J. Phys.: Condens. Matter 4 (1992) 1143–1212. Printed in the UK

REVIEW ARTICLE

Surface-enhanced Raman scattering

A Otto, I Mrozek, H Grabhorn and W Akemann

Lehrstuhl für Oberflächenwissenschaft (IPkM), Heinrich-Heine-Universität Düsseldorf, W-4000 Düsseldorf 1, Federal Republic of Germany

Received 2 September 1991

Abstract. On the basis of different types of experiments, we develop implicitly the model of surface-enhanced Raman scattering (SERS) of adsorbates on metal surfaces. The long-range enhancement by resonances of the macroscopic laser and Stokes field is separated quantitatively from the metal electron-mediated resonance Raman effect. The latter mechanism proceeds by increased electron–photon coupling at an atomically rough surface and by temporary charge transfer to orbitals of the adsorbates. This model can account for the chemical specificity and vibrational selectivity of SERS and (partly) for the SERS specificity of the various metals.

Contents

0953-8984/91/051143+70$04.50

1. Introduction

After the first observation of a Raman signal of pyridine adsorbed at a rough silver electrode by Fleischmann and co-workers [1] and the discovery of the 'surface enhancement' [2, 3] of about 6 orders of magnitude the research on 'surface-enhanced Raman spectroscopy' (SERS) was focused up to about 1985 on the enhancement mechanism(s), as documented by many review articles [4–13], 20 articles in [14], and [15–36]. About 85 selected papers on the SERS mechanisms will appear in [37].

Though considerable progress was made, a full understanding of all aspects of the enhancement mechanisms was and in the opinion of the authors is still missing (see section 6). In the meantime, SERS has become a domain of applied science. In 1989 and approximately the first half of 1990, about 170 publications listed in chemical abstracts were concerned with or used SERS, about 9% of them in biological, 22% from materials sciences, engineering and environmental, 41% from chemical, 9% from physico-chemical, 4% from applied industrial and 15% from physical laboratories. 19 SERS citations have appeared since 1989 in biological abstracts. A review of recent literature of the applied and mechanistic research on SERS is given section 8.

In the main part of this article we will present experiments and theoretical considerations of our own research group on the so-called classical and chemical origins of SERS (in the sense of a previous review article [17], where 'chemical' refers to resonance effects by charge transfer).

We have chosen the implicit method of representation, following our experimental, empirical and positivistic approach to the issue. This implies that in the course of the discussion we often have to refine or to replace some previous concepts or hypotheses. Therefore we have taken care to refer to these concepts in quotation marks with the exception of 'SERS' itself. For instance, we will proceed from the 'first-layer effect' (section 3) via 'SERS-active sites' (section 5) to adsorption sites not available at smooth low index surfaces of single crystals (so-called E-sites) (section 5.2) and the hypothesis of increased surface-electron–photon coupling (section 4.2). If the discussion of a particular point is resumed further below, this will be pointed out. Open questions and our present understanding of SERS are summarized in section 7.

2. Classical and resonance Raman aspects of SERS

Figure 1(*a*) displays the unenhanced Raman spectrum of a solid film of C_2H_4 (about 1.7 μm thick) frozen on top of a silver film. This silver film was deposited on a Cu

substrate at room temperature by thermal evaporation in ultra-high vacuum (UHV). In figure 1(*b*), the Cu substrate was cooled to 40 K before so-called cold deposition of the silver film. This sample yields the 'surface-enhanced' Raman spectrum. (In this case, 5 L corresponds to less than a monolayer, the quantitative evaluation of the enhancement is described in section 4.)

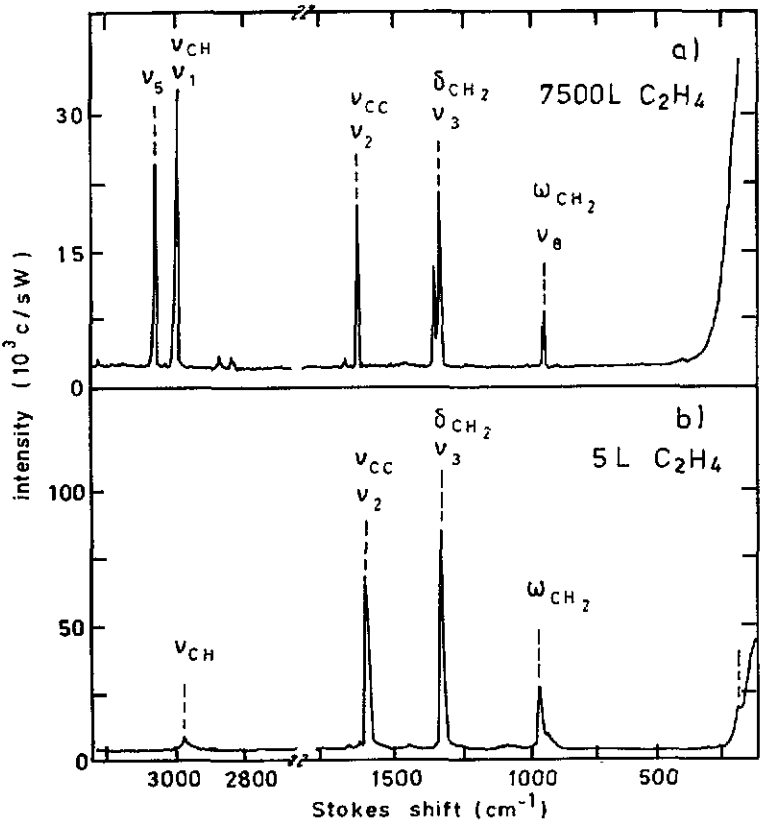

Figure 1. Raman spectra of ethylene (C_2H_4), laser wavelength 514.5 nm. Intensity (counts per second) is normalized for incident laser power. (*a*) Substrate is a 'smooth' silver film (deposited at room temperature in UHV), covered by a condensed film of C_2H_4 by exposure to 7500 L at the substrate temperature of 40 K; (*b*) substrate is a 'porous' silver film, thickness 100 nm, cold-deposited at 40 K, exposed to 5 L of C_2H_4. ν_2 is the C–C stretch mode ν_{CC}, ν_3 is the CH_2 scissor mode δ_{CH_2}, ν_8 is the symmetric CH_2 wagging mode ω_{CH_2} and ν_1 is the symmetric CH stretch mode ν_{CH}. For a comprehensive assignment see [38]. After [38].

In this example the presence or absence of SERS must be ascribed to unknown differences of the differently prepared silver surfaces. (The same holds for silver electrode surfaces at which the majority of SERS investigations are done—see section 8.) One difference is certainly the 'roughness'. The room-temperature deposited film has only some residual roughness, whereas cold-deposited films are highly porous (the ratio of true surface to apparent surface is about 20–40 [39], see also figure 16(*b*)).

Is the enhancement of Raman scattering of C_2H_4 caused (or partly caused) by the resonant enhancement of the local electromagnetic laser field $E_{loc}(\omega_L, r)$ within

'cavities' of the porous film? (The relevant literature on the porosity is given in section 8.) The intensity at frequency ω_L causing Raman scattering is enhanced by the factor

$$\left|\frac{E_{loc}(\omega_L, r)}{E_{inc}(\omega_L, \Omega_L)}\right|^2 \tag{1}$$

where E_{inc} is the field strength and Ω_L the direction of the incident laser beam, far away from the sample. Also the 'emissive power' of the molecule at the Stokes frequency ω_S into direction Ω_S is enhanced by local field resonances at frequency ω_S. According to the law of optical reciprocity, the emitted field in direction Ω_S is enhanced exactly as the local field is at r when light is incident on the sample with direction $-\Omega_S$. Given a statistically rough surface, one has to integrate over r.

This enhancement, which we call 'classical electromagnetic enhancement' (CEME) is usually approximated [18] by the product of the average local field intensity factors at the surface, on the vacuum (or electrolyte) side at the incident (inc) frequency ω_L and the emitted frequency ω_S, namely

$$\left\langle\left|\frac{E_{loc}(\omega_L)}{E_{inc}(\omega_L, \Omega_L)}\right|^2\right\rangle\left\langle\left|\frac{E_{loc}(\omega_S)}{E_{inc}(\omega_S, -\Omega_S)}\right|^2\right\rangle. \tag{2}$$

We now turn to the question of whether the enhancement is caused (or partly caused) by resonant Raman scattering in a kind of 'surface molecule' complex.

The molecule C_2H_4 has no internal electronic excitations in the visible spectral range, but when it is bonded to single neutral silver atoms (in other words if one forms silver–ethylene complexes by dispersing silver in solid ethylene or ethlyene–Ar matrices at low temperatures) one observes a pronounced optical absorption band centered around 550 nm (see figure 2). This band corresponds to the charge transfer excitation of an electron from the Ag 5s state to the lowest unoccupied molecular orbital (LUMO), a $\pi^* b_{2g}$ state [40]. (For a detailed discussion see section 6.6.) In the following, we will call these unoccupied orbitals 'affinity levels'. The band is not observed when silver is isolated in a C_2H_6 matrix [41] (see figure 2) since a hydrogen-saturated hydrocarbon molecule has neither occupied nor empty π-states. Tuning into this charge transfer (CT) band ($\hbar\omega_L = E_{CT}$, where E_{CT} is the charge transfer energy) should yield resonant Raman scattering by the CC stretch vibration. The $\pi^* b_{2g}$ state is C–C antibonding, and C–H non-bonding. If it is temporarily occupied by an electron this will push apart the carbon atoms, but not change the distance between C and H atoms. This naive picture translates within Lee and Heller's short time-domain picture of resonant Raman scattering [42] into the scheme of figure 3.

The Ag–M complex is quasi-instantaneously excited by photon annihilation to the charge transfer state. Thus, the conformation of the ligand M is not changed by the transition and the starting point of nuclear dynamics is the ground state wavepacket $n = 0$. The wavepacket $n = 0$ propagates along the normal coordinate Q(C–C) of the CC stretch vibration: the propagation along Q(C–H) is negligible. After transition into the electronic ground state by quasi-instantaneous photon emission, there is a finite overlap of the propagated wavepacket with the excited vibrational states of the electronic ground state leading to a final state with $n = 1$ given by the Frank–Condon factor $F = \langle n = 0, \text{propagated}/n = 0, \text{ground state}\rangle$. The Raman intensity is proportional to $|F|^2$ [42]. The time for propagation is given by Heisenberg's uncertainty

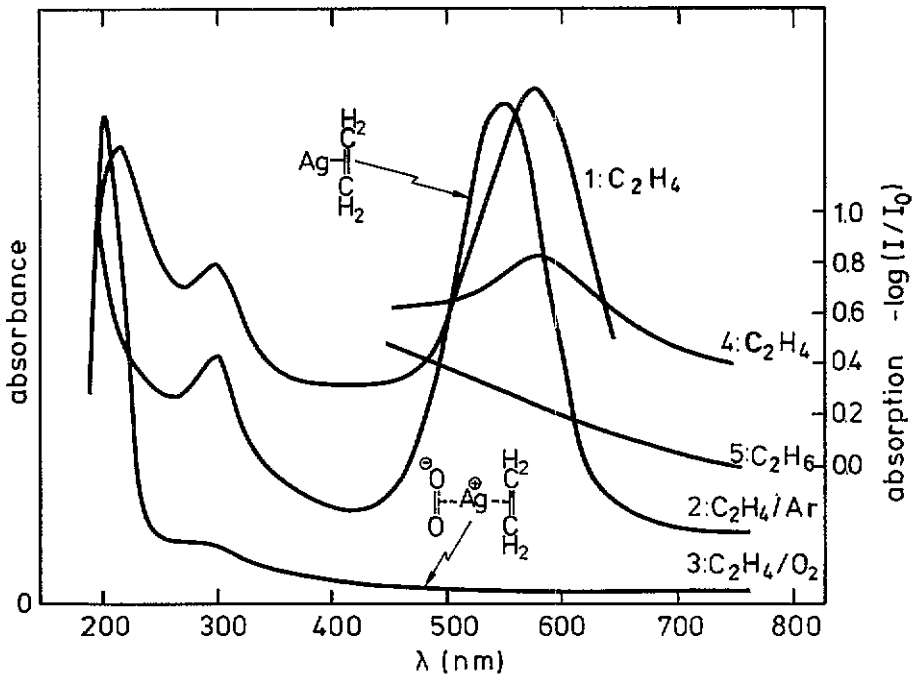

Figure 2. Absorbance spectra (left scale, arbitrary units [40] for silver atoms in matrices at 10–12 K, silver concentration not quoted. 1: undiluted C_2H_4; 2: C_2H_4: Ar = 1: 10; 3: C_2H_4: O_2 = 1 : 1. The schemes of the Ag complexes are from reference [40]. Absorption spectra from reference [41], right scale 4: C_2H_4-film, d = 4 μm, Ag concentration $C_{Ag} = 7.8 \times 10^{-4}$; 5: C_2H_6-film, d = 5 μm, $C_{Ag} = 5.3 \times 10^{-4}$.

principle, $\theta = \hbar/|\hbar\omega_L - E_{CT}|$ [42]. $|F|$ will increase linearly with θ. Hence, Raman scattering will be resonant, the intensity given approximately by $(|\hbar\omega_L - E_{CT}|)^2$.

Figure 4 shows the result of Raman experiments with solid C_2H_4 matrices, in which silver atoms were dispersed at low atomic concentrations; the details are described in reference [41]. The hatched bands in the range of ν(CC), $\delta(CH_2)$ and $\omega(CH_2)$ were assigned to vibrations of C_2H_4 in Ag–C_2H_4 complexes. No new bands appear in the spectral range of the ν(CH) modes and in the case of matrix isolation in ethane C_2H_6. The new bands are assigned to the resonant Raman effect of about 2 orders of magnitude [41]. Inspection of the spectra in figure 4 and the SERS spectra in figure 1(b) reveals in both cases a conspicuous low intensity of the C–H stretch modes.

There is one further analogy. The CT band in the visible range is not observed when Ag is dispersed in a mixed C_2H_4/O_2 matrix—see figure 2 [40]. This is explained by the oxidation of Ag to Ag^+—see the inset in figure 2. Charge transfer excitation is now only possible from the Ag4d states to the $\pi^* b_{2g}$ state of C_2H_4, which yields the ultraviolet absorption bands in figure 2 [40]. In consequence, this must lead to a loss of the resonance Raman effect at a laser wavelength of 514.5 nm. When one adsorbs submonolayer quantities of oxygen before or after exposing the cold-deposited silver film to C_2H_4, SERS can be quenched below the detection threshold [45] (see also section 3.1). Is this the suppression of resonant Raman scattering within a 'surface–C_2H_4' complex?

Jiang and Campion [46] estimated an enhancement of 15–65 for the Raman scat-

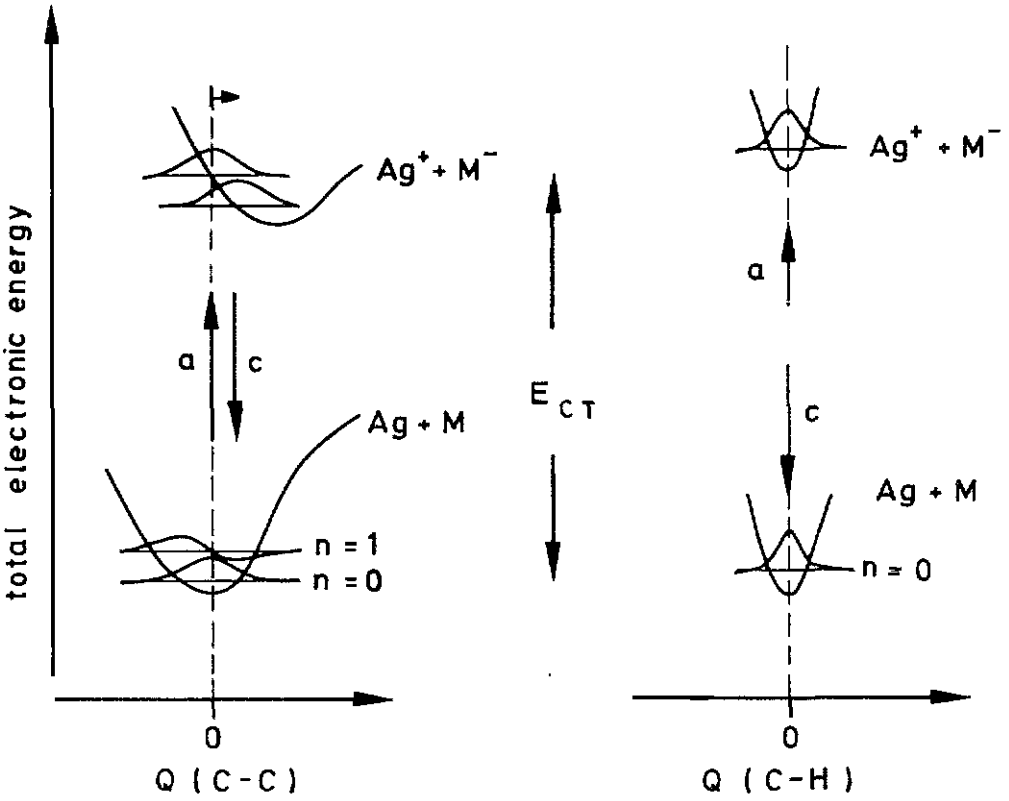

Figure 3. Scheme of resonant Raman scattering in a silver atom (Ag)-ligand (molecule M, e.g. C_2H_4) complex within the Born–Oppenheimer [43] and Frank–Condon [43] approximation. The potential curves of the total electronic energy of the ground state (Ag + M) and the charge transfer (CT) state ($Ag^+ + M^-$) versus the normal coordinates Q of the C–C stretch vibration (ν_2 in the case of C_2H_4) and of the symmetric C–H stretch vibration (ν_1 in the case of C_2H_4) are separated at $Q = 0$ by the charge transfer excitation energy E_{CT}. Nuclear wavefunctions in the ground ($n = 0$) and vibrationally excited ($n = 1$) states in the electronic ground state and the corresponding wave packets $n = 0$ in the CT state and their propagation along Q(C–C) are indicated qualitatively. Vertical arrows characterize quasi-instantaneous electronic transitions by photon annihilation (a) and creation (c).

tering intensity of pyridine adsorbed onto silver that was deposited on Rh(100) with a thickness of 10% of a silver monolayer. The Raman signal was assigned to pyridine chemisorbed to silver adatoms. This is comparable to the resonant Raman scattering in the isolated $Ag–C_2H_4$ complexes.

An obvious approach to the question of a surface-resonant Raman process is the search for short-range, or 'first-layer' SERS by adsorbing and condensing the Raman scatterers on well-prepared 'LEED-clean' low index faces of silver single crystals in UHV. With some exceptions, most investigators agree [32] that on Ag(111), Ag(100) and Ag(110) faces there is no special extra SERS for the adsorbed molecules with respect to molecules condensed on top of the adsorbed molecules; in other words, no

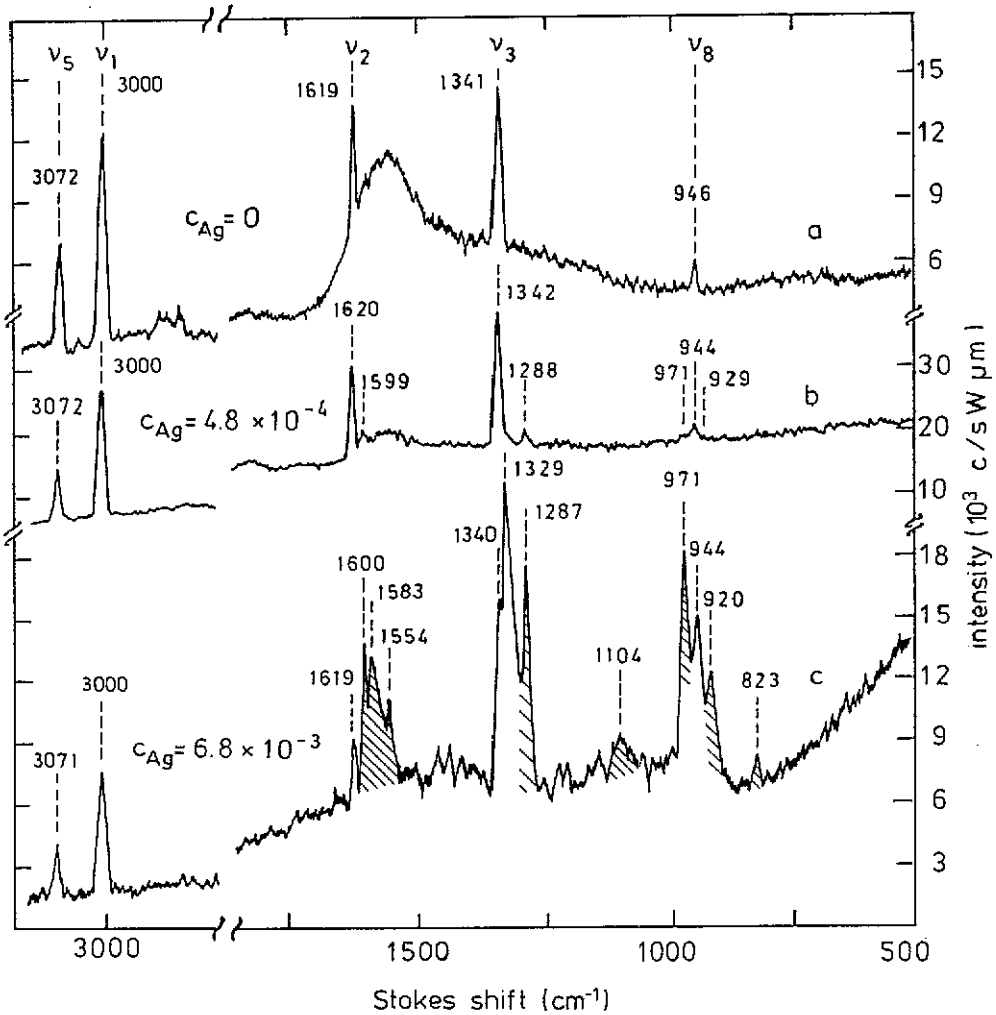

Figure 4. Raman spectra (normalized for film thickness and power) of a solid ethylene matrix [41]. The broad background structure in the upper spectrum is from the carbon-contaminated silver substrate [44]. Laser wavelength 514.5 nm, substrate temperature 10 K. The hatched structure is assigned to Ag-C_2H_4 complexes. (The ν_3 band at 1329 cm^{-1} may contain contributions from the Davydov couple, see figure 1, top). After [41].

'first-layer' effect [47–51] and no 'active sites' [52].

The classical electromagnetic enhancement model should be tested for samples of controlled and known roughness, for instance for the case of silver films deposited on an optical grating under UHV conditions—see inset in figure 5.

On metallic gratings, one may resonantly excite surface plasmon polaritons (SPP) (see for instance [54]) by angle tuning p-polarized light (e.g. [55]). On gratings with the optical constants of silver, laser field intensity enhancements ($\hbar \sim 2.5$ eV) of 20–200 may be expected directly above the silver surface [56–60]. This enhanced field decays exponentially over several hundred nanometres into the vacuum or into a dielectric layer (for instance about 250 nm into a thick benzene layer condensed on the grating

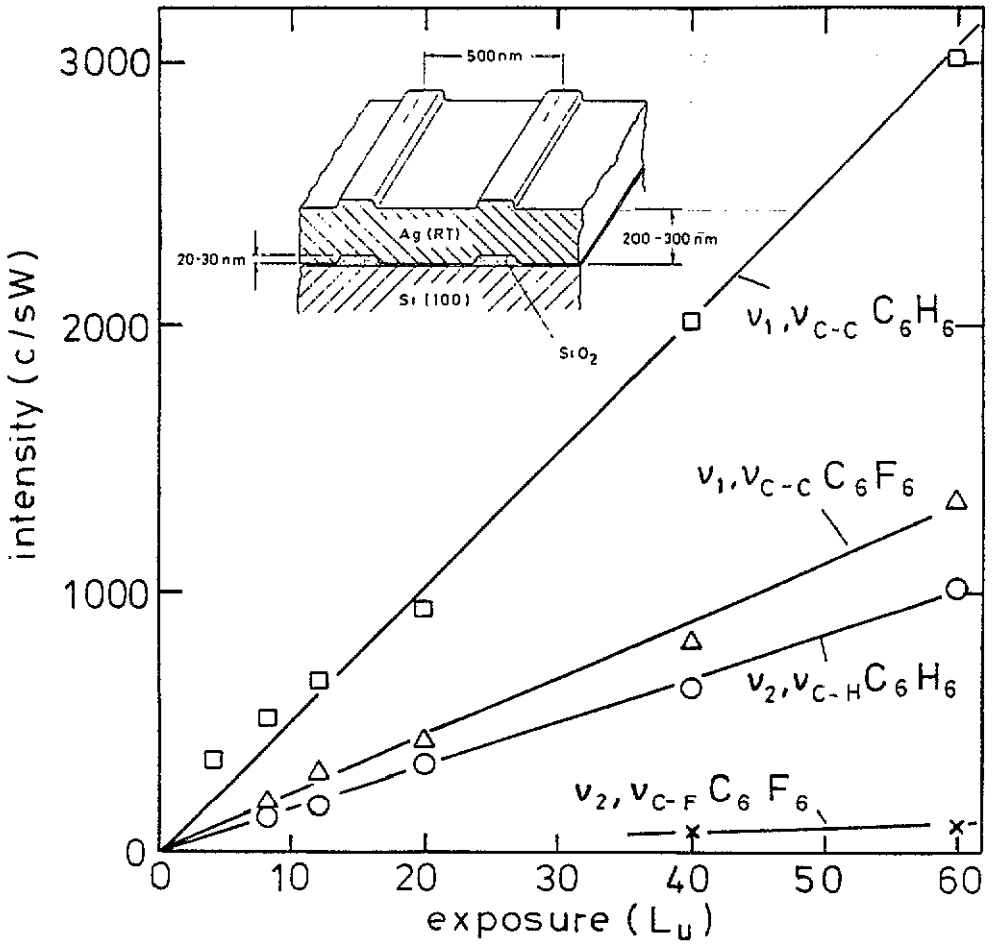

Figure 5. The peak intensities (normalized for incident power) of the indicated Raman bands of the a_{1g} vibrations of C_6H_6 and C_6F_6 versus exposure at a substrate temperature of T_E = 40 K. The actual spectra are depicted in figure 16(*b*). The substrate is a silver film deposited at room temperature onto an optical grating schematically depicted in the inset. The laser beam is tuned to the SPP resonance. The exposures are given in Langmuirs uncorrected for the gauge sensitivity factor (L_u). After [53].

shown in the inset of figure 5, as has been demonstrated experimentally [38]).

Thin condensed layers of benzene or hexafluorobenzene of only a few nanometres thickness, produced by the exposures given in figure 5 will thus be exposed to a constant, enhanced exciting field.

The Raman intensities grow linearly with coverage. (At T_E = 40 K the sticking coefficient of C_6H_6 and C_6H_6 is 1 and the extra first-layer enhancement is smaller than 2, if it exists at all.) This result corresponds to the absence of 'first-layer SERS' of C_2H_4 [61] and pyridine [62] adsorbed on a silver film deposited at room temperature on a smooth flat substrate in UHV.

Apparently, the residual roughness of the room temperature deposited silver films (e.g. observed by scanning tunnelling microscopy [63–65] does not induce a measurable

'first-layer effect'. We will come back to this point in section 6.

The results in figure 5 corroborate the nearly linear increase of the SERS intensity of the a_{1g}–CC mode of benzene condensed on Ag(111) reported by Hallmark and Campion [66]. They point to a nearly symmetric form of the Raman tensors of the a_{1g} vibrational modes of C_6H_6 and C_6F_6, as will be discussed in section 4.3.

From these examples is it obvious that for well-controlled surfaces there is no apparent 'non-classical' SERS. One might conclude that SERS is nearly exclusively explained by CEME, notwithstanding some less important effects due to molecular adsorption, orientation (see section 4.3), and depolarization (see section 8).

This conclusion is supported by the fact that the best metal substrates for SERS investigations are those which support strong electromagnetic resonances (see section 6.6). This conclusion discards the possibility that a significant resonance effect might exist at disordered metal surfaces because of states of adsorption and electronic properties (especially optical properties) of these surfaces that differ from those encountered at smooth surfaces. In the following sections we will focus on these problems.

3. Separation of 'first-layer' SERS and long-range classical electromagnetic enhancement

3.1. Silver island films

Thick cold-deposited silver films [24,67] and silver electrodes, activated for SERS by an oxidation–reduction cycle [22] are less well characterized than silver islands. For the latter, quantitative calculations of classical electromagnetic enhancement (CEME) [20,21,23,26] are available.

Deposition of silver from the vapour phase onto room temperature dielectric substrates in a quantity corresponding to an average thickness of 30–150 Å leads to discontinuous films of irregularly shaped islands (e.g. [68,69]). Silver island films or small separated silver islands on regularly spaced posts [70] or stochastically distributed posts [71,72] are considered as excellent 'classical enhancers' (e.g. [73]). Indeed, the concept of CEME was first introduced by Moskovits in connection with collective electromagnetic resonances in films consisting of silver islands [74]. The dependence of CEME on the distance d of a scatterer from the surface of a silver sphere of radius r and dielectric constant $\epsilon(\omega)$ has been calculated without approximations by Kerker *et al* [75], but more often quoted is the result of the dipolar plasmon approximation for silver spheres by McCall *et al* [76] for a molecule

$$\text{CEME} \sim \left(\frac{r}{r+d}\right)^{12} \tag{3}$$

or for a monolayer at a distance d [77]

$$\text{CEME} \sim \left(\frac{r}{r+d}\right)^{10}. \tag{4}$$

Following electrostatic calculations by Gersten and Nitzan [78,79] for spheroidal particles it is usually assumed that the distance dependence of CEME from irregularly

shaped islands also follows equation (3) or (4), where r is now the local radius of curvature of the part of the surface next to the Raman scatterer [31,80]. Any slower decays of CEME with d due to the collective resonances between bumps (discussed in [17]) is not considered. To our best knowledge, experimental data on the distance dependence of CEME have always been fitted to equation (3) or (4). This dipolar, local curvature approximation is also used in the field of surface-enhanced fluorescence [27].

The following results were obtained with silver island films on sapphire substrates, produced and kept in UHV. Experimental details are given in [84–86]. From comprehensive investigations of thermodesorption of Xe, C_2H_6, C_6H_{12} and the observation of ordering in the adsorbed layers (see detailed description in [86]) the following picture emerges: (a) the surface of the island films is a factor of three to four larger than the geometrical area of the sapphire substrate—the islands contain no 'pores'; (b) at low temperatures, one can form spacer layers, monolayers, bilayers and multilayers of cyclohexane. They separate other aromatic molecules, adsorbed or condensed on top of the spacer layer without intermixing by place exchange, provided the temperature is low enough.

The clean unexposed silver island films yield an intense and rather uniform background of inelastically scattered light [86]. (We will come back to this point in section 6.4 and 6.5.) The SERS bands of the adsorbed and condensed species are superimposed. Figure 6 shows the dependence of the intensities of the C–C and C–H Raman bands of benzene on exposure. The ν_{CC} intensity saturates at an exposure of about 5 L, corresponding to about 1.3–1.7 monolayers. The ν_2, C–H intensity is relatively weak, compared to the ratio of C–H to C–C intensities of benzene adsorbed on a silver

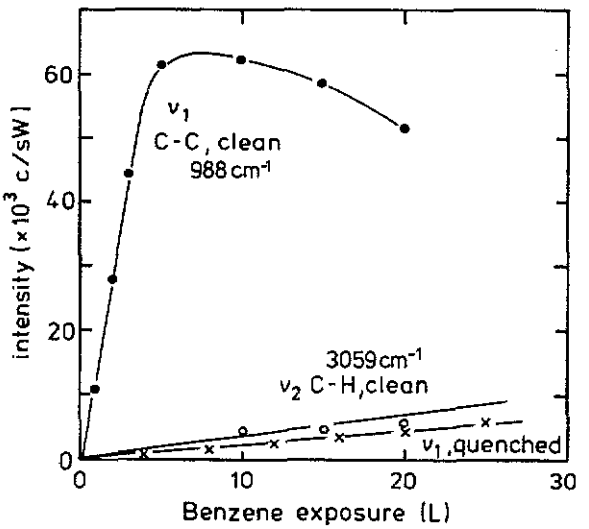

Figure 6. Coverage dependence of the peak Raman intensity of the totally symmetric C–C ν_1 and C–H stretch modes ν_2 of benzene (Wilson mode numbers). Full and open circles: ν_1 and ν_2 of benzene adsorbed on a silver island film of average thickness 42 Å and deposition rate 0.9 Å s^{-1}. Each exposure was performed at 28 K followed by a low- temperature anneal at 77 K to 'order' the adsorbate, see [86]. Crosses: ν_1 of benzene adsorbed at 10 K on a silver island film of average thickness 61 Å and deposition rate 0.9 Å s^{-1}, pre-exposed at 25 K to 5 L of O_2 and annealed to 75 K. All Raman spectra were recorded at a sample temperature of 28 K. After [86].

grating (see figure 5) and of liquid benzene (see figure 16(*a*)).

The saturation of the Raman intensity with coverage at about one monolayer, corresponding to an enhancement of the ν_1 band of benzene of about 10^4 (see section 3.4) is lost if the silver island films are first 'passivated' by oxygen (see figure 6). They are exposed at temperatures of about 30 K to 5–10 L of oxygen, then warmed up to about 50–80 K and cooled down again to 28 K. No change of the optical transmission and reflection spectra of the island films were observed, indicating that the classical electromagnetic resonances are not changed. This is consistent with the clear demonstration of electromagnetic resonances of silver island films in ambient air (e.g. [87, 88]). However, the inelastic featureless background is reduced by about 50%. (We will come back to this point in section 6.4.)

After the 'passivation' the long-range chemically unspecific CEME becomes observable by the increase of the Raman signal with growing thickness of the condensate. The initial gradient of Raman intensity versus exposure (see figure 6; the line marked 'ν_1, quenched' is about 200 counts $s^{-1}W^{-1}L^{-1}$—counts per second per Watt laser power, per L exposure) and eventually reaches the average gradient $\alpha_b \sim 0.7$ counts $s^{-1}W^{-1}L^{-1}$ of very thick condensed layers (averaging over the interference pattern at high exposures, for more details see [86]). This corresponds to an enhancement of about $200/0.7 \sim 300$—see below. CEME is observable up to a distance of about 13 nm [86].

The 'passivation' of the silver islands is envisioned as a 'decoration' of sites of atomic scale roughness with atomic oxygen, whereby (111) terraces remain clean from oxygen. The reasons are: oxygen physisorbed by an Ag(111) surface or by silver films deposited at room temperature desorbs at 44 K [45]. After this desorption, the Ag(111) surface is clean, as demonstrated by ultraviolet photoelectron spectroscopy [89]. This corresponds to the very low sticking coefficient of O_2 on Ag(111) of 5×10^{-6} at 150 K [90]. On room-temperature-desposited silver films there remains a low coverage of oxygen [89]. This result corresponds to (i) an initially increased sticking coefficient of 10^{-2} at 77 K, which drops to about 1.5×10^{-5} after an oxygen coverage of 1% [91] and (ii) to increased sticking after damaging an Ag(111) surface by ion bombardment [92]. Both results are explained by oxygen adsorption at defects [90]. The quenching mechanism will be discussed in section 6.4. Apparently, there exists a 'first-layer' SERS for silver island films—in contrast to SERS of adsorbates and condensates on the grating sample.

The first-layer effect of SERS of adsorbates on island films was clearly demonstrated with the help of two isotopic pyridine species (deuterated and hydrogenated) [93]. At low temperatures (30 K) the films were first covered with one monolayer of one isotopic species, on top of which was condensed a multilayer of the second species. Raman signals were observed only from the first monolayer adsorbed. After warming up above 100 K, the SERS spectrum contained signals from both isotopic species. The results are easily explained with two assumptions:

(i) There exists a short-range enhancement mechanism confined approximately to adsorbates within the first directly adsorbed monolayer in addition to the long-range classical electromagnetic enhancement.

(ii) Warming the sample from low temperature during exposure allows for molecular place exchange. In this way, molecules outside the short range of the extra enhancement have a chance to enter it at the expense of others which have to leave it.

3.2. Spacer experiments

The long-range electromagnetic enhancement is revealed by separating the Raman scatterers from silver island films and silver films deposited at room temperature on rough CaF_2 films by spacer layers of cyclohexane—see figure 7. The 'first-layer effect' of paranitrobenzoic acid on rough silver films (figure 7(*b*)) was not observed in previous experiments [94, 95]—the possible reasons for this discrepancy are discussed in detail in reference [85].

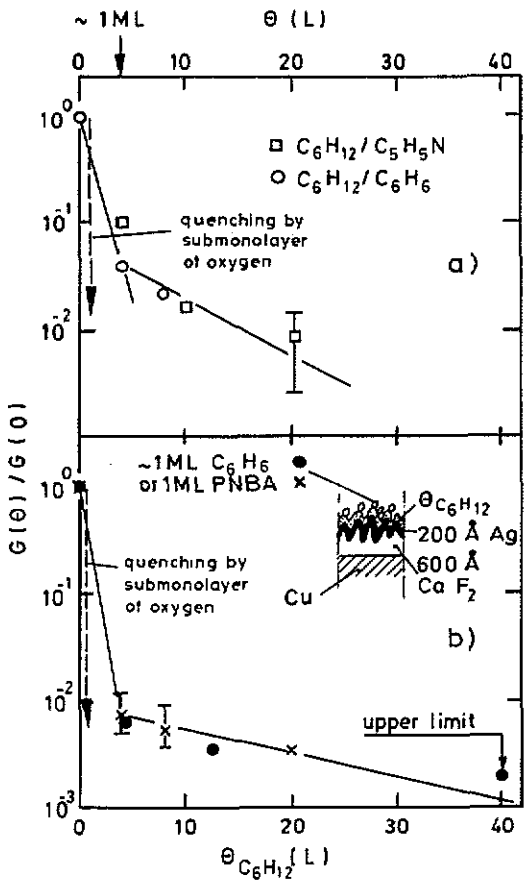

Figure 7. Relative Raman scattering enhancement $G(\theta)/G(0)$ as a function of the cyclohexane (C_6H_{12}) spacer layer thickness given by the exposure θ. (*a*) Silver island films, average thickness $d_m \sim 40$ Å. Rectangles: C–C–ν_1 mode of pyridine (1003/990 cm^{-1}), circles: C–C–ν_1 mode of benzene ($\sim$ 990 cm^{-1}). At $\theta = 0$, only one mark at ordinate one has been used for reasons of clarity. Arrow indicates approximately one monolayer of spacer; (*b*) silver films, deposited at room temperature on rough CaF_2 film (see insert). Circles: C–C–ν_1 mode of C_6H_6, crosses: ν_3 mode of paranitrobenzoic acid (PNBA) at 1598 cm^{-1}. After [85].

Fitting the long-range enhancement in figure 7 to equation (4) yields radii of local curvature of 50–100 Å and 100–200 Å in the case of the island films and the rough films on CaF_2, respectively. These radii correspond to the structure of the silver samples seen by electron transmission microscopy [96]. From SERS with a spacer configuration

(between PNBA and a silver film on CaF_2) different from the one depicted in the inset of figure 7, Murray and Allara deduced $r \sim 130$–260 Å [95].

3.3. Excitation spectra

The absolute 'first-layer enhancement' of the ν_1 and ν_2 modes of benzene and the ν_2 mode of cyclohexane on silver island films was evaluated at 6 different laser photon energies [96]. In figure 8(a) the individual enhancement factors are interpolated to yield a reasonable symmetric excitation spectrum. The normal-incidence transmission spectra (see figure 8(b)) of the same samples were taken immediately after preparation of the island films at room temperature before cooling down and exposure to benzene. They follow the shift in the resonance curve towards the red as the average film thickness d_m increases indicating collective electromagnetic resonances [97]. We believe therefore that the excitation spectra are dominated by electromagnetic resonances.

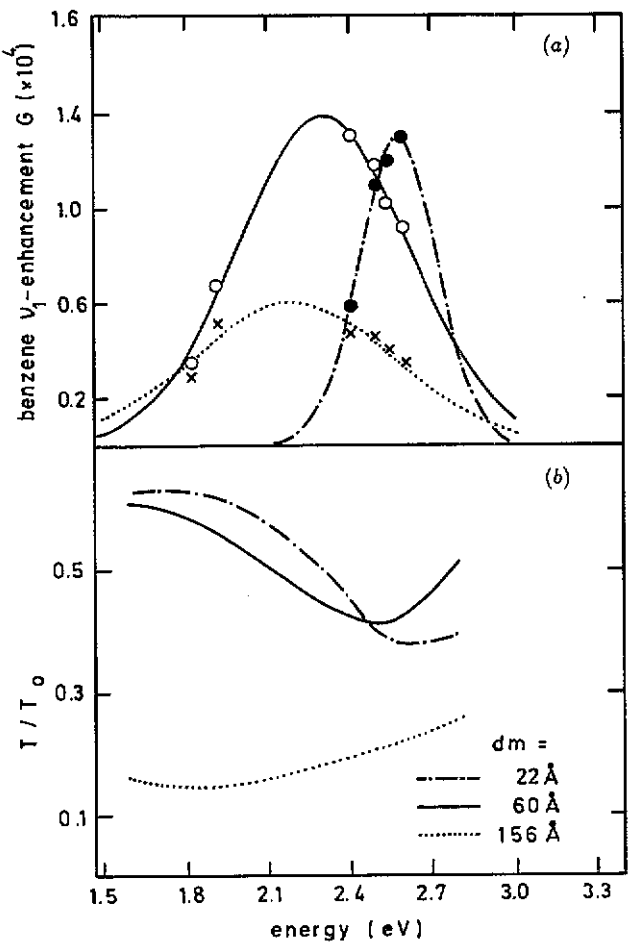

Figure 8. (a) Enhancement G of the ν_3 mode of benzene adsorbed on three island films of average thickness $d_m = 40$, 60, 156 Å and deposition rates 0.9, 1.3, 1.4 Å s^{-1} at 6 different laser photon energies $\hbar\omega_L$. For the connecting curves see text. (b) Transmission T spectra of the three island films above before exposure divided by the transmission T_0 of the sapphire substrate without island film. After [96].

However, there is a problem. We followed [98] the approximations of reference [87] and [88] which derive CEME from absorption and transmission [87] and absorption only [88]. In all cases we obtained CEME spectra in the range of 10^6 to 10^7 at 2.5 eV with a tendency to increase towards the red [98]. Considering the spectral shapes of the 'first-layer' excitation spectra in the case of island films and of cold-deposited silver films [99,100], they seem to follow the spectral shapes of the anomalous optical absorption (see also figure 16 in [67]) rather than that of the CEME approximations. The latter are dominated by the factor $|\epsilon(\omega_L)|^2\,|\epsilon(\omega_S)|^2$ [87,88] and increase enormously towards the red spectral range (see also section 6.5). This point needs further consideration.

3.4. DC resistance measurements

The methods described above to separate a 'first-layer' effect from long-range CEME fail for cold-deposited silver films. In this case, the 'first-layer' SERS effect can be clearly demonstrated by simultaneous Raman spectroscopy and 4-point contact DC resistance measurements [83,65] of continuous silver films on insulating substrates.

Condensation of Xe, CH_4, C_2H_6, C_5H_5N and C_2H_4 on smooth silver films leads to a positive resistance change ΔR that saturates at monolayer coverage [101]. Apparently, the adsorbates act as centres of electron scattering like impurities in the bulk. However, when thick cold-deposited silver films are exposed to the same species, the absolute gradients of $\Delta R/R$ versus exposure at low exposures are bigger than in the case of the smooth films. ΔR is positive for CH_4 and C_2H_6, but negative for C_5H_5N and C_2H_4 [101] and it saturates in all cases at submonolayer coverage of the porous films. This has been explained by increasing ($\Delta R < 0$) or decreasing ($\Delta R > 0$) the electron tunnelling rates by molecules in narrow 'tunnelling sites' in 'porous grain boundaries', according to the presence (C_5H_5N, C_2H_4) or absence (CH_4, C_2H_6) of low-lying unfilled molecular π^* orbitals [101]. (We will come back to this point in sections 4.2 and 6.2.)

Figure 9 demonstrates that only those molecules contribute to the Raman signal which contribute to ΔR. In other words only molecules in measurable interaction with the metallic electrons at the Fermi level (which are responsible for transport phenomena) yield an observable SERS effect. It should be noted that these molecules constitute less than one monolayer. This is one of the reasons to postulate 'SERS-active sites'—see section 5. The quenching of SERS by oxygen is connected with a relatively large ΔR, both phenomena already saturating at an exposure of only 3 L [83].

3.5. Quantitative separation of CEME and 'first-layer SERS' for various substrates

The extrapolation of the long-range enhancement inferred from spacer experiments to direct adsorption (no spacer layer) in figure 7 agrees approximately with the enhancement observed at low exposures after quenching the 'first-layer' effect by oxygen, as given by the vertical arrows in figure 7. Therefore we consider the enhancement observed after oxygen quenching quite generally as the contribution of CEME to the overall enhancement of the Raman scattering of adsorbates. In this sense we compare SERS of the ν_1 ring breathing vibration of benzene adsorbed on various Ag samples in the 'unquenched' and 'quenched' states in figure 10.

The submonolayer enhancement G has been evaluated in all cases by comparing the initial gradient of the Raman intensity versus exposure (see for instance figure 6) with the Raman intensity of condensed layers on various reference substrates. The fourth line in figure 10 is for silver deposited in UHV on a graphite single crystal, on coal and on exfoliated graphite (for details see [86]). As expected, the first-layer SERS

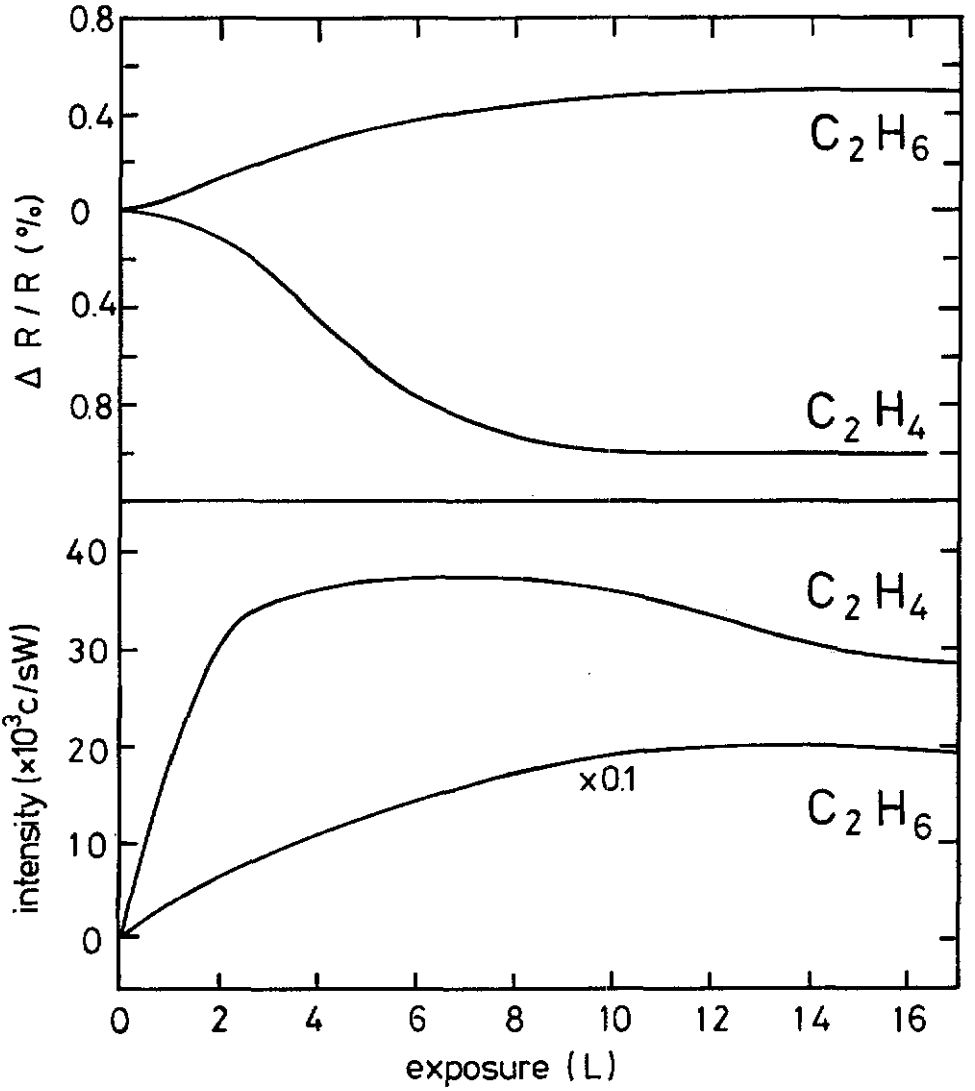

Figure 9. The change ΔR of the DC resistance of cold-deposited silver films on sapphire substrates (upper frame) and the scattered light intensity in Raman peaks during exposure (lower frame) versus coverage, with C_2H_6 and C_2H_4, respectively. The inelastic background has been subtracted from the Raman intensity. C_2H_4: silver deposited at T_S = 49 K, resistance R before exposure = 2.36 Ω, Stokes shift 1320 cm^{-1} (δ_{CH_2} *vibration*). C_2H_6: T_S = 46 K, R = 3.6 Ω, 985 cm^{-1} (*C–C* vibration). Monolayer coverage at about 20 L (after [83] and [102a]).

effect is quenched by oxygen passivation. After this no signal of benzene attributable to long-range CEME is observable. This is easily understood by a substantial suppression of the electromagnetic resonances of the silver islands (see for instance [103, 104]) by the carbonaceous substrates.

A nice demonstration of this effect is the work of Lyon and Worlock [105]. They

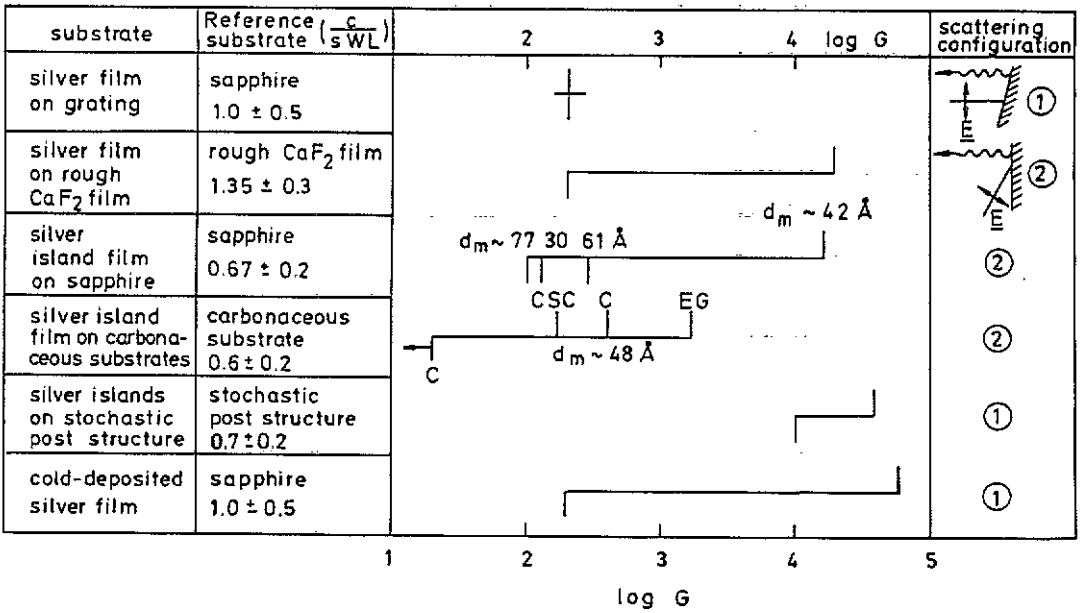

Figure 10. Submonolayer enhancement G of the peak Raman intensity of the ν_1-breathing mode of benzene on various silver substrates in scattering configurations 1 or 2, evaluated by comparison to the case of thick condensed benzene layers on silver-free reference samples. (The normalized signal from the condensates at constant spectrometer setting are indicated in the second column, but have not been used in the comparison of G of the different silver substrates.) Upper values: Clean silver substrates; lower values: oxygen-passivated silver substrates (arrows: signal below detection threshold). Numbers give average film thickness of island films. GSC: graphite single crystal, C: coal, EG: exfoliated graphite. For horizontal bars, see text. After [86] and [38].

produced a silver island film on a highly ordered pyrolithic graphite (HOPG) substrate partly covered by a wedge-shaped intermediate film of SiO_2. The Raman intensity of adsorbed PNBA on the island for a 20 nm intermediate SiO_2 layer was 300–500 times stronger than in the case of direct contact between the islands and HOPG. The excitation spectra (Raman intensity versus laser frequency) only displayed a resonance in the first case. The results were explained by a decrease of CEME by damping the plasmon-type resonances by the optical absorption of graphite.

Stochastic post structures [72] (line 5 in figure 10) are randomly distributed parallel SiO_2 posts on a quartz substrate with average spacing between the posts of 200–300 nm. Each post is 400 nm tall. Silver is deposited at 45° incidence, forming roughly ellipsoidal islands in the 100 nm range [72] on one side of the posts. These islands are bigger than those constituting the island films (average size about 30 nm). The laser beam was incident from the same direction as the Ag vapour beam, polarized in the plane of incidence with respect to the quartz substrate, and the Raman-scattered light was collected in a back-scattering configuration. (Also in this case, the first-layer effect evaluated with the help of cyclohexane or benzoic acid monomolecular spacer layers and oxygen quenching agreed approximately).

Pre-exposure of cold-deposited silver films suppresses SERS of the ν_1 mode of benzene to about 200–300 (see line 6 in figure 10). Cold-deposited silver films have a very high roughness factor of 20–40 [39] and probably the highest 'surface defect'

concentration—even in this case less than 10% of a monolayer of oxygen remains after desorption of physisorbed oxygen [45]. Also in this case, the inelastic background and the Raman intensity of internal vibrations of the silver substrate are reduced [106] (see also section 6.4). Except for the cold-deposited films the substrates of the silver samples (e.g. sapphire, stochastic post structure) served also as substrates of the thick condensed benzene reference films. Because of the comparatively low optical reflectivity of these substrates, the references should yield, within a factor of 2, the same Raman intensity as an ideal unsupported benzene film of equal thickness. But condensation of a film much thicker than the laser wavelength on an ideal plane mirror will enhance the Raman signal at normal incidence of the laser beam by a factor of about 8 (from the average of $(E_{loc}/E_0)^4$)—for more detailed considerations see [107, 108]. This explains the different intensities from the thick benzene reference films (second column of figure 10).

Whereas there is no 'first-layer' effect for the 'smooth' silver film on the grating, the benzene ν_1 Raman enhancement at submonolayer coverage of silver island films and of silver films on rough CaF_2 films is about 2 orders of magnitude bigger than CEME for the first layer. Interestingly, the 'first-layer effect' on the islands on the posts (size about 100 nm) is only about one order of magnitude, intermediate between the values for small islands (size about 30 nm) and 'smooth' silver films.

The best 'classical enhancers' are the islands on the posts where CEME reaches about four orders of magnitude, whereas the exclusive CEME for silver films on the grating reaches only two orders of magnitude. The latter case can be explained approximately by considering the two local-field enhancement factors in equation (2).

Even if $\omega_S \sim \omega_L$ the second factor is not necessarily equal to the first, if the direction Ω_L and $(-\Omega_S)$ of the incident and emitted beams are different, as discussed in [17]. This holds in particular for the silver film on the grating. Whereas the well-defined incident beam is angle-tuned to the surface plasmon polariton (SPP) resonance, the scattered radiation is collected in a wide $(-\Omega_S)$ range given by the 1 : 1 aperture of the collecting lens, and the SPP back-scattering emission is even partly blocked by a small mirror necessary to handle the incident beam. Thus the observed enhancement of about 200 is mainly attributed to the first factor in equation (2) (see also [109]), in reasonable agreement with theory [56–60].

In the case of the silver islands on SiO_2 posts and the Ag condensation described above and the scattering configuration described in figure 10, the two factors in equation (2) should be approximately equal. The average enhancement of the intensity at the surface of silver spheroids with major axis 100 nm and minor axis 50 nm, and the electric vector parallel to the major axis was calculated to be about 32.5 at the excitation wavelength λ_L of about 630 nm and about 15 at $\lambda_L = 514.5$ nm [110]. According to equation (2), this should yield a CEME of about 200 at $\lambda_L = 514.5$ nm, about two orders of magnitude less than observed.

In the case of the island and rough films the smaller absolute value and the range of CEME of oxygen-passivated silver island films are in good agreement with the results of Cotton *et al* [77] and Kovacs *et al* [111]—both groups studying SERS of organic molecules separated from silver islands (transferred to air) by Langmuir–Blodgett films. In summary, we have experimentally quantified CEME in special cases, but apart from the silver gratings we cannot yet rationalize the absolute values—see also section 3.3.

Long-range CEME has been separated from 'first-layer' SERS for roughened silver electrodes by Notholt and Ludwig [112]—see section 5.4. SERS at silver electrodes is

quenched by submonolayers of particular metals (see the literature review in section 8).

One might be tempted to assign the quotient of 'first-layer' SERS and CEME, observed after oxygen passivation, represented by the lengths of the horizontal bars in figure 10, to an extra, first-layer 'chemical effect'. This is premature—one would neglect the evidence for 'active sites' (see section 5). Before trying to understand the differences apparent in figure 10, we will discuss the 'chemical specificity' of the 'first-layer effect'.

4. Chemical specificity; evidence for resonant Raman scattering by charge transfer

4.1. Absolute 'first-layer' enhancement

The absolute enhancement G, evaluated from the initial gradients of intensity (integrated over the vibrational bands) versus exposure of the silver island films (see for instance figure 6) and of thick layers condensed on reference substrates, is very much dependent on the adsorbate and on the vibrational mode (see the results for CO, C_6H_6, C_5H_5N, C_6H_{12}, C_2H_4 and C_2H_6 in figure 11). The general trend is smaller enhancement G for saturated hydrocarbons and for C–H stretch modes (see also section 4.3

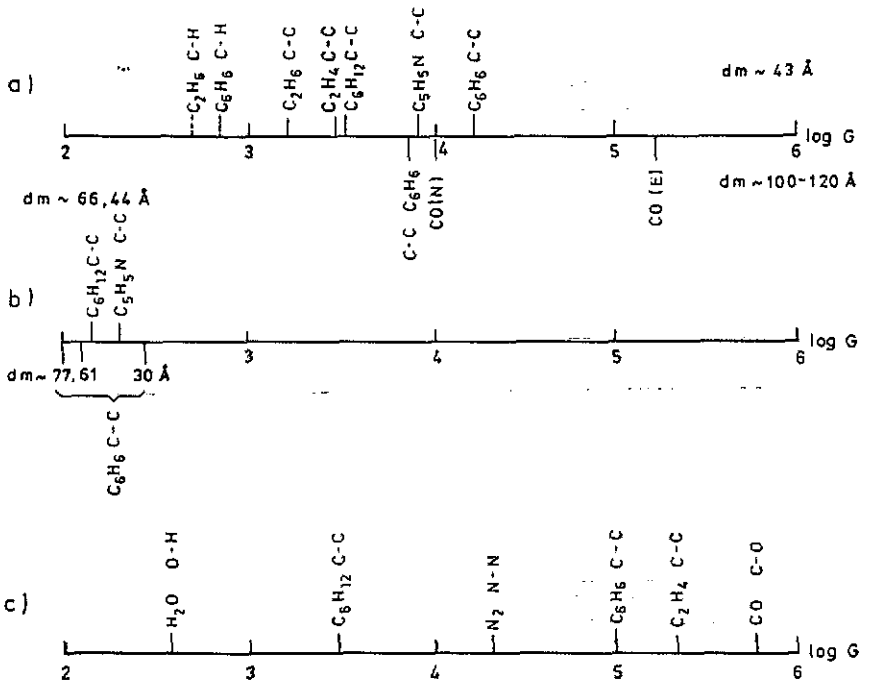

Figure 11. Enhancement G for the integrated Raman intensity of various modes of adsorbates (E: 'extra' line or 'chemisorbed', N: 'normal' line or 'physisorbed', see section 6.5) on three different substrates (errors of G are up to ± 0.5 orders of magnitude): (*a*) clean island films on sapphire, of average mass thickness d_m = 43 Å or 100–120 Å (for entries above or below the G-scale); references are thick condensed layers on clean sapphire; (*b*) oxygen-passivated island films on sapphire (d_m is indicated), references as in (*a*). (*c*) thick cold-deposited (30–60 K) silver films; References are thick condensed layers on the silver film itself. After [86] and [113].

and figure 14). Note that G does of course not only depend on the absolute SERS intensity but also on the Raman intensity of the condensed gases serving as reference. (For CO, the latter signal is, for instance, relatively weak.) Figure 11(a) indicates, for CO, separate entries for 'chemisorbed' (E) and 'physisorbed' (N) CO—this is discussed in detail in sections 5.2 and 6.5 and in [114] . After oxygen passivation, the remaining enhancement does not seem to be chemically specific (see figure 11(b)). This is to be expected for pure CEME.

The 'chemical specificity' of SERS of adsorbates on cold-deposited silver films (see figure 11(c)) displays a trend similar to that in figure 11(a). G for water is comparatively low. We cannot exclude the possibility that water does not 'penetrate' all the 'pores' (see the detailed discussion in [115]). In this case, the G value for water should not be discussed within the 'chemical specificity' model.

A contribution of a short-range quasi-first-layer effect of about 2 orders of magnitude to CEME, at roughness features of very small local radii of curvature less than 10 Å, according to equation (3) or (4) cannot be excluded *a priori*—see for instance reference [99], but also the footnote [80].

The clear 'first-layer' enhancement for silver island films, for room-temperature deposited silver films on rough CaF_2 films (see figure 7), and for cold-deposited films after 'smoothing' them by thermal annealing [116, 117] (see also section 6.5) would imply in any case approximately the same very small scale roughness. This is very unlikely. How does one explain the chemical specificity, vibrational selectivity and the quenching by oxygen, using this argument?

4.2. The relation between 'SERS' and the position of the affinity level

We now change from the correct description of the electronic state of a molecule in terms of total electronic energy (neutral molecule and free electron at the vacuum level: $E(\mathrm{M}) + E_{\mathrm{vac}}$; anion: $E(\mathrm{M}^-)$) to the single-electron orbital picture, by assigning the energy difference between two electronic states to the energy E_{a} of the orbital, whose occupation is different in the two electronic states, i.e.

$$E_{\mathrm{a}} - E_{\mathrm{vac}} = E(\mathrm{M}^-) - E(\mathrm{M})\,. \tag{5}$$

We call the highest occupied single-electron state of M^- or of the adsorbed species $\mathrm{M}^-_{\mathrm{ads}}$ the affinity level and $E_{\mathrm{vac}} - E_{\mathrm{a}}$ the electron affinity.

E_{a} will depend on the geometrical configuration of the molecule—if the electron is attached to the molecule M for a very short time, M^- will have the equilibrium conformation of M, and $E_{\mathrm{vac}} - E_{\mathrm{a}}$ is called the vertical electron affinity. If M^- relaxes to its equilibrium configuration, $E_{\mathrm{vac}} - E_{\mathrm{a}}$ is called the adiabatic electron affinity.

The adiabatic and vertical position of the affinity level above the vacuum level is obtained by electron transmission (ET) experiments in the gas phase (e.g. [118]), and its vertical position above the Fermi level without relaxation for adsorbed $\mathrm{M}^-_{\mathrm{ads}}$ is determined by inverse photoemission or Bremsstrahlung isochromat spectroscopy (BIS) (e.g. [119]). The positions of the affinity levels of some benzene-derived molecules are given in figure 12. (The figure does not include the position of the lowest σ^* resonance of benzene, about 7 eV above the vacuum level as observed for a 2–3 monolayer film of benzene on Ag(111) by BIS [120].) The differences of the zeros of the $E - E_{\mathrm{vac}}$ and $E - E_{\mathrm{F}}$ ordinates are the work functions ϕ of clean Cu(111) and Ag(111) surfaces, respectively.

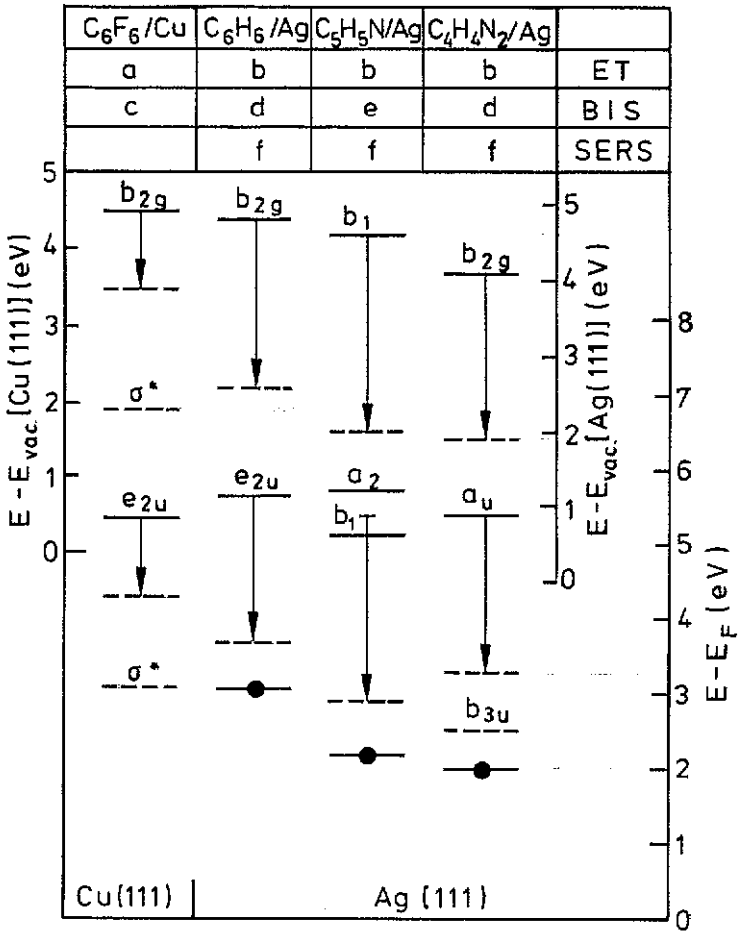

Figure 12. Energetic positions of the π^*-levels of hexafluorobenzene, benzene, pyridine and pyrazine above the vacuum level in the gas phase as deduced from electron transmission (ET) (full lines: adiabatic position for the lowest π^*s of C_6H_6, C_5H_5N and $C_6H_4N_2$, vertical positions for the upper π^*s)—the lowest σ^* level of condensed C_6H_6, about 11.2 eV above E_F of Ag(111) [120] is not displayed—and the position of π^* and C_6H_6-σ^* levels above the Fermi level E_F, when adsorbed at Cu(111) or Ag(111), as deduced from Bremsstrahlung isochromat spectroscopy (BIS) (broken lines, vertical position). The vertical arrows characterize approximately chemical and electronic relaxation shifts. The b_{3u} level of pyrazine cannot be observed by ET, and the lowest π^*-doublet of pyridine (a_2/b_1) was not resolved in BIS. Levels with dot are tentatively deduced from SERS experiments at silver electrodes at a potential $P = -0.68$ V_{SCE}, see text. Reference a: [121], b: [118], c: [122], d: [123], e: [124], f: [125].

To first order, the excitation energy E_{CT} of a metal electron at the Fermi level E_F into the affinity level is given by

$$E_{CT} = E_a - E_{vac} + \phi - C \tag{6}$$

where C is the sum of the 'chemical' shift by M^-–metal bonding and 'electronic relaxation' by the attractive potential between the electron in M^- and its image charge (or better its hybrid-image–exchange–correlation hole in the inhomogeneous

electron gas at the surface—see section 6.3). C corresponds to the vertical arrows in figure 12.

At a silver electrode, the variation of the potential of the electrode with respect to the potential of the electrolyte (characterized by the potential of the reference electrode) is given by the variation of the dipole layer at the electrode–electrolyte interface. In the vacuum-surface scientist's language, this corresponds to a variation of the work function ϕ. (For a tutorial introduction to SERS at electrodes, see [22].)

According to equation (6), the charge transfer excitation energy E_{CT} from E_F to the affinity level can thus be tuned in and out of resonance with the incident photon energy [126–136].

Thietke *et al* [125] measured the SERS intensity of the C–C ring breathing modes of benzene, pyridine and pyrazine as a function of electrode potential for different $\hbar\omega_L$. The potentials P_{max} of maximum SERS are plotted in figure 13 for different $\hbar\omega_L$. Of course the concentration and orientation of the adsorbed species as well as

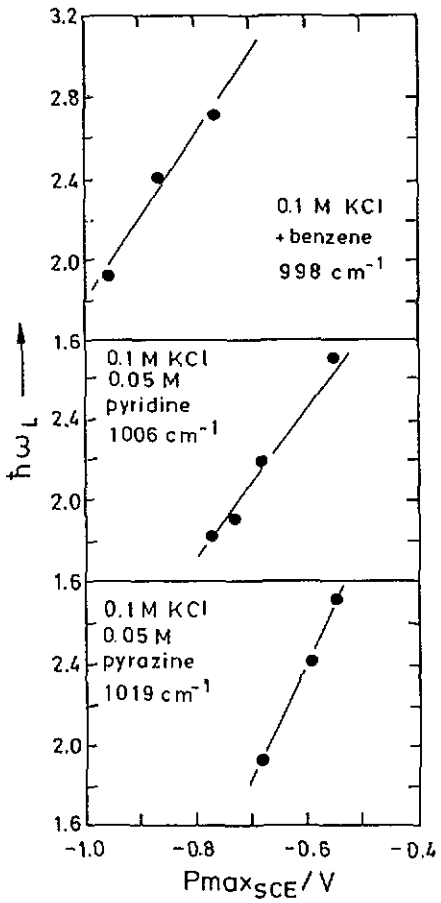

Figure 13. Full circles indicate the potential P_{max} (measured versus a saturated calomel electrode (SCE)) of maximum Raman intensity from the skeleton breathing modes of benzene, pyridine and pyrazine adsorbed at 'activated' silver electrodes in 0.1 M KCl electrolyte versus laser photon energy $\hbar\omega_L$. Full lines are guides to the eye. (Data from reference [125].)

the local potentials [127] will vary with potential, but it should not depend on the colour of the laser light. Thus one may tentatively interpret the $\hbar\omega_L$ versus P_{max} plots in figure 13 as E_{CT} (vertical) versus P. The positions of the affinity levels at an arbitrarily choosen P are given in figure 12. They scale quite well with the results of inverse photoemission BIS but they are lower, see section 6.2. It should be noted that we have assumed without justification that the electrons start at E_F. This problem will be discussed in section 6.4.

The search for the electron transfer excitations by optical reflection spectroscopy in our laboratory has so far been unsuccessful, both in electroreflectance from silver electrodes in pyridine-containing electrolyte [137] as in differential reflectance of clean and pyridine- or CO-covered thick cold-deposited silver films [138]. This corresponds to the missing change of the optical properties by the small amount of oxygen, which 'passivate' the substrates [106]. A more sensitive method for charge transfer excitations is electron energy loss spectroscopy [139,140] (see sections 6.2 and 6.3).

4.3. SERS selection rules

In many cases the relative vibrational band intensities in the SERS spectra are different to the Raman spectrum of the unadsorbed molecule (see for instance figure 1). The 'SERS selection rules', according to the different mechanistic models of SERS and relevant experiments have recently been discussed in a comprehensive article by Creighton [141]. In the spirit of the exclusive CEME model of SERS one neglects, in a first order approximation, the molecular symmetry reduction by adsorption. The molecule is characterized by its Raman tensor α unaltered by adsorption and its orientation, with respect to the surface. The enhancement of the various Raman active modes depends on the magnitude of the local field components parallel and perpendicular to the local surface. In this local cartesian frame (z is normal to the surface) the effective Raman tensor of a molecule adsorbed on an isolated sphere has been given in the small particle dipolar resonance approximation by Creigthon [142, 141] as

$$\alpha_{eff} = \frac{9}{[\epsilon(\omega_L)+2][\epsilon(\omega_S)+2]} \begin{pmatrix} \alpha_{xx} & \alpha_{xy} & \epsilon(\omega_S)\alpha_{xz} \\ \alpha_{yx} & \alpha_{yy} & \epsilon(\omega_S)\alpha_{yz} \\ \epsilon(\omega_L)\alpha_{zx} & \epsilon(\omega_L)\alpha_{zy} & \epsilon(\omega_L)\epsilon(\omega_S)\alpha_{zz} \end{pmatrix}. \tag{7}$$

Following reference [143], the 'SERS propensity rule' of the dominance of the α_{zz} component is often used to infer the adsorbate orientation at the rough surfaces (for instance [144,145]). Since in most cases the Raman tensors are not known, it is often assumed that the dominant diagonal Raman tensor components are fixed to the 'direction of the vibration' (neglecting the fact that in multiatomic molecules the vibrational patterns usually involve several bonds in different directions). This sequence of assumptions makes the 'SERS propensity rule' similar to the infrared surface selection rule—only vibrations with dynamic dipole perpendicular to the surface are observed.

Table 1 demonstrates the expectations for benzene based on the CEME selection rules. Benzene adsorbs flat on an Ag(111) surface as derived from energy loss spectroscopy [148]. We concentrate on the Raman active modes ν_6, ν_{10}, ν_1, ν_8 and ν_2. For the green Ar^+ laser line, $\hbar\omega_L = 2.41$ eV, and $|\epsilon| \sim 10$ [149]. Since the ν_1-Raman band of free benzene is polarized, a is of the order of b and hence one should expect

Table 1. The strongest SERS bands of benzene. Frequencies are listed for free benzene [146]. FR: Fermi resonance. Representations and activities (S: silent, R: Raman-active, IR: infrared-active) are for the case of free molecules. CEME is normalized to the enhancement of the internal field (given by the first factor in equation (7)). The intensity ratios of band intensities observed in SERS for C_6H_6 adsorbed on Ag islands on stochastic post structures and from the liquids are compared by setting the ratio for the ν_1 modes equal to one. For S and IR modes, values in brackets are SERS intensity ratios with respect to the ν_1 intensity. After [113] and [147].

Vibration, C_6H_6	ν_{16}	ν_6	ν_{11}	ν_{10}	ν_1(C–C)	ν_8	ν_2(C–H)
Frequency (cm^{-1})	404	606	671	849	992	1582/1606FR	3059
Representation	e_{2u}	e_{2g}	a_{2u}	e_{1g}	a_{1g}	e_{2g}	a_{1g}
Activity	S	R	IR	R	R	R	R
Raman tensor ($z \perp$ mol. plane)	—	$\begin{pmatrix} 0 & d & 0 \\ d & 0 & 0 \\ 0 & 0 & 0 \end{pmatrix}$ $\begin{pmatrix} d & 0 & 0 \\ 0 & d & 0 \\ 0 & 0 & 0 \end{pmatrix}$	—	$\begin{pmatrix} 0 & 0 & -c \\ 0 & 0 & 0 \\ -c & 0 & 0 \end{pmatrix}$ $\begin{pmatrix} 0 & 0 & 0 \\ 0 & 0 & c \\ 0 & c & 0 \end{pmatrix}$	$\begin{pmatrix} a & 0 & 0 \\ 0 & a & 0 \\ 0 & 0 & b \end{pmatrix}$	$\begin{pmatrix} 0 & d & 0 \\ d & 0 & 0 \\ 0 & 0 & 0 \end{pmatrix}$ $\begin{pmatrix} d & 0 & 0 \\ 0 & -d & 0 \\ 0 & 0 & 0 \end{pmatrix}$	$\begin{pmatrix} a & 0 & 0 \\ 0 & a & 0 \\ 0 & 0 & b \end{pmatrix}$
CEME, normalized parallel orientation $\lvert\epsilon(\omega_L)\rvert \sim \lvert\epsilon(\omega_S)\rvert \sim \lvert\epsilon\rvert$	—	d^2	—	$c^2\lvert\epsilon\rvert^2$	$a^2 + b^2\lvert\epsilon\rvert^4$	d^2	$a^2 + b^2\lvert\epsilon\rvert^4$
Int. (SERS)/Int. (liquid) normalized, stochastic post structure	(0.2 ± 0.15)	(0.35 ± 0.2)	(0.15 ± 0.6)	(4.6 ± 0.4)	1.0	(0.2 ± 0.05)	(0.25 ± 0.1)

that the intensity ratio SERS:liquid should scale roughly as $10^{-4} : 10^{-2} : 1 : 10^{-4} : 1$.

Since isolated silver islands on posts are good electromagnetic enhancers (see figure 10) they are well suited to test the 'classical selection rules'. The experimental ratios are given in the last line of table 1. They cannot be considered as a confirmation of the CEME selection rules. We come to the same conclusion for CO on copper—see section 5.3. The symmetry reductions or electric field gradient effects which might activate the modes that are non-Raman-active in free benzene but observed in SERS

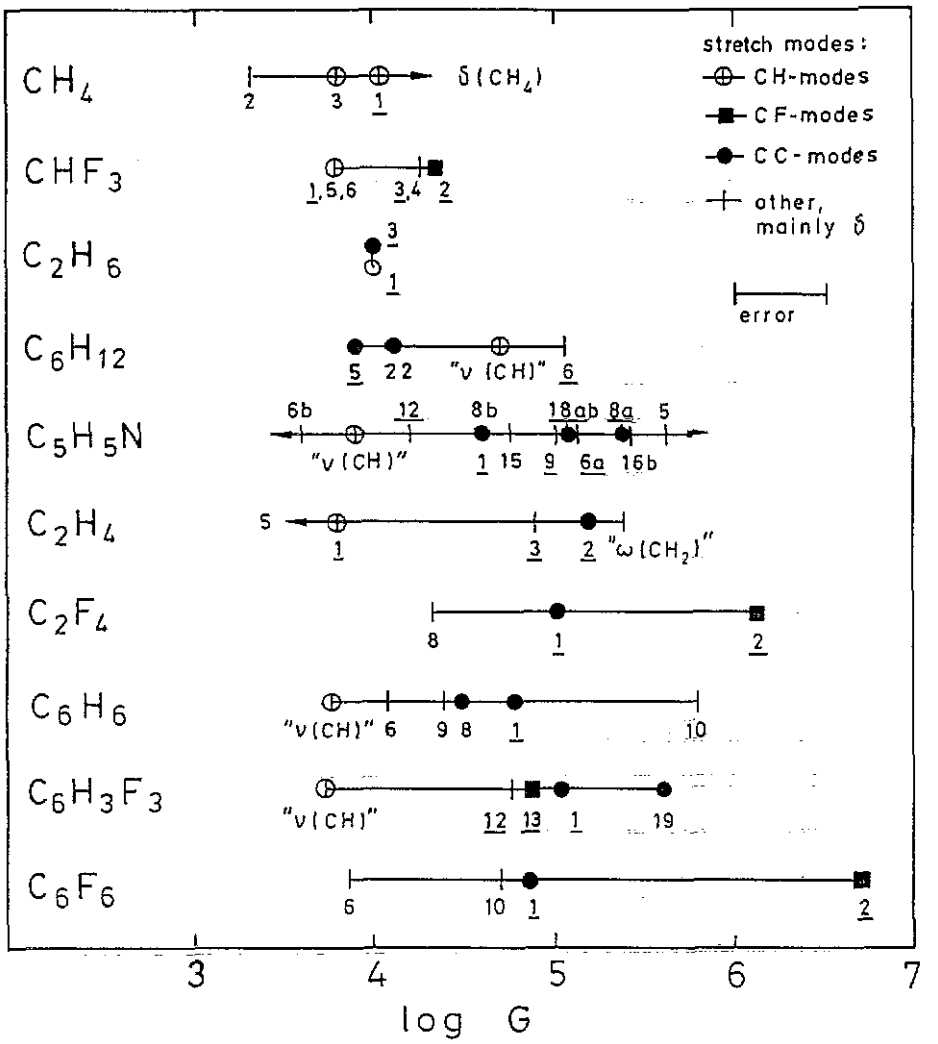

Figure 14. Absolute enhancement G of the integrated SERS bands of various adsorbate vibrations at submonolayer coverage of silver films, cold-deposited and exposed at 40 K. Reference samples are condensed films on sapphire. Notation of the vibration of the aromatic molecules are according to Wilson, and of the other molecules according to Herzberg. Arrows to the left or right denote vibrations with non-detectable SERS, respectively normal Raman bands. 'ν(C–H)' denotes the integration over all unassigned C–H stretch SERS bands normalized by the integral over all C–H stretch bands of the reference sample. '$\omega(CH_2)$' has the analogous meaning. Numbers of the totally symmetric modes are underlined. After [38].

(see table 1) have been discussed in reference [66]. Electron energy loss spectroscopy (EELS) in specular scattering configuration of benzene adsorbed on cold-deposited (60 K) silver [150] shows all vibrational modes in contrast to the infrared dipole selection rule operative, for instance, for benzene on Ag(111) [148]. According to reference [150] it is not known a priori whether EELS and SERS probe the same surface species. Ion resonances and impact scattering contributions should be considered [150]. These results demonstrate again the breakdown of selection rules, based on the model of classical macroscopic fields at a step-shaped metal surface in the case of highly disordered surfaces.

Figure 14 gives the relative and absolute submonolayer enhancements of the Raman intensities of the various vibrational modes of molecules adsorbed on cold-deposited silver films. We have only choosen modes whose assignment both in the SERS and the free molecule Raman spectra seems reliable to us. Like in the case of island films (see figure 11) the G values of the C–H stretch modes and of the C–C stretch modes of the saturated hydrocarbons are relatively low (except for C_6H_{12}, see below), but still at least one order of magnitude above G for the ν_1 mode of benzene after oxygen quenching (see figure 10). The SERS intensity of the C–C stretch modes of the hydrogen-unsaturated molecules is more prominent. If hydrogen is replaced by fluorine, SERS of the C–F stretch modes exceeds SERS of the analogous C–H stretch modes. This is most obvious for the ν_2 modes of the couple benzene–hexafluorobenzene (see also figure 16(a) and 16(e)).

We rationalize these trends with the help of the SERS model of Persson [151] (see figure 15(a)). It is based on the Newns–Anderson model (described for instance in [152]), featuring a free-electron metal, an affinity level E_a of an adsorbate, and a transfer amplitude V_{ak} of electrons between metal and E_a. A very simple *ansatz* of electron–photon interaction is given by $-eE_n l$, where E_n is the electric vector component of the laser field normal to the surface, and l is the distance between the metal surface (characterized by the image plane) and the 'centre of gravity' of the 'affinity orbital' (see figure 23(b)). (We will come back to this point in sections 6.1 and 6.3.) The electron–vibration coupling parameter is given by the gradient $\partial E_a(Q)/\partial Q$ (see figure 15(a)). This corresponds to the Jahn–Teller selection rules, discussed by Creighton [141]. The Raman cross-section is maximal when the charge transfer energy $E_{CT} = E_a(0) - E_F$ is equal to the photon energy of the incident or emitted light. Persson assumed that the optical transitions take place between filled and unfilled adsorbate-induced states. This emphasizes transitions starting immediately below E_F (see figure 15(a)).

This model can explain the resonance Raman effect in silver complexes (see section 2) when the electrons at E_F are replaced by an electron in the 5sp orbital of an isolated silver atom. (Obviously, this resonance Raman effect is absent at smooth surfaces; we will discuss this problem in the next two sections.)

We envision the lowest π^* affinity levels near resonance, with an appreciable coupling parameter $\partial E_a/\partial Q$ only for C–C stretch vibrations, the C–H stretch vibrations being excited via off-resonance charge transfer to the higher-lying C–H and C–C antibonding σ^*(C–H) states (see figure 15(b)). Only these σ^* affinity levels are present for the saturated hydrocarbons. (In reference [153] some arguments about the ratio of on- and off-resonance scattering have been presented, based on the analogy of the charge-transfer Raman mechanism and inelastic electron scattering in the gas phase. An estimate based on the yields of the surface photo-effect on the light emission yield by hot electrons and on the inelastic cross-sections in so-called shape resonances [154–

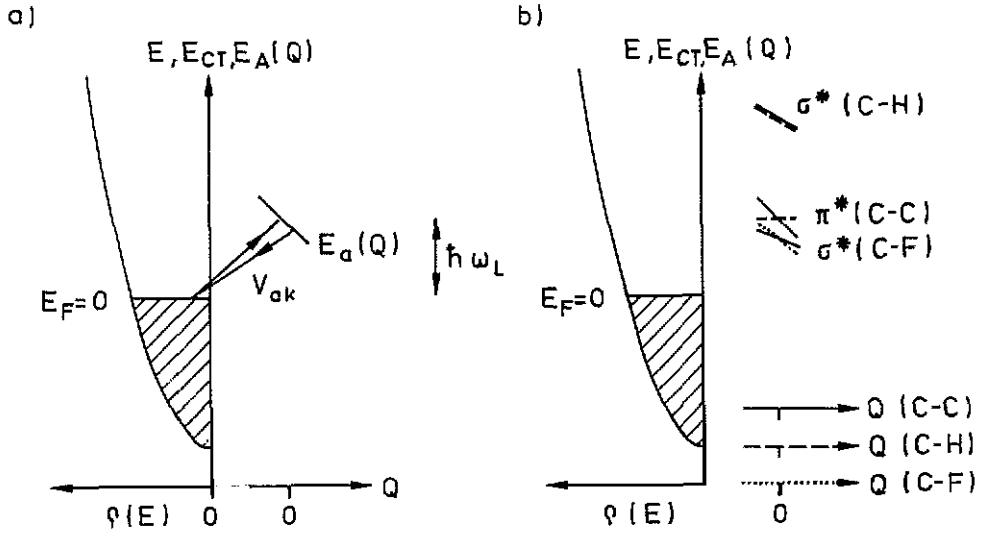

Figure 15. (*a*) Schematic diagram for Persson's model [151] of SERS. E: single electron energy, $\rho(E)$: density of states in the metal, E_F: Fermi energy. $E_A(Q) \sim E_a(Q = 0) - \partial E_a/\partial Q \cdot Q$: energy of the affinity level above E_F, for small normal coordinates Q of an adsorbate vibration, charge transfer energy $E_{CT} = E_A(Q)$, V_{ak}: electron transfer amplitude between metal and affinity level, $\hbar\omega_L$: Laser photon energy. (*b*) Qualitative scheme of positions of lowest π^* and σ^* affinity levels centred at C–C, C–H and C–F bonds, and of the electron–vibration coupling constants $\partial E_a/\partial Q_i$ for C–C, C–H and C–F stretch vibrations.

157] shows that the hypothetical Raman scattering process of figure 15 (at unordered surfaces, see section 5 and 6) may be the origin of 'first-layer' SERS [153]. From the relatively low intensity of overtones in SERS (the most noteworthy ones have been reported by Creighton [158]) residence times of the electron in the adsorbate of 10^{-15} s have been estimated [153].

We explain the dominance of the C–F stretch SERS signals by the strong electronegativity of fluorine, which leads to a lowering of the C–F antibonding σ^*(C–F) levels. For C_6F_6, the adiabatic electron affinity is even positive (see references in [53])—the lowest vertical σ^* affinity level of C_6F_6 adsorbed on Cu(111) derived by inverse photoemission [122] is below the lowest π^* affinity level—see figure 12.

In contrast, Moskovits and co-workers [159] explain the conspicuous increase of the Raman intensity of the totally symmetric ν_2–a_{1g} C–F breathing mode of C_6F_6 by the classical electromagnetic 'propensity rule'.

Moskovits *et al* assume that C_6H_6 and C_6F_6 are adsorbed flat. In this case, the Raman tensors of the a_{1g} modes are given in table 1, and $\alpha_{zz} = b$. The experimental facts are explained by Moskovits *et al* by arguing that the tensor component b of the C–C modes of C_6H_6 and C_6F_6 and the C–F mode of C_6F_6 is comparatively big, while that of the C–H mode of C_6H_6 is small. This assumption cannot be proven from the depolarization of Raman scattering of the free molecules, and contradicts experiment: the Raman intensity increases linearly with exposure of the silver grating for all the a_{1g} modes (see figure 5). This cannot be understood when the relative difference between a and b is large: since benzene adsorbs flat, but condenses to an amorphous or microcrystalline state, its orientation will nearly randomize with

increasing distance from the silver surface. (For a detailed investigation in the case of a Ru(001) substrate, see [160].) In the case of long-range CEME by the surface plasmon polariton resonances on the grating the electromagnetic propensity rule will also hold for condensed molecules even beyond the range of exposures given in figure 5. Thus, with increasing exposure, a and b will both contribute to α_{zz} and the intensity of the a_{1g}–C–H mode of C_6H_6 should increase superlinearly if $b \ll a$. This is not observed (see figure 5).

As discussed in section 3.5, the best substrate to demonstrate the electromag-

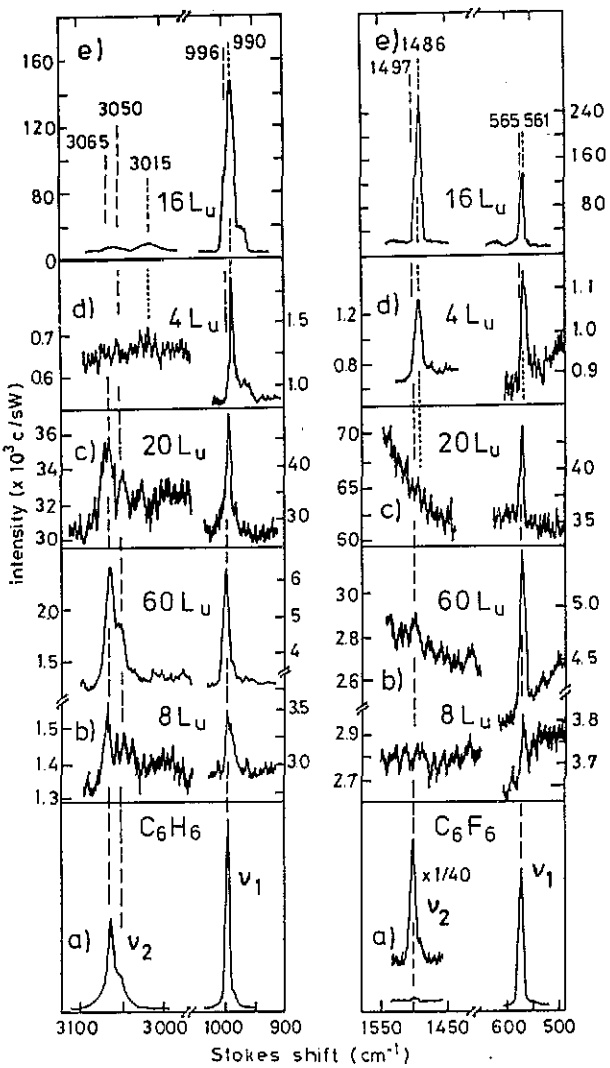

Figure 16. Raman spectra of C_6H_6 (left) and C_6F_6 (right) in the a_{1g} C–C, C–H, and the C–F mode range, respectively, (*a*) in liquid form, (*b*) adsorbed on the grating depicted in the inset of figure 5, (*c*) adsorbed on silver islands on the stochastic post structure passivated by oxygen exposure, (*d*) adsorbed on the grating in the inset of figure 5, precovered by 14 Å of silver at 40 K, (*e*) adsorbed on a thick cold-deposited silver film. Exposure is given in Langmuirs, uncorrected for the ion gauge sensitivity. After [53].

netic selection rule should be the silver islands on the stochastic post structure whose 'first-layer effect' is passivated by oxygen exposure. Nevertheless, the SERS spectra in this case show no conspicuous difference to the Raman spectra of the liquids (compare figures 16(*a*) and 16(*c*)). The conspicuous SERS of the C–F breathing mode is only observed when a small quantity of silver is cold-deposited on the grating (see figure 16(*d*), right half). We will come back to this point in the next section.

We have no explanation for the very broad and down-shifted SERS band of the C–H stretch modes of cyclohexane C_6H_{12} [38] and the relatively large value of the enhancement G—see figure 14. This might correspond to the broad and strong 'C–H' stretch band observed by electron energy loss spectroscopy of C_6H_{12} adsorbed on Ni(111) and Pt(111) by Demuth *et al* [161]. This latter phenomenon was attributed to a kind of hydrogen bonding of C_6H_{12} to the surface and related to dehydrogenation at higher temperatures.

Surprising is the clear presence of the ν_4 band of CH_4 (an asymmetric CH_4 angle-bending mode) which is neither observed in the Raman spectra of a condensed film of CH_4 [38] nor in the gas phase [162].

The selection rules by charge transfer excitation discussed above, based on the Jahn–Teller resonance Raman effect in complexes [141] or shape resonances [163], cannot explain the appearance of nearly all vibrational modes of adsorbates on thick cold-deposited films [24]. So far, the CT model assumes the residence of electrons in one orbital which is a good concept for relatively long residence times. For the short residence times envisioned in reference [153] the electron propagator might reach only a part of the adsorbate. This must be described by a coherent superposition of molecular anionic eigenstates which brings more vibrations into play, albeit with low intensity.

5. The search for 'SERS-active sites'

The by now undoubtable fact that there exists a chemically specific and vibrationally selective 'first-layer SERS' effect, but only at 'non-smooth' surfaces as indicated early in the work of Pettinger and Wenning [47], leads to the assumption that 'SERS-active sites' [164] are not present at smooth surfaces. Billmann *et al* [165] and one of the authors [7] introduced the 'adatom hypothesis': 'strong electron–photon coupling caused by atomic scale roughness' and 'tunnelling of the electron or hole from the metal via the adatom into electronic states of the adsorbate' [7], proposed among other mechanisms by Burstein *et al* [166] and by Gersten *et al* [167] albeit without atomic-scale roughness. In the following, several approaches to the problem are described.

5.1. Silver complexes at disordered surfaces

The proposals that the SERS-active sites at rough silver surfaces are presented by silver adatoms [165,168], Ag^+ sites [169–172], or Ag^{4+} clusters [173] lead to the search for resonant Raman scattering in isolated silver complexes with the adsorbates as ligands of the complex. The detection of charge transfer bands and of resonant Raman scattering in neutral $Ag–C_2H_4$ complexes has already been described in section 2.

The absence of resonant Raman scattering in Ag^+ pyridine complexes in acetronitrile was demonstrated in reference [62], corresponding to missing optical absorption in the visible spectral range [174]. The oxidation of Ag to Ag^+ in silver–CO complexes makes charge-transfer bands in the visible disappear [175], analogous to the silver–ethylene complexes described in section 2. (The correspondence to SERS is given by

the oxygen quenching of SERS of CO [176].) Apparently, the removal of the outer 5sp electron in Ag^+ quenches the resonant Raman scattering (see also section 6.6). Therefore, regardless of whether 'Ag^+-sites' in the sense of a single, fully charged silver cation exist at all at clean unordered silver surfaces, we do not include these sites into our list of possible candidates for 'SERS-active sites'.

However, in section 6 we propose to replace the concept of 'SERS active sites' by the concepts of 'adsorption sites of lowered affinity level' (so-called E-sites—see next section) and sites of 'increased surface-electron–photon coupling'. In this sense, we do not exclude the possibility that the E-sites might be sites of deficient electron density at disordered surfaces as assumed in Smoluchowski's model [177] (see figure 23(g)). This is further discussed in section 6.5. The relatively small difference of 0.2 eV in the work functions of 'SERS-active' and 'SERS-inactive' clean silver surfaces [39] does not indicate a relevant surface concentration of 'Ag^+ sites'.

5.2. 'Normal' and 'extra' Raman bands

The frequencies of the skeleton vibrational modes of molecules adsorbed in UHV by Ag(111) or by silver films deposited at room temperature or at low temperatures and then properly annealed at room temperature are nearly unshifted (within ± 3 cm^{-1}) from the free molecular case. This adsorption state has therefore been called 'physisorbed' [178, 179, 51]. On unordered, 'rough' silver surfaces one observes shifted bands attributed to 'chemisorbed' species at sites of atomic scale roughness [178, 179]. On cold-deposited Ag films, partly 'smoothened' by annealing at 250 K, one may observe both bands [116, 117]. (This will be further discussed in section 6.5.) We prefer to call the nearly unshifted bands the N-lines (N $\equiv$ normal), assigned to molecules adsorbed at 'N-sites' provided by atomically smooth parts of the surface and the shifted bands the E-lines (E $\equiv$ extra) of molecules at 'E-sites', i.e. at sites not available on atomically smooth, low-index surfaces. We prefer this nomenclature, because often a 'physisorbed' molecule A desorbs at higher temperature than a 'chemisorbed' molecule B (see table 2), and in order to avoid the impression that 'the chemical effect is caused by chemisorption'. (Note that the notion 'chemical effect' is often a euphemism for all the unravelled 'non-classical' aspects of SERS.)

The relative differences between N- and E-frequencies, measured within the course of many individual experiments in the Düsseldorf laboratory is given in table 2. In principle, we expect a small difference of N- and E-frequencies for any adsorbate. For weak intensity spectra of C_6H_6 the assignment of the ν_1 signal to either N- or E-bands is sometimes difficult. When Raman signals were obtainable from an adsorbed monolayer on 'smooth' silver films, only the N-bands were apparent—for pyridine see [62], for C_2H_4 see [61]. The E-bands are prominent in the SERS spectra of silver island films and cold-deposited silver films. In the latter case, only the species with the highest desorption temperature contribute to SERS. This is demonstrated by the comparison of the development of the SERS intensity and the downward shift of the desorption temperature of CO during submonolayer coverage of porous, cold-deposited silver films [183] (see figure 17). Desorption of bilayer and multilayer (condensed) CO below 35 K is only observed at CO exposures above 30 L. Experiments with mixtures of CO isotopes prove that the adsorption in the 'pores' is not geometrically ordered [180]. N-lines of CO have been detected only in SERS spectra of CO on silver island films [114], as further discussed in section 6.5. One should notice the correspondence of the results in figure 17 with the changes of the DC resistivity shown in figure 9, which demonstrates that the 'E-species' interact more strongly with electrons at E_F.

Table 2. Frequency differences (in cm^{-1} of the N- and E-bands of some totally symmetric vibrations, thermodesorption temperature T_D of N-type adsorbates on smooth silver samples and maximum desorption temperature T_{Dmax} after adsorption on thick cold-deposited Ag and Cu films. For pyridine, $T_D(N)$ and T_{Dmax} were derived from SERS experiments.

	C_6H_6/Ag	C_5H_5N/Ag	C_2H_4/Ag		CO/Ag	C_5H_5N/Cu	
vibration	ν_1, ν_{CC}	ν_1, ν_{CC}	ν_2, ν_{CC}	ν_3, σ_{CH_2}	ν_{CO}	ν_1	ν_{12}
$\nu_N - \nu_E$ (cm^{-1})	6 ± 2[a]	shifting from (-15) to (-10)[b]	33 ± 3[c]	15 ± 2[c]	shifting from 0 to 25[d]	-17[h]	-7[h]
$T_D(N)$		(220–240 K)[e]	90 K[f]		41 K[g]	~ 240 K[h]	
T_{Dmax}		(> 270 K)[e]	180 K[f]		100 K[g]	> 290 K[h]	

[a] [38].
[b] [24].
[c] [116].
[d] [180].
[e] [181] (evaluated by SERS).
[f] [182].
[g] [183].
[h] [184].

This is also supported by further resistivity experiments described in section 5.4 and by consideration of the shift and linewidths of the E-bands, see section 6.2.1. Our heuristic introduction of 'E-sites' implies that there may exist several distinct ones—see section 6.2.4.

5.3. CO on copper films

SERS of the stretch vibration of CO on cold-deposited copper films is only observed from E-species. The SERS spectrum (see figure 18) displays the CO stretch vibration at about 2102 cm^{-1}, the CO–Cu vibration at 352 cm^{-1} and a CO frustrated rotation at 279 cm^{-1}—these assignments are supported by SERS and IR data of different CO isotopes [190]. The feature at 24 cm^{-1} is assigned to a frustrated CO translation based on the scattering data of other systems. According to the representations of the vibrations of CO at high-symmetry adsorption sites (top and bridge) [191,192] and the corresponding finite Raman tensor components [193], the classical electromagnetic selection rules discussed in section 4.3 predict strong Raman signals from the C–O and CO–Ag stretch vibrations but only weak intensities from the frustrated rotation and translation, in contrast with the experimental result.

Included in figure 18 are the vibrational frequencies for CO on low-index faces of copper, obtained by infrared reflection absorption spectroscopy [194,187,185,195,196,188] and by inelastic He scattering [192]. The SERS band at 2102 cm^{-1} cannot be assigned to CO adsorbed on the top sites of Cu(111), Cu(100) and Cu(110). CO bands above 2100 cm^{-1} have been observed by infrared spectroscopy in the presence of steps [197] or defects at the Cu surface [186] or at polycrystalline Cu surfaces [194].

One cannot explain the dominance of a band at 2102 cm^{-1} over a band at about 2080 cm^{-1} by 'intensity borrowing'. This is a valid concept only in infrared spectroscopy [187,194] but not in Raman scattering, as demonstrated experimentally in references [180] and [114]. Hence, at least the C–O stretch SERS band is assigned to

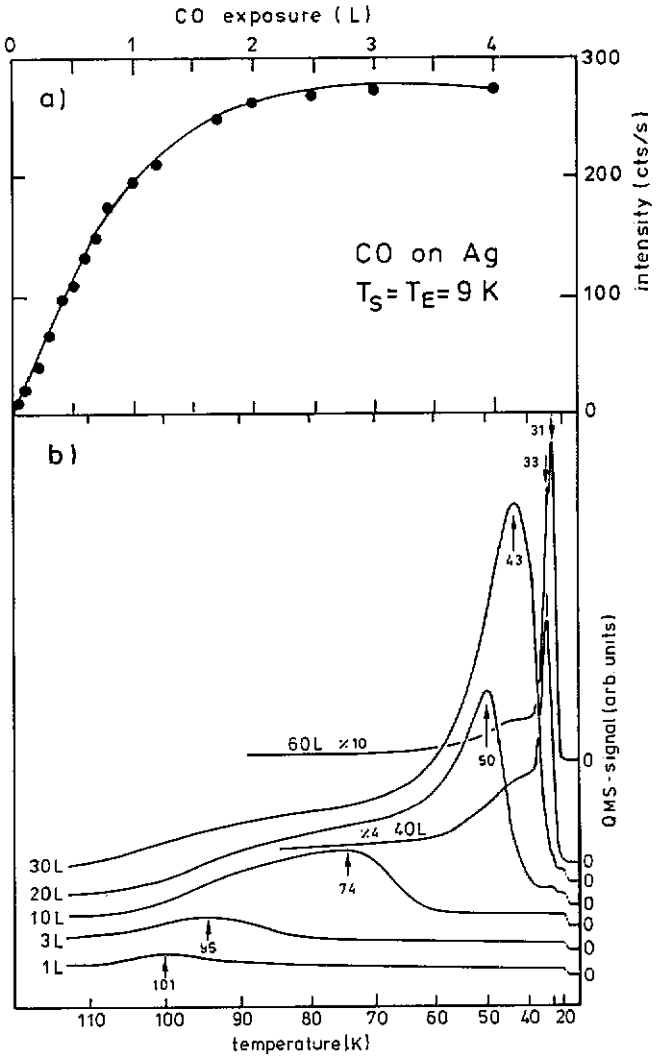

Figure 17. (*a*) Peak intensity of the CO stretch band in SERS from a cold-deposited silver film (at 9 K) versus exposure to CO (at 9 K). (*b*) CO thermodesorption (TDS) spectra. The silver film was deposited at 30 K and preannealed at 110 K in order to avoid film reconstruction during TDS . Parameter is the exposure to CO at 20 K, heating rate about 4 K s^{-1}. Bilayer and multilayer desorption below 35 K is only observed at exposures above 30 L. For 'smooth' silver films, bilayer desorption starts already at exposures of about 1.75 L. After [183].

CO at E-sites—whereas CO at sites of high local symmetry on microcrystalline terraces ('N-type CO') does not contribute. The increased C–O stretch frequency might indicate adsorption at a site of electron depletion as predicted by the Smoluchowski effect at disordered surfaces (see figure 23(*g*)). The increase of the C–O stretch frequency and a simultaneous increase in the desorption temperature of CO on Cu(100) have been observed in the presence of electron-withdrawing co-adsorbates [198] and have been explained by increased 5σ donation and decreased 2π backdonation [198]. An analogous increase was observed for CO on cold-deposited silver by oxygen coad-

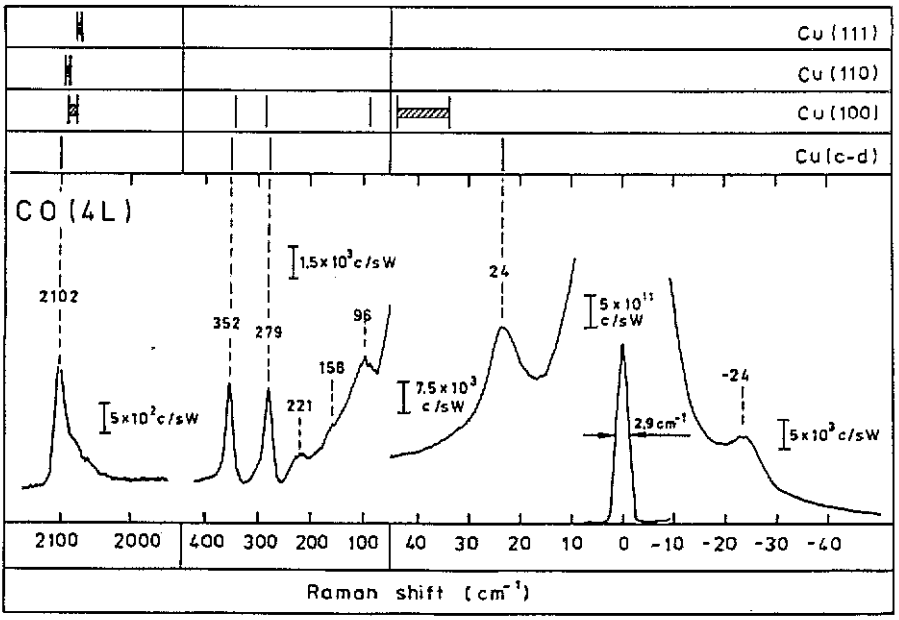

Figure 18. Raman spectrum of CO on copper. The thick copper film was cold-deposited at 40 K and exposed to 4 L of CO, subsequently warmed to 150 K and recooled to 40 K. The light scattering spectrum next to the laser frequency (wavelength 647.1 nm) was attenuated by a filter of transmission $T = 10^{-6}$. Above the SERS spectrum are indicated the ranges of the coverage dependent CO stretch frequencies of CO on low index single crystalline faces of Cu, from infrared reflection-absorption spectroscopy (IRAS) with Cu(111) [185], Cu(100) [186], and Cu(110) [187]. Also indicated are the positions of the CO–Cu stretch frequency (345 cm^{-1}) and a frustrated rotation of Cu(100) c(2 x 2) CO (at 285 cm^{-1}) obtained by IRRAS [188], of a non-dispersing mode at about 85 cm^{-1}, and the dispersing band of the frustrated translations from inelastic He scattering of CO on Cu(100) [189]. After [102b].

sorption before the quenching of SERS was complete [176]. One must expect that the double degeneracy of frustated rotational and translational modes of CO adsorbed at top sites is removed by adsorption at E-sites. However, we have so far only identified one frustrated rotation (shifting between 280 and 290 cm^{-1} [102b] and one frustrated translation ($\sim$ 24 cm^{-1})). The situation is complicated because of the Cu phonon structure below 240 cm^{-1}. IR data taken between 70 cm^{-1} and 300 cm^{-1} have produced no evidence of any vibrational mode other than the mode at 285 cm^{-1} (noise level is $\Delta R/R \sim 5 \times 10^{-5}$)—Y Chabal, private communication.

5.4. Small quantities of cold-deposited silver

The controlled preparation of sites of atomic scale roughness has not yet revealed the nature of the 'SERS-active sites'. Explicit experiments with pyridine adsorbed on stepped and kinked surfaces of silver single crystals were reported in references [199, 49, 200, 178]. According to Rowe *et al* [199], the first-layer enhancement produced by a 5° vicinal face of Ag(100) is less than 100, and according to Pettenkofer and Otto [49] the 'first-layer' extra enhancement produced by a 6° vicinal face of (110) (approximately (540)) is about 10. This result was not corroborated by Campion and Mullins [200, 178] at Ag(521), Ag(987) and Ag(540) surfaces, well characterized by LEED [178]. We will come back to this point in section 6.5.

Ar^+ bombardment of the Ag(521) surface kept at 100 K did not induce a 'first-layer effect' [178], in contrast to older positive reports by Smardzewski *et al* who sputtered polycrystalline silver [201] and Ag(521) [202] and observed a 'first-layer effect'. All the work described above was performed before it became known that oxygen quenches the 'first-layer effect'.

In order to test the hypothesis of SERS-active sites by atomic-scale roughness, silver was deposited at about 40 K with an average thickness d_{cold} on the grating shown in figure 5, following reference [203]. (The optical reflectivity changes of smooth silver films by cold-deposited silver (at 12 and 50 K) with $d_{\text{m}} < 60$ Å is smaller than 3% in the spectral range of 1.8–5.0 eV [204] (see also [205]), and thus there are no indications of short-range electromagnetic resonances within the thin cold-deposited silver film on top of 'smooth' silver films.) Subsequently, the samples were exposed to benzene. Besides weakening the long-range classical electromagnetic enhancement discussed in section 2.1, a 'first-layer' non-classical effect is induced by the cold-deposited silver. This effect 'boosts' the C–F stretch mode of C_6F_6 (compare figures 16(*b*) and 16(*d*)) as discussed in section 4.3. It saturates at a benzene exposure of about 2–5 L, independently of d_{cold}. When pyridine was used in these experiments allowing for an easier differentiation of E- and N-bands (see table 2), only E-bands were observed at $d_{\text{cold}} = 9$ Å. The 'first-layer effect' induced by $d_{\text{cold}} < 20$ Å (see figure 19) is chemically specific; for instance there is no apparent short-range enhancement for C_2H_6 [38]. The long-range enhancement G_{lr} is evaluated by comparing the gradients of Raman intensity versus benzene exposure, $\mathrm{d}J/\mathrm{d}\theta$, at 10–20 L exposure for the grating and the clean sapphire reference substrate.

The surface plasmon polariton resonance deteriorates with increasing d_{cold} as was reported earlier by Reed *et al* [206], and hence G_{lr} decreases with d_{cold} (see the lower frame of figure 19). (The initial increase at $d_{\text{cold}} \sim 4$ Å is caused by the increase of the angular halfwidth of the SPP resonance, allowing full tuning of the focused laser beam into the resonance.) The short-range enhancement G_{sr} is evaluated from the ratio of $\mathrm{d}J/\mathrm{d}\theta$ at 0–1 L and 10–20 L under the reasonable assumption that the 'first layer' enhancement is given by

$$G(\theta \to 0) = G_{\text{lr}}(\theta \to 0)G_{\text{sr}}\,. \tag{8}$$

G_{sr} grows nearly exponentially with d_{cold} for $d_{\text{cold}} < 20$ Å. This is analogous to [47]. As in the case of the silver island films and thick cold-deposited Ag films G_{sr} is quenched by oxygen without an observable change of G_{lr}.

A related experiment, using the method of attenuated total reflection to excite SPPs and electrochemical oxidation–reduction cycles to roughen the silver electrolyte interface has been described by Notholt and Ludwig [112] with a similar separation of electromagnetic and chemical enhancements.

Figure 19 also contains the short-range Raman enhancement reported by Ertürk and Otto [62] after first covering a smooth silver film with pyridine and then depositing extra silver at low temperatures. Though the possibility was not excluded that the silver, postdeposited at 40 K, makes contact only with the silver substrate at higher temperatures during a TDS scan [61], one of the authors (AO) thought this to be very unlikely. This belief was proven wrong by simultaneous Raman spectroscopy and DC resistance (R) measurements [207, 208]. When silver is postdeposited on a smooth silver film, covered by a few monolayers of benzene, there is an increase of about 2 orders in the ν_1–C–C Raman signal but no change of R. Warming up induces a big

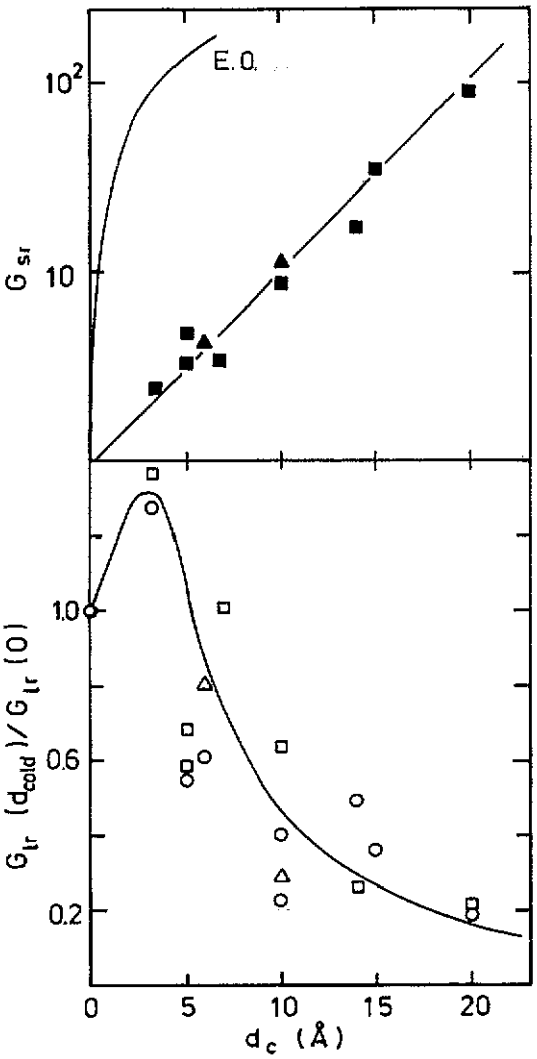

Figure 19. Separation (see text) of short-range G_{sr} and long-range G_{lr} enhancement of the Raman intensity of the C–C ring breathing mode ν_1 (squares, triangles) and the C–H-ring breathing mode ν_2 (circles) of benzene as a function of precovering the grating in figure 5 with the average thickness d_c of silver at 40 K (squares) or 10 K (triangles). Lines are guides to the eye. (Note that there is no short-range enhancement in the case of ν_2.) The curve E.O. reproduces the results of reference [62]—see text. After [38].

increase in R above 120 K and a strong decrease of the Raman signal of the order of the difference between the two curves in the G_{sr} frame of figure 19. Obviously, silver migrates above 120 K from a position on top of the benzene layer to the silver surface, inducing atomic-scale surface roughness. Simultaneously, the resonance Raman effect in the isolated silver–benzene complexes is replaced by the apparently weaker SERS. With the new interpretation the silver postdeposition experiments by Ertürk [62, 50, 61]—resulting in a negligible Raman enhancement for C_2H_6 [50] but a strong one for C_2H_4—are now in good agreement with the results of Raman spectroscopy of

isolated silver complexes [41]—see section 2.

If we exclude strong clustering of very small quantities of silver deposited at 40 K onto the silver grating, then the quasi-exponential increase of G_{sr} at $d < 20$ Å demonstrates that isolated silver adatoms on smooth silver are no potent 'SERS-active sites'. However, a submonolayer ($d_c = 0.8$ Å) of cold-deposited silver on a smooth film is sufficient to induce strong resisitivity changes $\Delta R/R$ [209], and it is easy to differentiate between E- and N-type adsorbates [209]. Apparently the adsorbates that induce strong ΔR yield strong SERS only in the case of cold-deposited Ag films of average thickness exceeding a monolayer. The exponential increase of the 'first-layer effect' in the range of $0 < d_{cold} < 20$ Å (see figure 19) cannot be explained by an exponential increase of the E-site density, since the 'first-layer' signal always saturates at the same exposure! We rationalize this with the assumption that the existence of E-sites is a necessary, but not a sufficient condition for SERS—see section 6.5.

6. Mechanistic considerations

In the following, we will replace the concept of 'SERS-active sites' by two necessary conditions: the availability of 'E-sites', and increased surface–electron coupling, in order to account for three independent classes of observations which will be discussed in the following sections.

(i) Adsorbates at 'E-sites' are present as demonstrated by DC resistivity measurements [209] (see section 5.4) or by electron energy loss spectroscopy (see section 6.3) without an appreciable 'first-layer enhancement' above one order of magnitude.

(ii) The so-called inelastic background (see section 6.4) is related to the SERS intensity (see section 6.5).

(iii) In special cases we observed besides the 'first-layer effect' by the E-band, also a 'first-layer effect' by the N-band, in contrast to the case of smooth surfaces (see section 6.5).

6.1. Smooth surfaces

The important experimental result of missing 'physical' or 'chemical' first-layer Raman enhancement at smooth surfaces is only trivial within the CEME model.

Shortly after the discovery of SERS, the so-called 'image dipole model' by Van Duyne and co-workers [210] was discussed frequently. Though it is understood that the very high enhancements calculated at those times [211] were caused by extrapolations of the classical model of screening which do not hold [212], a corresponding 'physical enhancement' still appears when screening is treated within the self-consistent jellium model using the dynamical density-functional approach [213]. Gies and Gerhardts modelled silver by a jellium with $r_S = (4\pi n/3)^{-1} = 3$, ($n$ is the electron density) and assumed pyridine to sit as a classical dipole with a polarizability of 12 Å^3, 2 Å in front of the jellium and to vibrate at the laser frequency (6×10^{14} s^{-1}). The electromagnetic enhancement was calculated to be about 700 [213]. In order to introduce the possibility of Raman scattering, in spite of the assumption of a point dipole, it was implicitly assumed that the polarizability of this localized classical dipole is modulated by an internal vibration. Obviously, this calculation does not reproduce the experimental result. The assumed distance of 2 Å is comparable to the small number of data available on species adsorbed at Ag(111) (illustrated in the lower part of figure 23(*c*)). Thus

the adsorbates are probably embedded in the tail of the electron density distribution (as indicated in figure 23(*c*)). According to TDS, CO, Xe and hydrocarbons are all weakly bonded to smooth silver surfaces—see table 2. For a jellium surface with a density appropriate for Al, Lang and Williams [214] determined that Xe lies almost completely outside the electrostatic dipole layer potential of the substrate while it lies almost entirely within the region where the exchange correlation potential is appreciable. The latter varies as the cube root of the density $n(z)$ and therefore approaches zero more slowly than $n(z)$ itself. The neglect of the internal electronic structure of the adsorbed molecule and of the extension of its orbitals may perhaps explain the failure of the classical point dipole model of Gies and Gerhardts [213]. Furthermore, confirmation that the response of the inhomogeneous electron gas to the coherent superposition of the incident field, the emitted field and the vibrating molecule may be modelled by the response to a classical dipole may be helpful. No self-consistent calculation of static screening at a metal surface with adsorbates is known to us.

The 'chemical' SERS models of 'photon-driven' charge transfer from metal to adsorbate also meet difficulties since they have been derived with a smooth surface in mind. For instance Persson's model, which we have discussed in section 4.3, does qualitatively explain resonant Raman scattering in silver complexes—but why does one not observe the analogue 'first-layer effect' at a smooth silver surface? That may have two reasons:

(i) The positions of the affinity levels of the adsorbates are off-resonance at smooth surfaces but may be lowered at 'E-sites' which brings them closer to resonance. This will be considered in sections 6.2 and 6.3. Nevertheless, according to the results in figure 12, one should be in pre-resonance or even resonance condition for N-type pyridine or pyrazine, respectively. We will offer an explanation for this discrepancy in section 6.4.

(ii) The simple *ansatz* of electron–photon coupling as $-E_n(\omega)l$ ($E_n(\omega)$ is the electric field strength normal to the surface, l the distance from the surface to the centre of gravity of the affinity orbital—see figures 23(*a*), (*b*)) does not consider the screening of the light fields at a metal surface. This will be discussed in sections 6.4 and 6.5.

6.2. Position of affinity levels of adsorbates at 'E-sites'

There are several indications that the affinity levels of the E-type adsorbates are below those of the N-type adsorbates (see figure 20).

6.2.1. Frequencies and line shapes. All E-type adsorbates (adsorbed at sites not available at smooth low-index faces) have a stronger interaction with the metal electrons than the N-types as demonstrated by their increased influence on the DC resistivity (see section 3.4 and [209]) and the shift of the E-bands of the total symmetric stretch modes to lower frequencies (see table 2), with the exception of pyridine (see [220]). The latter is explained by a partial population of the lowest antibonding affinity level (empty in the free molecule) by adsorption [223].

According to the Newns–Anderson model [152] this population is increased by lowering the position E_A of the affinity level and/or increasing the electron transfer amplitude V_{ak}, see figure 15. Within the Newns–Anderson model, the damping of an adsorbate vibration by electron–hole pair excitation increases with the adsorbate induced density of states at the Fermi energy, $\rho_a(E_F)$ [225]. The measured halfwidth of all the E-bands given in table II is bigger than that of the N-bands. Though a

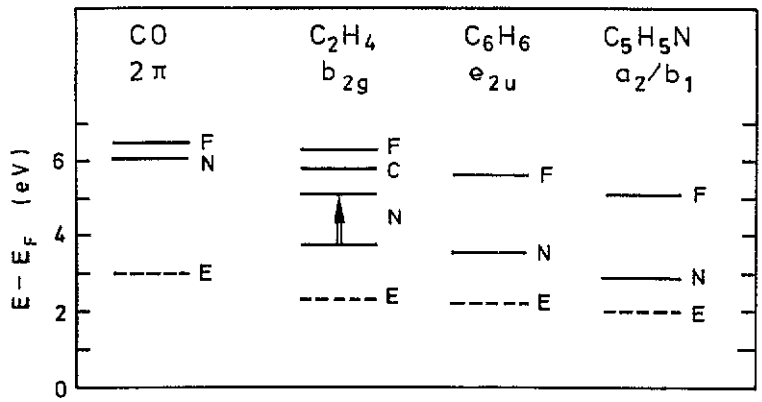

Figure 20. Position above E_F of the lowest affinity levels (with assignment) of free (F) adsorbed (or condensed (C)) molecules, determined by EELS in the case of CO [215,216]—see text. For free C_2H_4, C_6H_6, C_5H_5N the positions were obtained by electron transmission spectroscopy [217,118], the values concerning N-type adsorbates on Ag(111) were determined by inverse photoemission. C_2H_4 (C): reference [218], N shifting upwards with coverage: [219], C_6H_6: [123], C_5H_5N: [124]. Values concerning E-type adsorbates were determinded by SERS—see text. The work function of Ag(111) is 4.5 eV [39].

contribution of inhomogeneous broadening to the halfwidth probably exists, the results may equally well be explained by a stronger e–h damping of the E-type vibrations which would indirectly confirm the lowering of the affinity level.

6.2.2. Electron energy loss spectroscopy (EELS) of CO/Ag. Demuth *et al* observed a 'surface-shape resonance' in the cross-section of the CO stretch vibrational excitation at a kinetic energy of the electrons of 1.55 eV, assigned to the position of the $2\pi^*$ affinity level of CO about 6.05 eV above E_F [215]. This value may be attributed to N-type CO [180]—see figure 20. For CO on cold-deposited silver a strong loss at 3.0 eV was observed and assigned to a charge transfer excitation [216]. We assign this value to E_{CT} for E-type CO—see figure 20.

6.2.3. Excitation profiles of SERS. Inverse photoemission of C_2H_4 at a coverage of about 2 monolayers on Ag(111) by Koch and co-workers [218] yields the π^* b_{1g} level 5.8 eV above E_F. This may be assigned to condensed C_2H_4. On cold-deposited Ag films, this level shifts from 3.8 to 5.1 eV above E_F [219] with increasing exposure.

In this case the signal will be dominated by the majority species namely the N-type adsorbates. Will the affinity level of the most tightly bound E-types be lowered to about 2.3 eV above E_F, corresponding to the charge transfer energy observed in silver-ethylene complexes (see figure 2)?

The charge transfer energy of E-type adsorbate should become apparent by excitation spectroscopy, e.g. the dependence of the Raman intensity of E-type vibrations on laser frequency. Due to the varying contributions of classical electromagnetic enhancement and 'first-layer charge transfer Raman scattering' to SERS, the interpretation of an experimentally determined excitation profile is not trivial.

The SERS excitation profiles of adsorbates on thick cold-deposited silver films, as reported by Pockrand [99,24] and Seki [226] are chemically rather unspecific. This was confirmed by the excitation profile of the C–H stretch mode of C_2H_6 [153]. If the

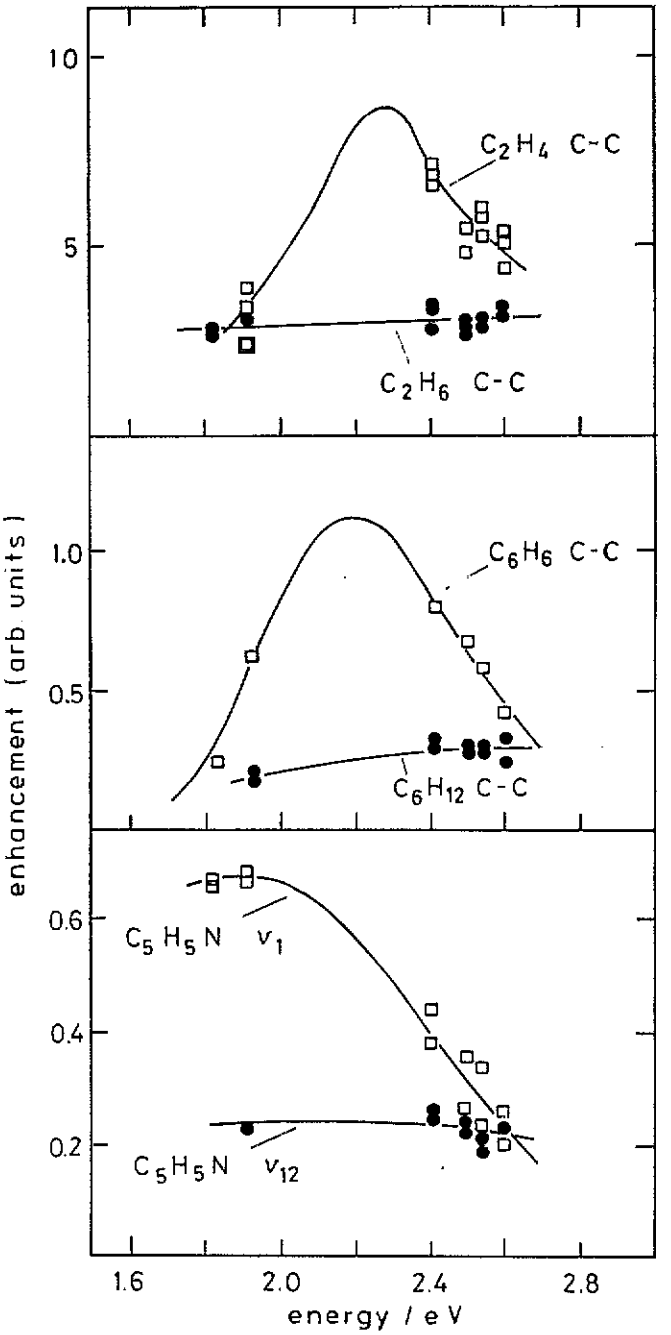

Figure 21. Relative enhancement at 6 different laser photon energies $\hbar\omega_L$ obtained by normalization to the Raman intensity of thick-condensed layers on sapphire. Substrates are silver films of thickness $d_c = 10$ nm, cold-deposited at 40 K on 'smooth' silver. (In the case of C_6H_6 and C_5H_5N the films were annealed at 90 K before exposure, after exposure at 40 K the films were annealed again at 90 K—see the so-called 'low-temperature anneal' in [229, 230, 45].) Exposures are, in all cases, 4 L at 40 K. All Raman spectra were taken at 40 K. For explanation of the curves, see text. After [38].

SERS excitation profiles of different vibrational modes are plotted versus the Stokes frequency, they all have the maximum near a Stokes photon energy of about 2.0 eV [227], irrespective of the chemical nature of the adsorbate. This fact is not properly understood but it favours an explanation of the observed broad resonance of about 1–2 orders of magnitude by electromagnetic resonances [227, 24]. This electromagnetic resonance is observed as so-called 'anomalous optical absorption' by optical reflection spectroscopy ([228] and references therein). It is probably caused by electromagnetic resonances within small internal voids (but still of supra-atomic size) within the porous structure of the thick cold-deposited films ([115] and references therein). The 'anomalous optical absorption' is not observed for relatively thin cold-deposited silver films (thickness $d_c < 20$ nm) on thick smooth silver films [204, 205]. Apparently, the resonating 'cavities' are only formed at larger d_c. On the other hand, the short-range extra contribution to SERS, characterized by the E-bands, is already induced by $d_c \sim 1$–2 nm (see section 5.4).

Therefore, one might hope to observe the excitation profile of the charge transfer processes under the condition $d_c = 10$ nm. This is complicated by the observation that the Raman intensity versus exposure plots depend on the exciting laser frequency [38]. (A tentative explanation will be given in section 8 in connection with the discussion of depolarization effects.) We have arbitrarily chosen the exposure of 4 L (above 8 L, the intensities are saturated) and compare the relative excitations of the C–C stretch modes of C_2H_4 (C_6H_6) and its hydrogen saturated counterpart C_2H_6 (C_6H_{12}) in the upper (middle) frame of figure 21. It is possible to connect the data points by the assumption of a resonance for the unsaturated hydrogens and a missing resonance for the saturated hydrocarbons (see section 4.3). If one tentatively follows this curve fitting one obtains the affinity level of C_2H_4 approximately 2.3 eV above E_F, which agrees with the charge transfer excitation energy in silver–C_2H_4 complexes (see section 2).

In this sense, the lowest charge transfer excitation energy of E-type pyridine—apparent from the fit for the ν_1 mode in the lowest frame of figure 21—is approximately 2.0 eV [231], i.e. about 1 eV less than expected from the results of inverse photoemission measurements (see figure 12).

6.2.4. Different 'E-sites' on cold-deposited copper. Despite a lack of detailed characterization we have identified two different 'E-adsorbate sites' on cold-deposited copper films by comparing the SERS bands of CO_2 and N_2 on cold-deposited silver and potassium films, respectively (see figure 22).

The SERS band of the N_2 stretch vibration of N_2 adsorbed on cold-deposited silver films has a lower frequency than the stretch vibration of N_2 physisorbed on Ag(111)—compare the top three entries in figure 22(*a*). Analogously to all other adsorbates listed in table 2 (with the exception of pyridine) the down-shifted SERS band is assigned to E-type adsorption. The N_2-SERS band of N_2 on cold-deposited potassium is shifted downwards by about 500 cm^{-1}, and in the case of a K colloid in solid N_2 a weaker and less shifted band has also been observed [233]. The different downward shifts are easily explained by various permanent electron transfers into the lowest antibonding π_g affinity level of N_2 [235]—the shift of about 500 cm^{-1} was assigned to the formation of N_2 [233]. For N_2, adsorbed on cold-deposited copper, we observed two SERS bands, reflecting different occupancies of the π_g level—see lowest entry in figure 22(*a*).

For free CO_2 only ν_{sym} is Raman-active and the overtone of δ and the fundamental of ν_{sym} lead to a Fermi resonance, yielding the doublet at 1286 and 1388 cm^{-1} (see

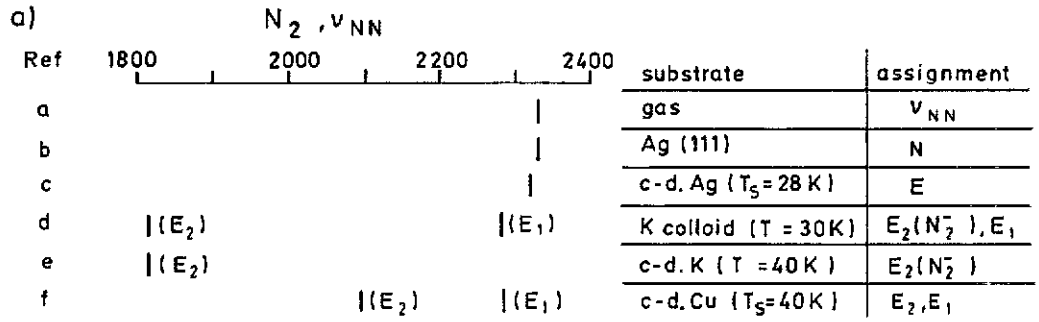

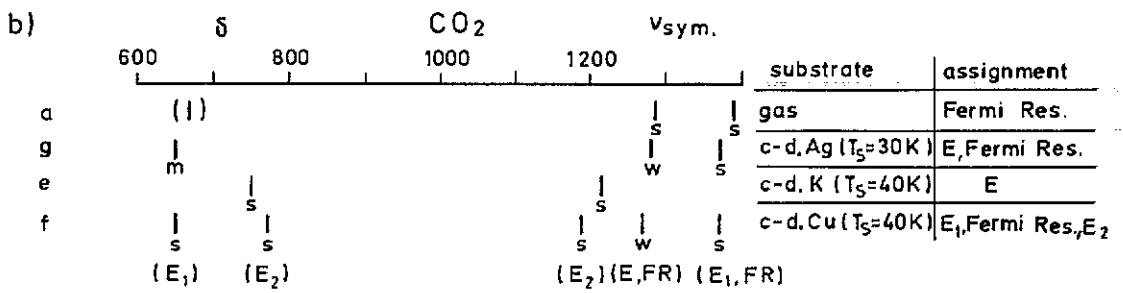

Figure 22. (*a*) Frequencies and assignment of the stretch mode of N_2 adsorbed on various substrates. (*b*) Frequencies and assignment of the bending mode δ (not Raman-active for free CO_2) and the symmetric CO_2 stretch mode ν_{sym} of CO_2 adsorbed on various substrates. c-d.: cold-deposited at substrate temperature T_s. Intensities: w: weak, m: medium, s: strong. References: a = [146], b = [51], c = [45], d = [233], e = [234], f = [102c], g = [116].

figure 22(*b*), first entry).

The lowest affinity level of CO_2 (a linear molecule in the neutral ground state) is a π_u antibonding level [154]. Its occupation leads to lengthening of both C–O bonds and O–C–O angle bending [154]. Therefore, the symmetric CO_2 stretch vibration and the O–C–O bending mode δ are prominent in the SERS spectra [102c] as well as in the shape resonance of inelastic electron scattering at 3.8 eV [154] . The asymmetric stretch mode (at 2349 cm^{-1} for free CO_2) is barely observed in the SERS spectra.

The shift of the δ-band of the E-species on cold-deposited silver is about equal to the shift of the high frequency component of the Fermi doublet. Therefore, the condition $2\omega(\delta) = \omega(\nu_{sym})$ is less well fulfilled, and accordingly the low-frequency component of the Fermi doublet (approaching $2\omega(\delta)$) becomes weaker. On potassium, the increased partial occupancy of the π_u affinity level induces considerable shifts (see figure 22(*b*), third entry) and no Fermi doublet is apparent. The SERS spectrum of CO_2 on cold-deposited copper shows more bands than in the case of Ag and K, and very roughly looks like a superposition of the CO_2 SERS spectra of Ag and K. Tentatively, we assign the two SERS bands of N_2 on cold-deposited copper, and the two δ bands and the three bands in the spectral range of the ν_{sym} vibration of CO_2 on cold-deposited copper to two different E-type adsorption sites, which we call E_1 and E_2 (see figure 22). This assignment is proofed by annealing the copper films, cold-deposited at 40 K, to 200 K.

Recooling to 40 K and exposing the restructured films to N_2 or CO_2 yields only the E_1-SERS bands [102c]. The N_2 and CO_2 molecules resemble messengers from 'odd sites', destroyed by annealing. These sites are certainly not steps of Cu(111) surfaces, since these are annealed only at higher temperatures, between 375 and 665 K [236]. The different partial occupancies of the affinity levels and/or the different electron transfer amplitudes V_{ak} of the E_1 and E_2 species are also reflected in the halfwidth of the stretch bands. Those of the E_2-bands are considerably broader than those of the E_1-bands irrespective of inhomogeneous broadening [102c]. The results and interpretation of this section support the interpretations of the previous one.

6.3. Screening at smooth surfaces

We resume the question of section 6.1 concerning the missing resonance Raman effect of pyridine on Ag(111). We attribute the missing 'first-layer SERS' at smooth single crystalline Ag surfaces to screening.

Screening has to be discussed without self-consistency by resorting to screening at clean metal surfaces. In the case of isolated silver atoms and molecules the internal electronic excitations start in the UV spectral range; therefore the incident and emitted electromagnetic fields are not significantly screened within the complex and Persson's *ansatz* $-elE_n$ for the electron–photon coupling is reasonable when l is taken as the distance between the centres of the Ag atom and of the ligand, and E_n is taken as the component of the electric vector of the exciting light in the direction connecting the two centres (see figure 23(a)). However, in the metal case (where l is the distance between the image plane and the centre of the adsorbate and E_n is the field component normal to the surface—see figure 22(b)) an external field is very effectively screened. It is easily calculated in a quasi-static approximation that the surface charge density $\sigma = E_n/4\pi$ which screens the laser field under the usual experimental conditions (50 mW power, focused to 1 mm $\times$30 μm, $\lambda_L = 514.5$ nm) amounts to only 1.42×10^{-7} electrons per surface atom of an Ag(111) surface. The centre of gravity of the static screening charge at an Ag(100) surface was calculated by Aers and Inglesfield [241] to lie about 1.0 atomic units (1 au = 0.53 Å) to the vacuum side from the geometrical surface (the plane where the bulk is chopped in two). According to jellium models (see section 6.4) the centre of the dynamical screening charge at ω_L or ω_S is still at the vacuum side. Consequently, Perssons field E_n within the first silver atom layer is considerably screened (for further discussion see section 6.4.2). This point is related to the fact that charge transfer excitations in EELS of pyridine and pyrazine on Ag(111) are weak [148]. Our judgement 'weak' is based on an EELS result of Campion: he reported [242] a charge transfer excitation at 1.89 eV for pyridine on a Ag(540) surface that was stronger than any of the internal electronic π–π^* excitations of pyridine. Of course, this result and the missing SERS of the same system [200] seem to contradict any correlation between SERS and CT excitations [242]. This problem will be addressed further below.

6.4. Increased surface-electron–photon coupling

Considering the results of cold-deposition of small quantities of silver in section 5.4 and the EELS results described above (section 6.3) it seems that a position of the affinity level appropriate for resonance is a necessary but not a sufficient condition for 'first-layer' SERS. We think that the second necessary condition is increased electron–photon coupling at the surface. We see two possibilities:

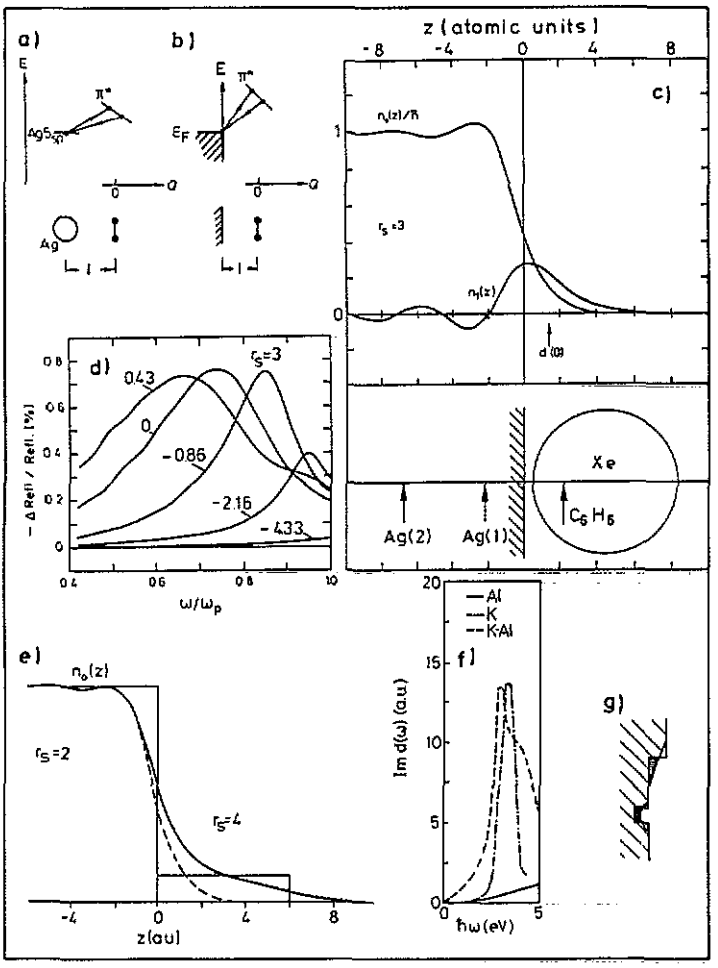

Figure 23. (*a*) Resonant Raman effect in a silver-unsaturated hydrocarbon molecule complex by electron transfer from the Ag 5s,p level to the lowest unoccupied molecular orbital π^* of the molecule. Q is the normal coordinate of a C–C stretch vibration, l is the distance between the centres of the silver atom and the ligand molecule. (*b*) SERS model of Persson [151] (see also figure 15), l is the distance between the image plane of the metal surface and the centre of the adsorbed molecule. (*c*) Upper part: ground-state electron density distribution $n_0(z)$ and static screening charge distribution $n_1(z)$ (in arbitrary units) with centroid $d(0)$ at the edge of a jellium of $r_S = (4\pi n/3)^{-1} = 3$. n = electron density, 1 au $\sim$ 0.53 Å. (After [237].) Lower part: Ag(111) surface, first and second layer of the centres of the silver atoms are indicated, the jellium edge is set equal to the geometrical surface. The position of adsorbed Xe is taken from the average distance of Xe at Ag(111) of 3.55 ± 0.1 Å evaluated by LEED [238], the position of the C_6H_6 ring plane is from a cluster calculation [239]. (*d*) non-local corrections ΔR to the Fresnel reflectance R, angle of incidence 45°, p-polarized, as a function of photon frequency for jellium $r_S = 3$, $\omega_p^2 = 4\pi ne^2/m$. Parameters are the applied static electric field in units of V Å^{-1}. (After [240].) (*e*) Equilibrium electron density profile for an Na ($r_S = 4$) monolayer on an Al ($r_S = 2$) substrate. The electronic density profiles of the clean Al and Na surfaces are indicated by the broken and full curves, respectively. (After [237].) (*f*) Im d(ω) for jellium models of pure K ($r_S = 5$), pure Al ($r_S = 32$) and a monolayer of K on Al. After [252] and [253]. (*g*) Smoothing of ground-state electron distribution at sites of atomic-scale surface roughness (Smoluchowski effect [177]).

(i) According to Ljungbert and Apell [243] electron hole pair excitations at the surface can dominate the optical absorption of small metal spheres. This and other theoretical work (e.g. [244, 245]) was motivated by the wish to explain the 10–100 times enhanced photo-yield of small silver particles suspended in gas [246, 247]. On the other hand, near threshold, photoemission of small Cu and Au island and thin films in UHV showed no drastic changes with respect to the bulk [248].

These experiments were repeated with increasing quantities of silver deposited on oxidized silicon wafers in UHV, forming island films and eventually continuous 'smooth films' [249]. The photoelectric yield at 4.89 eV photon energy (about 0.8–0.4 eV above the threshold), did not exceed the yield from thick films [249]. Nevertheless, we cannot exlude the possibility that increased surface-electron–photon coupling is caused simply by confinement of electrons in structures smaller than the coherent mean free path of electrons.

(ii) Next we present our hypothesis of 'active sites' of surface-electron–photon coupling. First, we discuss the theoretical situation at smooth surfaces. Static screening at a jellium surface, treated by Weber and Liebsch [237] in the density functional approach is shown in figure 23(*b*).

The distance of the centre of gravity of the screening charge distribution $n_1(z)$ from the jellium edge is denoted by d [250]. In the static case $d(0)$ at frequency $\omega = 0$ represents the position of the so-called image plane. In dynamic screening, the surface photoabsorption cross-section is proportional to Im $d(\omega)$ [250], with [252]

$$d(\omega) = \int_{-\infty}^{+\infty} \mathrm{d}z\, z n_1(z,\omega)/\sigma(\omega) \tag{9a}$$

$$d(\omega) = \int_{-\infty}^{+\infty} \mathrm{d}z\, n_1(z,\omega) \tag{9b}$$

where $n_1(z,\omega)$ is the dynamic screening charge distribution.

The best choice of the homogeneous electron density for the case of silver is $r_s \sim 3$. In this case $d(\omega)$ increases only very little from $d(0)$ with increasing ω (see figure 2(*a*) in [253]). The jellium approximation for silver will hold qualitatively only below $\hbar\omega \sim 3.5$ eV, the onset of d-band transitions. Positive $d(\omega)$ has recently been confirmed experimentally to be the negative dispersion of surface plasmons on K and Na [251]. Inspection of figure 23(*c*) shows that most of the electron density of the surface layer of silver is screened from the outside field. In the classical sense, there is only the weak internal field $E_n/\epsilon(\omega)$ for $z < d(\omega)$. For frequencies below the plasma frequency the contribution to the matrix element of surface-electron–photon coupling comes from the region of strong gradients in the electromagnetic field and the electron density profile at $z > d(\omega)$ [250]. Thus, compared to the free silver complex, the electron–photon coupling within the surface layer of silver atoms (see figure 23(*c*)) is smaller than in isolated Ag complexes and only a number of electrons much smaller than one per silver surface atom can be involved in the resonance Raman model of Persson [151]. The electronic tail at $z > d(\omega)$ consists nearly exclusively of electrons at the Fermi energy with the component of the k vector parallel to the surface approximateley zero. Therefore the surface-electron–photon coupling involves mainly electrons at E_F. These points have been discussed in detail by Persson and co-workers [254, 255]. Consequently, experimental verifications of the surface-electron–photon coupling by photoemission [256] or inverse photoemission [257] involve initial or final states near E_F, respectively.

The 'softer' the tail of the inhomogeneous electron gas at the surface, the stronger is the surface-electron–photon coupling, characterized by Im $d(\omega)$. This point is supported by two theoretical approaches: Gies and Gerhardts [240] presented the time-dependent local density response theory of strongly charged metal surfaces (e.g. electrode–electrolyte interfaces). Depending on the sign of the static external field strength, the tail of the electron distribution is either further extended from the jellium edge (e.g. cathodic electrode) or the electron density profile near the jellium edge becomes steeper (e.g. anodic electrode) (see figure 1 in [258] and figure 3 in [259]). In the first case, the non-local corrections to the Fresnel reflectance calculated from the surface response function $d(\omega)$ is increased, in the second case it is nearly suppressed (see figure 23(d)).

The second approach is by Liebsch [252] who successfully explained the enhancement of optical second harmonic generation (SHG) by several orders of magnitude after covering rhodium [260] or silver [261] by submonolayers of alkali metals. The more diffuse the electron density profile (figure 23(e)), the more susceptible it is to the optical fields as demonstrated by the low frequency loss function Im $d(\omega)$ in figure 23(f). The backing of the low density tail by an electron gas of higher density increases the low-frequency surface-electron–photon coupling [252] (compare the spectra for K and K–Al below 3 eV in figure 23(f)). The peak increases with decreasing density in the overlayer [252] and shifts to lower photon energy. Within the jellium model, partial coverages (e.g. of alkali metal on Al) are equivalent to lower average electron densities in the overlayer [252]. The increased surface-electron–photon coupling was observed by photoemission of Cu covered partially by Na [262] and by electron energy loss spectroscopy of Cu(100) with submonolayer coverage of K [263]. Atomic scale 'pockets' of low density electron gas with a diffuse profile backed by high electron density material will also exist near sites of atomic-scale roughness where the electrons smoothen the surface profile given by the cores of the surface atoms (so-called Smoluchowski effect [177]) as schematically depicted in figure 23(g). These sites are considered to be the active sites of surface-electron–photon coupling (see also the discussion in [153]).

As described in section 3.1 oxygen adsorbs preferentially at sites of atomic scale roughness. The electron density in the 'floppy' tail will be depleted by electron transfer to the localized O 2p orbitals, 2.9 eV below the Fermi level, as observed by photoemission [264, 265]. In this way active sites of increased surface-electron–photon coupling are 'passivated'.

Light emission from tunnel junctions [266, 267] was used to demonstrate these mechanisms. A silver film, deposited at room temperature on a rough CaF_2 film (see insert of figure 7(b)) shows a pronounced 'non-classical' 'first-layer effect' (see section 3.2). Similar silver films were produced in ultra-high vacuum as the top electrodes of Al–Al_2O_3 tunnel junctions on rough CaF_2 substrates (see the insert in figure 24 [268]).

The intensity and the spectral distribution of the emitted light of a given junction depends on the polarity of the junction bias—there is about 3 times more intensity, when the electrons tunnel from the Al to the Ag electrode than there is in the opposite direction even though the tunnelling currents are larger in the second case. This excess intensity is quenched by a 1 L exposure to oxygen at about 40–50 K, see figure 24. These experiments clearly demonstrate the increased photon emission by hot electrons at sites of atomic scale surface roughness. Of course the time-reversed process, which is the first step of the electronic Raman scattering (see section 7), exists as well. The hot-electron picture of light emission from tunnel junctions was first proposed

by Kirtley *et al* [269,267], albeit without the concept of increased electron–photon coupling at sites of atomic scale roughness. However, according to reference [269], a very interesting puzzle arose from their results, since light emission from tunnel junctions was symmetric, or nearly so [266] with respect to the bias voltage polarity. Note that these results were obtained with the junctions in air—the results of Hänisch [268] in ultra-high vacuum (see figure 24) have solved this puzzle.

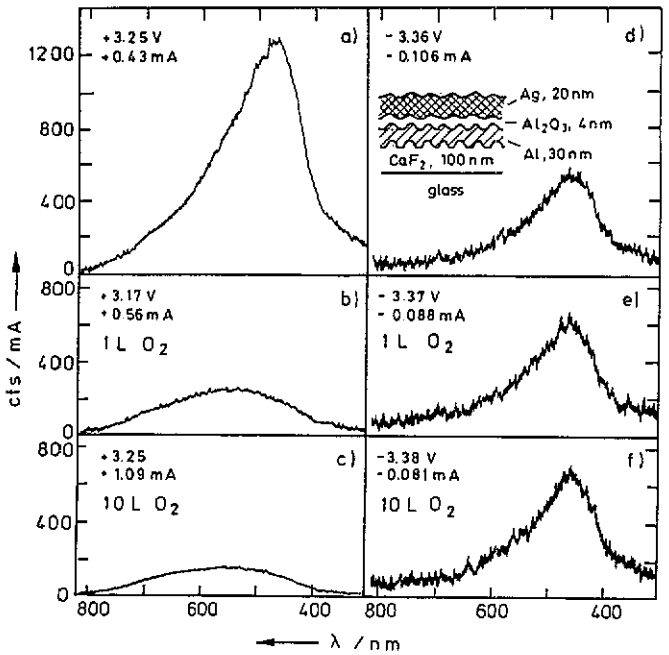

Figure 24. Light emission spectra (uncorrected for wavelength-dependent spectral sensitivity, normalized for tunnelling current) of two (left-hand side, right-hand side) tunnel junctions on rough CaF_2 substrates (see insert in (*d*)). The silver top electrodes were produced in UHV by vapour deposition at room temperature; (*a*)–(*c*): silver electrode biased positively, electron tunnelling towards the silver electrode (defined as positive direction of current); (*d*)–(*f*): Silver electrode biased negatively; (*a*) and (*d*): clean silver surfaces; (*b*) and (*e*): exposed to 1 L of O_2 at 50 K; (*c*) and (*f*): exposed to 10 L of O_2 at 50 K. Bias voltage and diode current are given in every case. After [268].

The only observed exception from SERS quenching by oxygen passivation is oxygen itself. The Raman spectrum of silver films deposited at 30 K, exposed to oxygen only displays a broad band around 335 cm^{-1} (see figure 25(*b*)), which was assigned to the Ag–O vibration of dissociated oxygen [45,270] based on the agreement with the Ag–O frequency at 325 cm^{-1} of dissociated oxygen on Ag(110) [271]. However, when the films are deposited at 120 K, one also observes SERS from peroxidic and superoxidic dioxygen [270]. The excitation mechanism is probably hole transfer rather than electron transfer [272].

With the concept of surface-electron–photon coupling one may explain why the Fermi level is the discrete lower energy level of the charge transfer excitations (see section 4.2). Originally Ueba [273] and one of the authors (AO) in [274] introduced a hypothetical increased density of states near E_F at silver adatoms (which could not be confirmed by photoemission [275,39]) in order to explain the discreteness of

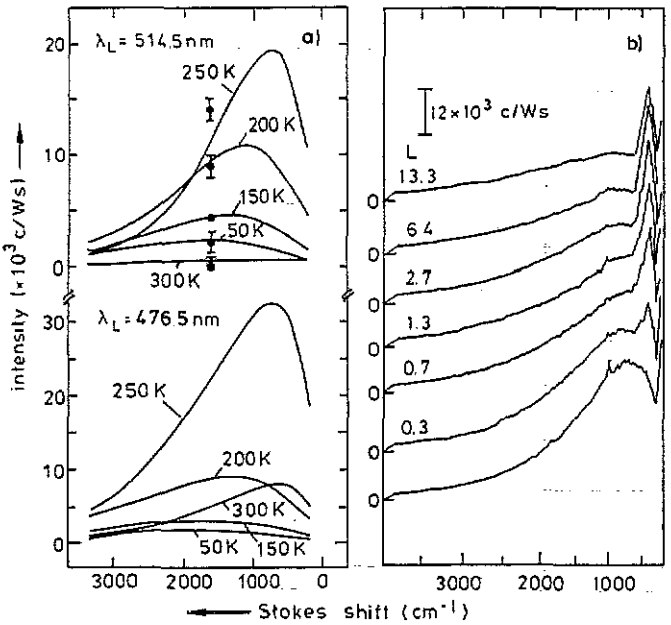

Figure 25. (*a*) Inelastic background spectra of two (upper and lower frame) unexposed silver films of about 100 nm thickness, deposited at 50 K, annealed to the indicated temperatures T_A and recooled to 50 K. Laser wavelengths λ_L = 514.5 nm and 476.5 nm. Angle of incidence 65°, p-polarized, scattered light cone normal to the surface. Noise and a small peak caused by CO are omitted. (*b*) Development of the background spectrum of a silver film of about 200 nm thickness, deposited at 35 K, annealed to 250 K, as a function of exposure to oxygen at 35 K. Structure at about 335 cm^{-1} is an Ag–O vibration. (After [102a].) Bars in the upper part of (*a*) are the normalized (at T_A = 150 K) peak intensities of the N-band of the ν_2-C–C stretch vibration of C_2H_4 after 5 L exposure at 40 K of various cold-deposited Ag films, annealed to the indicated T_A's. After [117].

the excitation. Now this may as well be understood by the surface-electron–photon coupling being mainly restricted to electrons at E_F.

We think that the increased surface-electron–photon coupling is also manifest in the so-called inelastic background (see figure 25(*a*)) which one already observes in the uncovered clean state of those silver samples which yield a 'first-layer' SERS effect ([276, 17] and references therein, [277]). The low-frequency part of the spectra in figure 25(*a*) is not displayed—it contains the vibrational structures of silver itself [278]. Since the spectral structure of the background of cold-deposited and partly annealed silver films shifts with the laser frequency ω_L (see figure 25(*a*)), it is tempting to assign this background to Raman scattering by electron–hole pair excitations [102a]. In any case, the quenching of the inelastic background by oxygen (see figure 25(*b*)) that is also observed for other 'SERS-active' samples demonstrates that the background is a surface phenomenon—as, for instance, second harmonic generation [279, 280].

The intensity increase of the background between 300 and 1000 cm^{-1} was assigned to the increasing three-dimensional phase space for e–h excitations [277], the decrease at higher frequency shifts to inelastic scattering of photons by fluctuations in the number of electrons in an adatomic quasi-level [281]. Monreal *et al* [282] calculated Raman scattering by electron–hole pairs at metal surfaces using the semi-classical infinite barrier model—the classical polariton skin effect field distribution provides the

momentum needed to excite an electron above the Fermi level. In this model it cannot be understood why the background is quenched by oxygen, given the unchanged optical reflectivity. Electron Raman scattering of spherical particles filled by Sommerfeld's free, non-interacting electron gas has been treated in reference [283].

The background at $T_A = 250$ K resembles qualitatively the theoretical spectra [284, 285] of Raman scattering in metals with bulk impurities in the 'dirty limit' when the mean free path of electrons is smaller than the skin depth. However, the SERS background seems to be connected with 'surface impurities'. We think that the nature of the background is not yet properly understood.

6.5. 'Non-locality'

The apparent similarities between resonant Raman scattering in AgC_2H_4 complexes (section 2) and SERS from 'E-type' C_2H_4 (see section 6.2.3) may be considered as indicating a localized interaction due to direct neighbourhood of a site of increased electron–photon coupling and an E-adsorption site (for instance adjacent sites of electron accumulation and depletion in the case of CO on copper—see section 5.1).

On the other hand, one might envision the extreme 'non-local' case of electrons confined to a small silver island, coupling to light, and interacting with the adsorbates (E- and N-types) on the island surface (see section 6.4(i)).

The combination of increased surface-electron–photon coupling and CT excitations is revealed by genuine 'first-layer SERS' of N-type adsorbates. When there is no increased surface-electron–photon coupling, indicated by a very low inelastic background, for instance, at well-prepared low-index silver single crystalline surfaces, there is no 'first-layer SERS' of N-types (E-types do not exist in this case). On cold-deposited silver films (30–120 K) one observes no N-bands of CO [183], a very weak N-signal of C_2H_4 [117], but the N-signal of pyridine is about 20% of the corresponding E-signal (see for instance [286, 99]—at the time of these publications the porosity of the films was not yet known; today it is certain that the N-bands are observed at submonolayer coverage). This trend corresponds to the position of the affinity levels of N-adsorbates in figure 20—at $\hbar\omega_L = 2.41$ eV one is out of resonance with N–CO, but close to resonance with N–C_5H_5N. Apparently, this is the long-searched-for first-layer resonance Raman effect. It does not require special adsorption sites and is active because of increased surface-photon–electron coupling.

Accordingly, the intensity of the N-bands should follow the development of the inelastic background with annealing temperature (see figure 25). For the example of the C–C stretch vibration of N-type C_2H_4, excited with the green Ar^+ laser line ($\lambda_L = 514.5$ nm) we have a good match to the inelastic intensity at the frequency of the N-band (see figure 25). Oxygen, which adsorbs only at surface defect sites (see section 3.1) quenches both E- and N-type Raman signals [117] without changing noticeably the electromagnetic resonances. Oxygen will not stick at the 'N-sites'. If it passivates the hypothetical sites of increased electron–photon coupling (section 6.4) this demonstrates non-local interaction by the electron propagators between sites of increased electron–photon coupling and sites of N-type adsorption. A very high background is displayed by the silver island films [96]. In this case, even CO displays 'first-layer SERS' of N-type CO (see figure 11(*a*) and reference [114]).

Apparently, the SERS intensities of N- and E-adsorbates are influenced by four factors: the increased surface-electron–photon coupling (represented by the background), the charge transfer energy (different for E- and N-type adsorbates), the transfer amplitudes V_{ak} (about which we know little) and the surface concentration of E-sites.

We attribute the quasi-absence of SERS of pyridine at adsorbed Ag(540) reported by Mullins and Campion [200] in spite of a strong CT excitation [242] (see section 6.3) to very weak surface-electron–photon coupling as indicated by a very weak background that is comparable to that of the Ag(111) surface [200, 287]. This holds also for silver films deposited at room temperature. In the same way we rationalize the small enhancement at about a monolayer of cold-deposited silver described in section 5.4.

As pointed out by Mal'shukov [288], the recent observation of strong SERS at near-infrared excitation (see section 8.2) raises problems: (i) can plasma resonances in the infrared give the observed SERS effect? (ii): If 'chemical enhancement' is present in the near-infrared 'one should either exclude all theories based on resonance effects or try to find a model which assumes a wide spectrum of electronic transitions'. Point (i) is related to the discussion in section 3.3. According to the approximation of small-particle electromagnetic dipole resonances, the factor $|\epsilon(\omega_L)|^2|\epsilon(\omega_S)|^2$ would increase enormously towards the infrared spectral range. But why do most excitation spectra decrease in the red visible range? Concerning point (ii), the range of 'non-locality' scales with the elastic mean free path of 'hot' electrons [153] which also increases strongly with decreasing energy above E_F [153]. In summary, these problems need further consideration.

6.6. The 'SERS specificity' of various metals

Besides the noble metals, the alkali metals are good substrates for SERS (see also section 8). For Al, the high reactivity with minute quantities of oxygen is a problem [289] but SERS of pyridine has been demonstrated by Gao and Lopez-Rios [290] and by one of the authors [102a]. The electromagnetic enhancement of Al islands on posts in air was observed by Liao and Stern [291]. Raman, optical reflectivity, DC resistance and oxygen passivation experiments on cold-deposited indium films have revealed the same qualitative trends [102a] as those reported here for silver.

It is certain that for these nearly free electron metals classical electromagnetic enhancement contributes to SERS—whereas weaker contributions are expected for transition metals (see the references in [292]). Recently, Bilmes *et al* [292] reported SERS of pyridine in electrodispersed platinum electrodes. The Raman intensity for adsorbed pyridine was enhanced by at least one order of magnitude after taking the increase in the electrode area into account. Nothing is known about screening and surface-electron–photon coupling at transition metal surfaces.

The approximate correspondence between the charge transfer excitation bands in isolated Ag-C_2H_4 complexes and the SERS excitation profile of E-type C_2H_4 (see section 6.2.4) raises the question of the energy of charge transfer excitations in complexes of C_2H_4 with other metals.

Figure 26 compiles the results of a literature survey on matrix-isolated complexes with CO and C_2H_4 ligands. There are no absorption bands above a wavelength of 400 nm from the transition metals, and the absorption bands of the noble metal complexes in the visible region are suppressed by oxidation (see the lowest frame of figure 26). These differences between the complexes with group I_b (Cu, Ag, Au) and the group VIII atoms Ni, Pd, and Pt may be understood with the example of SCF–Xα-SW results of orbital energies in Ni and Cu [305], Cu, Ag, Au [40], and Ni, Pd, Pt [306] complexes with one moiety of C_2H_4 (see figure 27).

The orbitals of the complexes may be discussed as belonging to four groups by projecting them on the atomic orbitals of the metal atoms and molecular orbitals of C_2H_4: (i) the low-lying orbitals representing the five σ and the one π bond of

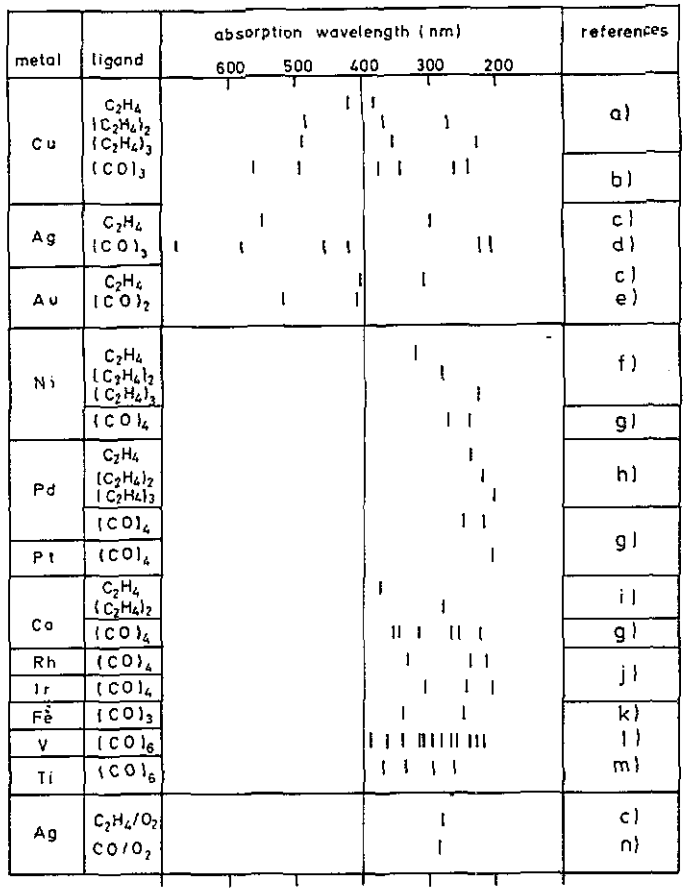

Figure 26. Centre position of assigned optical absorption bands in various matrix-isolated complexes of noble metals (upper frame), of transition metals (middle frame) and of Ag^+ (by mixing O_2 into the matrix (lower frame, see also figure 2)). References: (*a*) [293], (*b*) [294], (*c*) [40], (*d*) [295], (*e*) [296], (*f*) [297], (*g*) [298], (*h*) [299], (*i*) [300], (*j*) [301], (*k*) [302], (*l*) [303], (*m*) [304], (*n*) [175].

C_2H_4, including some d–π hybridization ($3a_1$), usually addressed as donation; (ii) five narrowly spaced d-orbitals, including d–π hybridization ($5a_1$) usually addressed as 'back donation'. (Apparently—using the approximation of atomic orbitals—the chemical bonding energy between Ni and C_2H_4 accounts for the energy of about 1.83 eV to transform the $3d^84s^2$ ground state of a Ni atom into a closed $3d^{10}$ shell (figure 7.30 of [307]). The details of d–π hybridization for the different 'metal atoms' depend on the relative position of the d and π orbitals. (iii) An empty (Pd) or filled (Ag) Pd(Ag)–C_2H_4 antibonding orbital ($6a_1$), mainly composed of the 4s (Pd) or 5s (Ag) state hybridized with the C_2H_4–π state. (iv) The empty π^* state ($6a_1$).

The lowest optical absorption band of the group Ib–C_2H_4 complexes is assigned to the $6a_1 \rightarrow 3b_2$ transition, which is approximately the $s \rightarrow \pi^*$ charge transfer excitation [40]. This excitation is lost by depleting the $6a_1$ level by the transformation of M_{1b} to M^+_{1b} by oxidation [40]. Relatively unaffected by oxidation is the quasi-'intrametal' transition from the 'd-states' to the half-filled (M) or empty (M^+_{1b}) $6a_1$—which corresponds approximately to an internal transition in M_{1b} or M^+_{1b}. This transition is

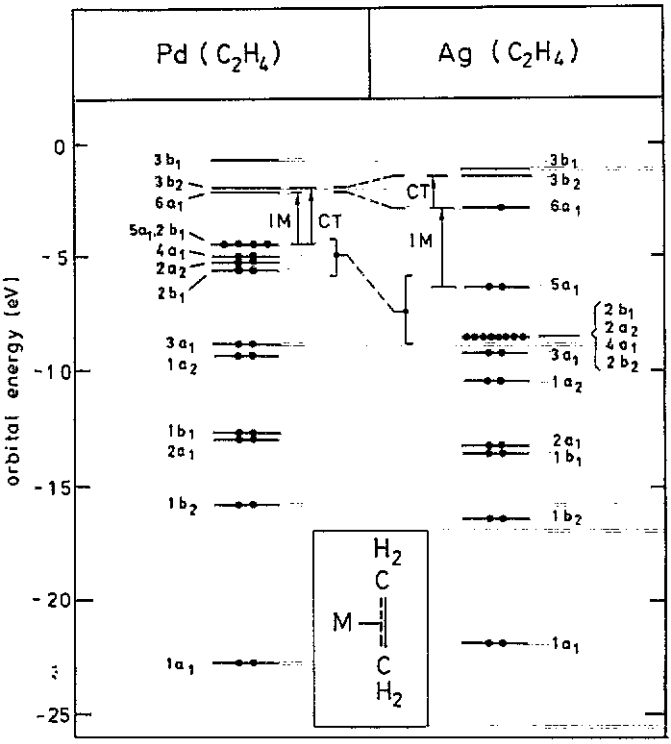

Figure 27. Orbital energies of Pd–C_2H_4 [306] and Ag–C_2H_4 [40] from SCF–Xα–SW calculations. CT: charge transfer transition. IM: 'intra-metal-atom' transition.

the lowest one possible in the M_{VIII}–C_2H_4 complexes. In the right frame of figure 26, the bands below a wavelength of 400 nm will have various degrees of 'internal' and 'charge transfer' character, and therefore will induce various Jahn–Teller distortions in the excited states [308]. Hence the result of a search for a resonance Raman effect by ligand vibrations cannot be predicted.

It seems that s-electron metals are good SERS substrates for three reasons:

(i) The collective screening by the nearly free electrons allows for high-quality electromagnetic ('surface plasmon type') resonances (below the onset of d-electron excitations in the case of the noble metals [309,100]).

(ii) Discrete charge transfer excitations in the visible spectral range are possible. Nevertheless, a systematic survey of smooth and rough metal surfaces concerning this point is missing.

(iii) 'Hot electrons' of 2–3 eV energy above E_F have a relatively high coherent mean free path [153] allowing for 'non-local SERS' [153] (see section 6.5).

7. Summary

In this article we review our present understanding of the enhancement mechanism of surface-enhanced Raman scattering (SERS) by adsorbates on 'rough' metal surfaces. Beyond the contribution of surface-plasmon-type resonances of the incident and emitted light fields (the so-called classical electromagnetic enhancement (CEME)) SERS

displays many features depending on the electronic configuration of the combined metal-adsorbate system and its resonant excitation by the incoming laser field.

Our experimental results clearly reveal the existence of an extra enhancement of the Raman signal confined to a part of the adsorbed molecules in the first monolayer for many different 'rough' metal surfaces studied, e.g. silver films with thickness from 1 nm up to 100 nm deposited on metal substrates whose temperature was held below 50 K, silver island films, silver films deposited on a rough CaF_2 substrate, silver island films on a stochastic post structure, and silver electrodes.

On the other hand, this first-layer enhancement is missing for an Ag(111) single-crystal surface and for continuous, polycrystalline silver films annealed at room temperature or above. It is also missing for atomically smooth silver films with a 500 nm wide grating structure that facilitates the excitation of the surface-plasmon–polariton resonance by the incoming laser light.

In each case the value of the 'first-layer' enhancement depends on the chemical nature of the adsorbate and on the mode of vibration. It is characterized by the appearence of vibrational bands (extra (E-)lines) which are frequency-shifted with respect to adsorption at atomically smooth surfaces (normal (N-)bands).

A clear conceptual identification of CEME is only possible when the electronic effects (substrate–adsorbate–photon interaction) are excluded by separating the Raman scatterers from the surface. In the case of silver island films and 'macroscopically rough silver films deposited on rough CaF_2 we succeeded in discriminating between first-layer enhancement and long-range classical electromagnetic field enhancement (CEME) by using monomolecular spacer layers to bring the top molecules out of range of electronic interaction with the surface. In this way the chemically and vibrationally unspecific, long-range classical field enhancement for multilayer adsorbates becomes apparent. In the case of thick cold-deposited silver films, the 'first-layer' effect is demonstrated by simultaneous DC resistance and SERS experiments.

Empirically, the 'first-layer' effect is suppressed by 'oxygen passivation' of the surface—we interprete SERS of the adsorbates after 'oxygen passivation' as 'first-layer CEME'. It reaches about 10^4 at separated silver islands in the 100 nm size range, but only about two orders of magnitude for silver island films and 'macroscopically rough' silver films. Room-temperature-deposited silver films on an optical grating are quasi-pure classical enhancers of about 2 orders of magnitude.

Conceptually and empirically it is difficult to identify CEME of cold-deposited 'porous' silver films—the upper limit is about 2 orders of magnitude. Transition metals do not support electromagnetic resonances of the same quality as nearly free electron metals or noble metals (at photon energies below the d-excitation threshold) because of a continuum of optical transitions between d-band states. This explains partly the relatively poor performance of d-metals as 'SERS substrates'.

Given all our experimental results, we consider the electronic Raman process by substrate–adsorbate–photon interaction to operate in the following steps:

(i) Laser photon annihilation by excitation of electrons at E_F by a considerably increased surface-electron–photon coupling at rough surfaces. The increased surface-electron–photon coupling in the case of 'macroscopically rough' silver films was directly observed via light emission from tunnelling junctions.

(ii) Propagation of the electron into affinity levels of the adsorbates (charge transfer) and back towards the metal.

(iii) Jahn–Teller distortions of the internal adsorbate configuration according to

the residence time of the electron in the affinity level. The lifetime and consequently the vibrational excitation is maximal when the photon energies (incoming laser or scattered Stokes frequency) are equal to the charge transfer energy.

(iv) Stokes photon creation by the time reversed process (i).

Points (i) and (iv) account for the fact that electronic Raman scattering at smooth silver surfaces has not been observed. The ability of a metal surface to screen adiabatically the external field is reduced by roughness and surface defects. The damping of the polarization currents by electron–hole pair excitations involves preferentially electrons at E_F because only those have a considerable amplitude in the region of the unscreened optical field. The 'oxygen passivation' is caused by depletion of the susceptible inhomogeneous electron gas at sites of atomic-scale roughness. 'Oxygen passivation' also quenches the so-called inelastic background scattering observed from many 'SERS-active' surfaces. This background demonstrates the increased surface-electron–photon coupling. Point (iii) accounts qualitatively for the chemical specificity and vibrational selectivity of SERS.

The resonance character of the charge transfer process explains the order of magnitude differences in the enhancement of the Raman signal of different molecules, especially of the C–C vibrations of saturated and unsaturated hydrocarbons adsorbed at cold-deposited silver films. The resonance condition, namely matching of laser photon and charge transfer energy, is not fulfilled for saturated hydrocarbons within the optical range, so they are only excited via an off-resonance charge transfer process similar to electron impact scattering.

The highest electronic contribution to SERS is observed for CO on cold-deposited silver films. It is at least 3 orders of magnitude. The vibrational selectivity, as demonstrated by the example of the C–C, C–H and C–F vibrations of hydro- and fluorocarbons, may be explained by the different coupling of nuclear motions to the charge transfer state. Point (ii) introduces 'non-locality'. Interestingly surfaces simultaneously displaying E- and N-lines, always support an extra first-layer enhancement for N-type adsorbates as well. In these cases we have to assign the N-lines to molecules adsorbed on terraces or generally smooth parts of the surface.

We explain the first-layer SERS for N-type adsorbates as a non-local charge transfer excitation, consisting of electron excitation at sites of enhanced electron–photon interaction and subsequent propagation to N-type adsorption sites. Thus the missing SERS from smooth surfaces is due to weak surface-electron–photon coupling.

By comparison of inverse photoemission results and SERS excitation profiles of E-bands we conclude that the affinity level of the adsorbates yielding the E-bands is lower than that of the N-species. Accordingly, in many cases (e.g. CO, benzene, ethylene, pyridine) the E-species are closer to resonance than the N-species. An affinity level closer to E_F implies increased electronic damping of the adsorbate vibration [225]. Experimentally the E-bands are broader than the N-bands. For N_2 and CO_2 on Cu, we observe two extra bands. Again, the more extensively shifted E-bands are broader which can be understood within the Newns–Anderson model.

The poor performance of d-metals as 'SERS substrates' can be explained partly by the absence of charge transfer excitations in the visible spectral range and by a comparatively small coherent mean free path of 'hot electrons'.

Our picture of 'first-layer SERS', though accurately based on our empirical knowledge, is tentative because there are still open problems: In spite the direct experimental demonstration of increased electron–photon coupling at disordered, SERS-active

surfaces, its impact on the non-local SERS effect and the inelastic background needs further clarification. It seems to us that electron–photon coupling is most effective on surfaces with only a modest concentration of atomic defects but dominant roughness on a more macroscopic level. This stems from the observation that SERS from N-type adsorbates is very pronounced on silver island films and cold-deposited silver films subsequently annealed to 250 K and not pronounced on cold-deposited silver films, which on the other hand provide the highest concentration of E-sites. Therefore, the relationship between collective resonances in small particles and the electron–photon coupling has to be addressed.

Another problem is that in spite of the identification of E-sites through the shifts of the vibrational frequencies of adsorbed molecules we have no further characterization of these sites. We only know that they have to be special defects on an atomic scale. Finally, although CEME is understood in principle there remain open questions. CEME is always treated within the macroscopic field approximation. This is certainly alright for condensed molecules which are separated from the surface. However we do not know how to treat CEME for E- and N-type adsorbates as yet (see section 3.3).

8. Literature review

8.1. Biological research

The application of SERS to biological or biochemical systems has been reviewed in [310–313]. Examples are neurotransmitters [314], immunglobulin G [315], enzymes and aminoacids [316], cytochrome c [317], nuclear acids (e.g. [318]), eye lens pigments [319], and intermediate states of rhodopsin [320]. It is particularly interesting that the DNA double helix adsorbed at silver electrodes [310] or at silver hydrosol [321] yields Raman signals of the bases (usually within the double helix not in direct contact with the silver surface) only after modification by γ-irradiation or from destabilized regions. SERS seems to be the most sensitive detection method in biochemical research.

8.2. Applied research

Much effort has been devoted to develop silver substrates for trace analysis as reviewed in [322]. Among them are silver-coated filter paper [323], silver-coated latex [324] and polystyrene spheres [325], silver islands on stochastically distributed posts [71, 326, 72] or silver-coated Sn spheres [327]. Electroplating with dilute $KAuClO_4$ or $AgClO_4$ solutions yields strongly enhancing arrays of spherical nodules [328].

Technical developments using SERS were made in the areas of remote sensing using optical fibres [329, 330], efficient optical collection systems using the surface plasmon polariton resonance at smooth surfaces [331, 332] (allowing to observe the displacement of paranitrosodimethylaniline adsorbed at a smooth silver surface by Cl [52]), high spatial resolution [333], rotating electrode [334], detection of short-lived intermediates in electrochemical reactions using time-resolved SERS [335], and extension to near-infrared excitation either with weak diode lasers and a CCD camera [336], or with Nd-YAG excitation (1.06 μm) and Fourier-transform infrared spectroscopy [337–340, 336, 341].

The potential of SERS for trace analysis has been assessed, for example, for subsurface water contaminants [342], nitrogen-containing drugs [343], and dioxines [344].

SERS is used to analyse the pattern of substances fractionated by chromatography, for instance by spraying silver colloid on high-performance thin-layer chromatography plates [345–349] or by flow injection of silver sol into the effluence of a liquid chromatograph [350–353].

8.9. Chemical research

Major applications of SERS in chemistry comprise for instance studies of polymers and polymerization [354–360], apparently yielding information on the polymer–silver interface [145]. Other studies have been concerned with surfactants [361,362], Langmuir–Blodgett films [363–365], phtalocyanines [366–368], and haemoglobin [369], other dyes (for instance [370–372]) and photographic sensitization [373–377] including formation of Ag colloids from Ag^+ by photosensitizing dyes [378]. In this context, surface-enhanced resonant Raman scattering (SERRS) is often observed, for instance of methylviologen dichloride [379] used as an electron relay for the photochemical splitting of water.

In the early work it was found and explained that RRS is less 'surface-enhanced' than normal Raman scattering [380,381] (see also the enhancement between 100–300 of 'type I'-methylviologen radical cation at a silver electrode [379]). Detailed experiments on the quenching of fluorescence and surface-enhanced resonant Raman scattering (SERRS) of rhodamine 6G adsorbed to silver colloids have been described in [382] (and references therein), [383–385]. According to reference [382], in aqueous sols without Cl^-, the quenching of fluorescence and SERRS occurs at identical molecular adsorption sites. Adsorption of Cl^- creates 'active sites' (about 3.3 per silver particle), which leads to an overall increase of the SERRS signal by a factor of 70. The quenching of the fluorescence by adsorption is a prompt process [383,384], whereas the SERRS bands of Rh6G only appear after minutes (apparently independently of Cl^- [383,384]). The peak SERRS bands reach about the same intensity as the broad spectral distribution of fluorescence (quantum yield 0.2) before quenching. From this fact, the enhancement of the Raman intensity is estimated as about 10 orders of magnitude [384]. Based on the idea that excitation–relaxation and resonance Raman processes compete [380] ([381] and references therein) the classical electromagnetic enhancement to SERRS follows, according to reference [386], the sixth power of the field enhancement. Consequently, the SERRS of Rh6G after Cl^- addition has been assigned to those molecules adsorbed within 'cavity sites' between silver particles, which have coagulated under the influence of Cl^- [385]. (Resonant) Raman scattering of Rh6G adsorbed on Al roughened by mechanically polishing in air was not observable in reference [387].

Corrosion inhibitors on Cu have been studied by SERS ([388–392] and references therein) and on brass [393] as well as catalytic reactions with oxygen of SO_2 [394,395], NO, NO_2/NO_4 [396,397] and ethylene [398,399] and of SO_2 with adsorbed NO_3 [400] at the gas–silver interface. Sometimes, the reactions induce strong changes of the inelastic background [400]. On cold-deposited silver films, adsorbed oxygen reacts with CO_2 to form carbonate [401].

SERS from adsorbates on silver electrode surfaces in non-aqueous electrolytes has been described in [379,402–409]. SERS of water apparently needs the breaking of hydrogen bonding in water (see references in [17] and [338], and [410–413]). In this case, a metal cation effect on the SERS of interfacial D_2O and H_2O is observed [414]. The same holds for ammonia [415]. Water enters the pores of cold-deposited silver films only at temperatures just below thermodesorption [115].

8.4. Substrates for SERS activation and quenching

Besides the noble and alkali metals, cold-deposited Ga [416] and In films [28] are well enhancing substrates, whereas only weak signals have so far been observed in the case of Al ([290] and references therein, [387]).

Enhanced Raman scattering has been reported for $Pt(CN)_4^{2-}$ on Pt colloids [417], benzene on Pt [418], pyridine on Pt [292] and Rh electrodes [419] and on supported Rh particles [420] and on β-palladium hydride [421, 422], for pyridine on α-Fe_2O_3 colloids [423], as well as for Cu-phtalocyanide on small GaP particles [424]. In the last case, the enhancement factors of up to 700 have been assigned to electromagnetic resonances, rather than to resonant Raman scattering by coupling the intramolecular transitions to excitons [425, 426]. Earlier reports of SERS from Hg could not be confirmed [427]. Unenhanced Raman spectra of 4-cyanopyridine adsorbed on a rhodium electrode [428] and of ClO_4^- on a smooth Pt electrode [429] have been observable, as well as resonant Raman scattering of heptylviologen [430] and crystal violet [431] on platinum.

In order to use the well-established 'enhancing power' of silver and gold for vibrational spectroscopy at other interfaces, two approches have been pursued:

(i) Deposition of small amounts (submonolayer to several monolayers, averaged) of transition metals on noble metals, for instance Pt and Pd on Au [432], Rh and Ru on Au [433], Rh on Ag [434], Ni and Co on Ag [435, 436], Fe on Ag [437–439] or of SiO_2 on Ag [440], or of Si on Ag [441].

(ii) Deposition of silver on non-metallic substrates, for instance on semiconductors [442–444] on carbonaceous substrates [103, 104, 445], on corrosion layers on iron [446, 447], on SnO_2 [448], and on polymers [449, 450].

SERS is enhanced by adding Cl^- to the aqueous solutions, for instance for colloids [382, 451, 452, 321] (also in some cases without evidence of particle aggregation [382]), electrodes [453] and Cu(111) faces in UHV [454]—the action of Br^- and J^- being comparable [382, 455, 456]. The initial stages of growth and the subsequent reduction of AgCl films at a silver electrode in aqueous chloride solutions was studied in reference [457]. Reduction of three-dimensional AgCl nuclei is characterized by two cathodic peaks, the more cathodic one is related to the creation of 'SERS-active sites (adatoms)' [457]. This reduction peak is not observed when the electrode is kept for some time at negative potential before the weak ORC is performed. This is analogous to cathodic quenching of SERS (see below). The action of trace chloride on roughening, annealing and dissolution of Au(111) was observed by in-situ scanning tunnelling mircroscopy (STM) in an electrochemical cell [458]. Chloride induces faster step motion and promotes gold dissolution during oxidation and reduction. Roughness, if present at all, anneals too fast for observation [458].

Photoelectron spectroscopy on chlorine on silver electrodes emersed from 0.02 M NaCl aqueous electrolytes shows two chlorine species with a difference in the 2p electron binding energy of 1.3 eV. The majority species at the 'smooth' silver electrode has the higher 2p binding energy (assigned to adsorbed Cl), whereas after an oxidation reduction cycle the low-binding-energy species (assigned to Cl^-) dominates [459]. This is discussed as evidence of cationic (Ag^+) SERS-active sites [459].

On the other hand, SERS of adsorbates on roughened silver electrodes is quenched by very small quantities of adsorbed lead [460, 461, 435, 462], thallium [389, 460, 463, 435] and cadmium [464] and by cathodic quenching [465, 466] ([467] and 17 references therein). Nobody has yet addressed the problem of why in some cases foreign metal deposition on 'activated' (roughened) Au and Ag electrodes allows for

Raman spectroscopy of molecules adsorbed to the foreign metal (see further above) and in some cases quenches SERS (see above).

The 'surface flattening' [468] on large scale by the coalescing nodular structure, within 19 hours after a heavy ORC (400 mC cm^{-2}) in 0.1 M Cl^- aqueous electrolyte was observed by scanning electron microscopy and scanning tunnelling microscopy (STM) [469]. In this work, a fine structure on the nanometre scale on the nodule surface (immersed 15 hours in Ar-saturated water) was revealed by STM [469]. STM of polycrystalline silver in Cl^- aqueous electrolyte before, during and after the ORC demonstrated roughness on an atomic scale after the reduction [470]. More SERS and second harmonic generation is observed, when the electrode is illuminated during the oxidation–reduction cycle (ORC) (e.g. reference [471]). This so-called 'photoactivation' was studied as a function of intensity and exposure time [472] and assigned to the formation of organometallic complexes, which survive subsequent 'dark' ORCs and are re-adsorbed at the surface at negative potentials, leading to a 'memory effect' [472].

Photoemission at 488 nm and 514 nm wavelength of a silver electrode into the electrolyte is enhanced by 2–3 orders of magnitude by an ORC [473]—see also the discussion in [153]. The changes of the optical reflectivity by the cathodic quenching [474,464] are negligible [467,475]. However, a change of optical absorption by cathodic quenching was observed by photoacoustic spectroscopy [476]. Raising the electrode temperature to about 40–80° also quenches the Raman signal [474,464]. Active hydrogen evolution at the electrode before the ORC yield stronger SERS intensities [477]. Probably all these phenomena are related to submicroscopic restructuring of the surfaces or self-edges and changes of the local electronic structure including the adsorbate. Many explanations are based on the formation, decay [478,479] and stabilization (for instance by Cu [480–482]) of 'SERS-active sites'. A large effort in discriminating between macroscopic and atomic-scale roughness in this respect has been reviewed by Pemberton and co-workers [483].

Underpotential deposition of silver on platinum (yielding a coverage up to one monolayer) has frequently been used to demonstrate the 'chemical SERS effect' [484,485,171,172,486]. Also in this case, a roughening oxidation–reduction cycle increases the Raman intensity [172]—it is under debate whether this leads to surface *structures supporting electromagnetic resonances* [487,486].

8.5. Porosity

SERS under UHV conditions has been investigated mainly at cold-deposited silver films [24]. These films are porous [488–490] and the roughness factor of films of 2000 Å thickness may reach a value of 40 [39]. They display a so-called anomalous optical absorption, probably caused by electromagnetic resonances in internal cavities [228,115] of the porous film. The excitation spectra of SERS follow roughly this resonance [99,227,24] (reviewed in [67]). Classical electromagnetic SERS calculations for various geometrical forms of the cavities have been presented in [488], [491–495], [288] and [496]. Based on these theoretical results, the cavities are envisioned as the 'SERS-active sites' and the SERS mechanism is the classical one [489,488,497,498]. No in-situ investigations of cold-deposited silver films at low temperatures by STM are known to us, but only after (partial) annealing by transfer to air [63,499,500]. STM cannot reveal a hypothetical nodular structure, as observed by scanning electron microscopy of 'activated' silver electrodes (see the simultaneous application of both microscopies in reference [469]). The Auger signal of Pd and Ag during the covering of a cold-deposited silver film by Pd shows the completion of the first Pd layer at

approximately the same quantity of Pd as a smooth silver film [501]. Surprisingly, the light scattered elastically by a cold-deposited film is relatively low—it increases considerably during the irreversible loss of 'SERS-active sites' by annealing to room temperature [278]. Platinum carbon replica of Ag films, deposited at 83 K on mica are smooth [502], not displaying any sign of the 'bump-column' structure of films deposited at room temperature [502,503]. Do these three independent results indicate that the 'external' surface is rather smooth in spite the larger roughness factor?

Recent reports of SERS of molecules 'trapped' [504] or 'intercalated' [505] (see also earlier conjectures [506]) within the silver electrode self-edge by the roughening oxidation-reduction cycle (ORC) may perhaps be related to adsorption within the 'pores' of cold-deposited silver films. Hindered or slow migration of molecules within porous grain boundaries might explain some slow (on the order of 10 minutes) intensity changes observed at electrode surfaces [507,467]. On shorter time scales, SERS of pyridine on silver electrodes only depends on the pyridine concentration within the electrolyte during the ORC—it cannot be changed by variation of this concentration after the ORC [508].

8.6. Resonant Raman scattering

An overview of the different contributions to resonance Raman scattering of adsorbates on metals has been given in [509]. Beyond the references in [17], the theory of photon driven charge transfer excitations has been extended in references [167,510,273,511,380,512], the ground state dynamic charge transfer theory in references [513–515], the latter extending a previous model of the modulation of the effective barrier potential by adsorbate vibrations [516,517].

In order to explain the enhancement of non-totally-symmetric modes besides totally symmetric modes and the weak overtone spectrum of SERS [518], a photon driven charge transfer model including Herzberg–Teller coupling was developed in [511].

Weak overtones not observed in the case of normal Raman scattering by the free molecules have been reported in references [24] (figure 11), [519,233,520] and relatively strong ones in [158]. The first demonstration of photon-driven electron transfer to the adsorbates is given in references [126–128], the first 'reversed' adsorbate to silver photon-driven electron transfer was reported in references [129,130]. Systematic trends in substituted pyridines and saturated nitrogen heterocycles were observed in [131]. Further evidence for resonant Raman scattering by photon driven charge transfer is contained in [125,506,132,521,133,135,522,136,523].

Charge transfer excitations relevant for the SERS mechanism have been observed by electron energy loss spectroscopy (see references in [17]). There is only one report on the optical detection of a charge transfer excitation, namely of pyridine adsorbed on silver islands [524,525]—a search for it on electrode surfaces by electroreflectance was negative [137].

Polarization-dependent Raman excitation spectra of vibrations of dyes yielded the following results: various vibrational modes of free-base phtalocyanine adsorbed flat on silver island films follow only the lowest π–π^* transition (polarized parallel to the molecular plane, shifted slightly (31–44 nm) toward the red) [526]. In contrast, Raman scattering by the central carbon breathing mode of positively charged crystal violet (CV^+), adsorbed flat on smooth gold shows not only the influence of the intramolecular π–π^* transition, but furthermore for the zz-Raman tensor component (z normal to the surface) a profile, monotonously increasing towards the red, assigned to electron transfer from Au to CV^+ [527,528] .

The excitation spectra of SERS of adsorbates on colloids is often explained by the aggregation of the colloid particles (see references in [17,529–531])—but the excitation spectra of adsorbed cyclohexane displayed a maximum, though the absorption spectrum of the sample did not show any maximum in the visible region [532]. The overlap of the excitation profile with the absorption spectrum was virtually negligible for adsorbed vanadate (no aggregation in this case) [533].

8.7. Distance dependence

Often, experiments on the dependence of SERS on the distance between scatterer and the silver surface did not reveal a 'first-layer effect', but only long-range classical electromagnetic enhancement. Spacers were polymer films [94,95] or Langmuir–Blodgett films [111,77,534] on CaF_2 roughened silver films or island films of silver in air.

When electrochemically roughened gold electrodes are covered by an overlayer film (e.g. nickel oxide [535]), the integrated SERS intensity of the overlayer grows with film thickness provided the film has not yet become opaque. This is explained with the long-range electromagnetic enhancement to distances of 20–30 Å from the gold surface [535].

The following interpretations do not agree with the conclusions of this article in sections 1–3: silver island films on glass were covered by copper-phtalocyanine (CuPc) layers of various thickness d, and SERS was recorded with the samples in air [108]. Strikingly, the absolute SERS intensity increased with decreasing d, reaching the absolute maximum at one monolayer, corresponding to an enhancment of about 10^4. Maximum 'first layer enhancement' was observed at an average silver island of about 5 nm—which lead to the conclusion that the large enhancement is caused by surface plasmon polariton modes [108] (see, however, section 3). In reference [536] silver island films and continuous thicker films were deposited on the base plane of a prism—the SERS intensity of adsorbed and condensed CuPc was observed as a function of the total reflection (ATR) and of the polarization of the incident light. In the case of island films, the extreme first-layer effect of [108] was reproduced; in the case of the continuous silver films the long-range enhancement in the surface plasmon polariton mode without 'first-layer effect' was reproduced (analogous to our own results of island films and films on optical gratings (see figure 10)).

Following the conclusions of [108] a 'chemical effect' was ruled out, and the first-layer effect in the case of silver islands was assigned to local fields within cavity sites, e.g. pores and crevices [536]. The angular and polarization dependence of SERS could be fitted to the square of the incident field in the interior of a homogeneous film with effective dielectric constant $\epsilon(\omega)$ [536].

SERS of $(Ru/NH_3)6^{3+}$ at silver electrodes was assigned to the species within the outer Helmholtz layer, and therefore not to a 'first-layer effect' [537]. On the other hand, the 'first-layer effect' was used as indicator of diffusion of C_2H_4 and Xe through thin pyrazine films condensed on cold-deposited silver films [538].

8.8. Depolarization

The local electromagnetic field at a surface changes with adsorption [18]. According to references [539–541], within the model of exclusive electromagnetic enhancement, the SERS intensity should first increase and then decrease with the coverage as a function of the adsorbate due to the depolarizing field from neighbour molecules. A very strong variation, following the predicted trend, was indeed observed for pyridine

on cold-deposited silver [286, 542] and interpreted by depolarization [542]. A more comprehensive experimental study showed very different dependencies of the Raman intensity versus coverage for different molecules of comparable optical polarizability, even different trends for the various vibrational modes of the same adsorbate [543]. This was found to be inconsistent with the depolarization model and was tentatively assigned to coverage-dependent shifts of the affinity levels. This may perhaps also explain that the development of the SERS intensity as a function of coverage is strongly dependent on the exciting laser wavelength (see section 6.2.3).

A weaker decrease of SERS of pyridine with increasing coverage of macroscopic rough silver was found in reference [544], but no decrease at all for silver island films in UHV [84], probably because 'first-layer SERS' cannot be explained solely by classical electromagnetic enhancement. On smooth polycrystalline gold electrodes in ClO_3^- aqueous electrolyte it was convincingly demonstrated that the Raman intensity of the breathing mode of pyridine depends only on the pyridine surface coverage (evaluated with the differential capacity [545, 546]). At relatively low coverages, the intensity grows quasi-linearly with coverage and does not depend explicitly on potential as it is expected for pure electromagnetic enhancement. A small decrease of the Raman intensity beyond a coverage of about 3.2×10^{-10} mol cm^{-2} (equivalent to about 2×10^{14} mol cm^{-2}) is explained by depolarization.

The dependence of Raman intensity on coverage changes drastically after one or several oxidation–reduction cycles [546]; also the SERS signal now reaches full intensity at comparatively low coverages analogous to our results from cold-deposited films (see section 5.2).

References

[1] Fleischmann M, Hendra P J and McQuillan A J 1974 *Chem. Phys. Lett.* **26** 123
[2] Jeanmaire D L and VanDuyne R P 1977 *J. Electroanal. Chem.* **84** 1
[3] Albrecht M G and Creighton J A 1977 *J. Am. Chem. Soc.* **99** 5215
[4] VanDuyne R P 1979 *Chemical and Biological Applications of Lasers* vol 4, ed C B Moore (New York: Academic)
[5] Furtak T E and Reyes J 1980 *Surf. Sci.* **93** 351
[6] Creighton J A 1980 *Springer Series in Chemical Physics* vol 15 (Berlin: Springer) p 145
[7] Otto A 1980 *Appl. Surf. Sci.* **6** 309
[8] Yamada H 1981 *Appl. Spectrosc. Rev.* **17** 227
[9] Birke R L and Lombardi J R 1982 *Advances in Laser Spectroscopy* vol 1, ed B Garetz and J R Lombardi (Philadelphia, PA: Heyden) p 143
[10] Dornhaus R 1982 *Springer Tracts in Modern Physics* vol 22 (Berlin: Springer) p 201
[11] Cooney R P, Mahoney M R and McQuillan A J 1982 *Advances in Infrared and Raman Spectroscopy* vol 9, ed R E Hester and R J Clark (London: Heyden) ch 4
[12] Marinyuk V V, Lazorenko-Manevich R M and Kolotyrkin Ya M 1982 *Advances in Physical Chemistry* ed Ya M Kolotyrkin (Moscow: Mir)
[13] Ueba H, Ichimura S and Yamada H 1982 *Surf. Sci.* **119** 433
[14] Chang R K and Furtak T E (eds) 1981 *Surface-enhanced Raman Scattering* (New York: Plenum)
[15] Furtak T E 1984 *Advances in Laser Spectroscopy* vol 2, ed B Garetz and J R Lombardi (Chichester: Wiley) p 175
[16] Schatz G C 1984 *Acc. Chem. Res.* **17** 370
[17] Otto A 1984 *Light Scattering in Solids* vol 4, ed Cardona M and G Güntherodt (Berlin: Springer) ch 6
[18] Arya K and Zeyher R 1984 *Light Scattering in Solids* vol 4, ed M Cardona and G Güntherodt (Berlin: Springer) ch 7
[19] Wokaun A 1984 *Solid State Phys.* **38** 223
[20] Metiu H 1984 *Prog. Surf. Sci.* **17** 153

[21] Metiu H and Das P 1984 *Ann. Rev. Phys. Chem.* **35** 507
[22] Chang R K and Laube B L 1984 *CRC Crit. Rev. Solid State Mater. Sci.* **12** 1
[23] Ford G W and Weber W H 1984 *Phys. Rep.* **113** 196
[24] Pockrand I 1984 *Springer Tracts in Modern Physics* vol 104 (Berlin: Springer)
[25] Campion A 1984 *Comment. Solid State Phys.* **11** 107
[26] Kerker M 1985 *J. Colloid Interface Sci.* **105** 297
[27] Wokaun A 1985 *Mol. Phys.* **56** 1
[28] Moskovits M 1985 *Rev. Mod. Phys.* **57** 783
[29] Efrima S 1985 *Modern Aspects of Electrochemistry* vol 16, ed B E Conway, R E White and J O'M Bockris (New York: Plenum) p 253
[30] Weitz D A, Moskovits M and Creighton J A 1986 *Chemistry and Structure at Interfaces* ed R B Hall and A B Ellis (Weinheim: Chemie) ch 5
[31] Murray C A 1986 *Advances in Laser Spectroscopy* ed B A Garetz and J R Lombardi (New York: Wiley) p 49
[32] Chang R K 1987 *Ber. Bunsenges. Phys. Chem.* **91** 296
[33] Birke R L and Lombardi J R 1988 *Spectroelectrochemistry, Theory and Practice* ed R J Gale (New York: Plenum)
[34] Mal'shukov A G 1988 *Chemical Physics of Solvation* part C, ed J Ulstrup, E Kalman, R R Dogonadze and A A Kornyshev (Amsterdam: Elsevier) p 433
[35] Stencel J M 1990 *Raman Spectroscopy for Catalysis* (New York: Van Nostrand) ch 5
[36] Kneipp K 1990 *Exp. Techn. Physik* **38** 3
[37] *SPIE milestone Series* 1990 ed M Kerker
[38] Grabhorn H 1991 *PhD Dissertation* Universität Düsseldorf
[39] Eickmans J, Otto A and Goldmann A 1986 *Surf. Sci.* **171** 415
[40] McIntosh D F, Ozin G A and Messmer R P 1980 *Inorg. Chem.* **19** 3321
[41] Brings R, Mrozek I and Otto A 1991 *J. Raman Spectrosc.* **22** 119
[42] Lee S-Y and Heller E J 1979 *J. Chem. Phys.* **71** 4777
[43] Weissbluth M 1978 *Atoms and Molecules* (New York: Academic)
[44] Tsang J C, Demuth J E, Sanda P N and Kirtley J R 1980 *Chem. Phys. Lett.* **76** 54
[45] Pettenkofer C, Eickmans J, Ertürk Ü and Otto A 1985 *Surf. Sci.* **151** 9
[46] Jiang X and Campion A 1987 *Chem. Phys. Lett.* **140** 95
[47] Pettinger B and Wenning U 1978 *Chem. Phys. Lett.* **56** 253
[48] Campion A and Mullins D R 1983 *Chem. Phys. Lett.* **94** 576
[49] Pettenkofer C and Otto A 1983 *J. Physique Coll.* **10** 337
[50] Ertürk Ü, Gherban D and Otto A 1988 *Surf. Sci.* **203** 554
[51] Veirs D K, Chia V K F and Rosenblatt G M 1989 *Langmuir* **5** 633
[52] Byahut S and Furtak T E 1991 *Langmuir* **7** 508
[53] Grabhorn H and Otto A 1990 *Vacuum* **4** 473
[54] Otto A 1976 *Optical Properties of Solids, New Developments* ed B O Seraphin (Amsterdam: North-Holland) p 677
[55] Teng Y Y and Stern E A 1967 *Phys. Rev. Lett.* **19** 511
[56] Numata H 1982 *J. Phys. Soc. Japan* **51** 2575
[57] Neviere M and Reinisch R 1982 *Phys. Rev.* B **26** 5403
[58] Mills D L and Weber M 1982 *Phys. Rev.* B **26** 1075
[59] Yamashita M and Tsuji M 1983 *J. Phys. Soc. Japan* **52** 2462
[60] Garcia N 1983 *Opt. Commun.* **45** 307
[61] Ertürk Ü and Otto A 1988 *Chem. Phys. Lett.* **149** 284
[62] Ertürk Ü and Otto A 1988 *Europhys. Lett.* **6** 251
[63] Gimzewski J K, Humbert A, Bednorz J G and Reihl B 1985 *Surf. Sci.* **162** 961; *Phys. Rev. Lett.* **55** 951
[64] Benistant P A M, van de Walle G F A, Van Kampen H and Wyder P 1986 *Phys. Rev.* B **33** 690
[65] Schumacher D 1991 *Habilitationsschrift* Universität Düsseldorf (*Springer Tracts of Modern Physics* submitted)
[66] Hallmark V M and Campion A 1986 *J. Chem. Phys.* **84** 2933
[67] Otto A 1988 *Indian J. Pure Appl. Phys.* **26** 141
[68] Sennett R S and Scott G D 1950 *J. Opt. Soc. Am.* **40** 203
[69] Murray C A 1983 *J. Electron Spectrosc. Relat. Phenom.* **29** 371

[70] Liao P F, Bergman J G, Chemla D S, Wokaun A, Melngailis J, Hawrylak A M and Economou N P 1981 *Chem. Phys. Lett.* **82** 335
[71] Meier M, Wokaun A and Vo-Dinh T 1985 *J. Phys. Chem.* **89** 1843
[72] Goudonnet J P, Inagaki T, Ferrell T L, Warmack R J, Buncick M C and Arakawa E T 1986 *Chem. Phys.* **106** 225
[73] Chen C Y and Burstein E 1980 *Phys. Rev. Lett.* **45** 1287
[74] Moskovits M 1978 *J. Chem. Phys.* **69** 4159
[75] Kerker M, Wang D-S and Chew H 1980 *Appl. Opt.* **19** 4159
[76] McCall S L, Platzman P M and Wolff P A 1980 *Phys. Lett.* **77A** 381
[77] Cotton T M, Uphaus R H and Möbius D J 1986 *J. Phys. Chem.* **90** 6071
[78] Gersten J I and Nitzan A 1980 *J. Chem. Phys.* **73** 3023
[79] Gersten J I and Nitzan A *Surface-enhanced Raman Scattering* (New York: Plenum)
[80] The limit of r below which the concept of CEME breaks down is not known. Isolated Na_8 clusters still display a surface plasma resonance [81], whereas Au_{55} clusters, stabilized by a ligand cell do not [82]. Electromagnetic resonances localized at atomic scale surface protrusions on a scale of $\lambda V_F/c$ will be heavily damped by the non-local dielectric response, whereas narrow (> 1 Å) gaps in silver may still support electromagnetic resonances [83].
[81] Selby K, Vollmer M, Masui J, Kresin V, de Heer W A and Knight W D 1989 *Phys. Rev.* B **40** 5417
[82] Fauth K, Kreibig U and Schmid G 1989 *Z. Phys.* D **12** 515
[83] Holzapfel C, Akemann W, Schumacher D and Otto A 1990 *Surf. Sci.* **227** 123
[84] Mrozek I and Otto A 1989 *Recent Trends in Raman Spectroscopy* ed S B Banerjee and S S Jha (Singapore: World Scientific) p 224
[85] Mrozek I and Otto A 1989 *Appl. Phys.* A **49** 389
[86] Mrozek I and Otto A 1990 *J. Electron Spectrosc. Relat. Phenom.* **54/55** 895
[87] Bergman J G, Chemla D S, Liao P F, Glass A M, Pinczuk A, Hart R M and Olson D H 1981 *Opt. Lett.* **6** 33
[88] Weitz D A, Garoff S and Gramila T J 1982 *Opt. Lett.* **7** 168
[89] Schmeisser D and Jacobi K 1985 *Surf. Sci.* **156** 911
[90] Campbell C T 1985 *Surf. Sci.* **157** 43
[91] Hall P G and King D A 1973 *Surf. Sci.* **36** 81
[92] Albers H, Van der Wal W J J and Bootsma G A 1977 *Surf. Sci.* **68** 47
[93] Mrozek I and Otto A 1990 *Europhys. Lett.* **11** 243
[94] Murray C A, Allara D L and Rhinewine M 1981 *Phys. Rev. Lett.* **46** 57
[95] Murray C A and Allara D L 1982 *J. Chem. Phys.* **76** 1290
[96] Mrozek I 1989 *Dissertation* Universität Düsseldorf
[97] Yamaguchi T, Yoshida S and Kinbara A 1984 *Thin Solid Films* **21** 173
[98] Mrozek I, Stephan N and Otto A unpublished
[99] Pockrand I 1982 *Chem. Phys. Lett.* **92** 509
[100] Pockrand I 1982 *Chem. Phys. Lett.* **85** 37
[101] Holzapfel C, Stubenrauch F, Schumacher D and Otto A 1990 *Thin Solid Films* **188** 7
[102a] Akemann W 1992 *Dissertation* Universität Düsseldorf, in preparation
[102b] Akemann W and Otto A 1992 *J. Raman Spectrosc.* at press
[102c] Akemann W and Otto A 1992 *Surf. Sci.* at press
[103] Ishida H, Fukuda H, Katagiri G and Ishitani A 1986 *Appl. Spectrosc.* **40** 322
[104] Rubim J C, Kannen G, Schumacher D, Dünnwald J and Otto A 1989 *Appl. Surf. Sci.* **37** 233
[105] Lyon S A and Worlock J M 1983 *Phys. Rev. Lett.* **51** 593
[106] Ertürk Ü, Pettenkofer C and Otto A 1986 *J. Electron Spectrosc. Relat. Phenom.* **38** 113
[107] Crawford O H 1988 *J. Chem. Phys.* **89** 6017
[108] Hayashi S and Samejima M 1984 *Surf. Sci.* **137** 442
[109] Tsang J C, Kirtley J R and Theiss T N 1980 *Solid State Commun.* **35** 667
[110] Barber P W, Chang R K and Massoudi H 1983 *Phys. Rev. Lett.* **50**
[110] Barber P W, Chang R K and Massoudi H 1983 *Phys. Rev. Lett.* **50** 997
[111] Kovacs G J, Loutfy R O, Vincett P S, Jennings C and Aroca R 1986 *Langmuir* **2** 689
[112] Notholt J and Ludwig P K 1988 *Chem. Phys. Lett.* **143** 609
[113] Mrozek I unpublished
[114] Mrozek I, Pettenkofer C and Otto A 1990 *Surf. Sci.* **238** 192
[115] Mrozek I, Bornemann T and Otto A 1988 *Surf. Sci.* **204** 358

[116] Pettenkofer C 1986 *Dissertation* Universität Düsseldorf
[117] Grewe J unpublished
[118] Nenner I and Schulz G J 1975 *J. Chem. Phys.* **62** 1747
[119] Dose V 1985 *Surf. Sci. Rep.* **5** 337
[120] Frank K-H, Yannoulis R, Dudde R and Koch E E 1988 *J. Chem. Phys.* **89** 7569
[121] Frazier J R, Christophorou L G, Carter J G and Schweinler H G 1978 *J. Chem. Phys.* **69** 3807
[122] Dudde R, Reihl B and Otto A, 1990 *J. Chem. Phys.* **92** 3930
[123] Dudde R 1989 *Dissertation* Universität Hamburg
[124] Otto A, Frank K H and Reihl B 1985 *Surf. Sci.* **163** 140
[125] Thietke J, Billmann J and Otto A 1984 *Dynamics on Surfaces* ed B Pullmann, J Jortner, A Nitzan and B Gerber (Dordrecht: Reidel) p 345
[126] Billmann J and Otto A 1982 *Solid State Commun.* **44** 105
[127] Otto A 1983 *J. Electron Spectrosc. Relat. Phenom* **29** 329
[128] Furtak T E and Macomber S H 1983 *Chem. Phys. Lett.* **95** 328
[129] Furtak T E and Roy D 1983 *Phys. Rev. Lett.* **50** 1301
[130] Billmann J and Otto A 1984 *Surf. Sci.* **138** 1
[131] Lombardi J R, Birke R L, Sanchez L A, Bernard J and Sun S C 1984 *Chem. Phys. Lett.* **104** 240
[132] Irish D E, Guzonas D and Atkinson G F 1985 *Surf. Sci.* **158** 314
[133] Takahashi M, Goto M and Ito M *Chem. Phys. Lett.* **121** 458
[134] Guzonas D, Irish D E and Atkinson G F 1986 *Proc. 10th Int. Conf. Raman Spectroscopy* ed W L Petticolas and B Hudson p 5
[135] Rubim J C and Sala O 1986 *J. Mol. Struct.* **145** 157
[136] Otto C, de Mul F F M and Greve J 1988 *Proc. 11th Int. Conf. Raman Spectroscopy* ed R J H Clark and D A Long p 281
[137] Kannen G, Bilmes S A and Otto A 1989 *Electrochim. Acta* **34** 1147
[138] Bornemann T 1989 *Dissertation* Universität Düsseldorf
[139] Avouris Ph and Demuth J E 1983 *Surface Studies with Lasers (Springer Series in Chemical Physics)* (Berlin: Springer) p 33
[140] Avouris Ph, DiNardo N J and Demuth J E 1984 *J. Chem. Phys.* **80** 491
[141] Creighton J A 1988 *Spectroscopy of Surfaces* ed R H J Clark and R E Hester (New York: Wiley) p 37
[142] Creighton J A 1985 *Surf. Sci.* **158** 211
[143] Moskovits M 1984 *J. Phys. Chem.* **88** 5526
[144] Moskovits M and Suh J S 1988 *J. Phys. Chem.* **92** 6327
[145] Boerio F J, Hong P P, Clark P J and Okamoto Y 1990 *Langmuir* **6** 721
[146] Weidlein J, Müller U and Dehnicke K 1982 *Schwingungsspektroskopie* (Stuttgart: Thieme)
[147] Stephan N 1990 *Diplomarbeit* Universität Düsseldorf
[148] Avouris Ph and Demuth J E 1981 *J. Chem. Phys.* **75** 4783
[149] Johnson P B and Christy R W 1972 *Phys. Rev.* B **6** 4370
[150] Wolkow R A and Moskovits M 1986 *J. Chem. Phys.* **84** 5196
[151] Persson B N J 1981 *Chem. Phys. Lett.* **82** 561
[152] Lundquist B I, Hjelmberg H and Gunnarsson O 1978 *Photoemission and the Electronic Properties of Surfaces* ed B Feuerbacher, B Fitton and R F Willis (New York: Wiley) p 227
[153] Otto A, Bornemann T, Ertürk Ü, Mrozek I and Pettenkofer C 1989 *Surf. Sci.* **210** 363
[154] Schulz G J 1979 *Electron-Molecule Scattering* ed S C Brown (New York: Wiley) p 1
[155] Herzenberg A 1984 *Electron-Molecule Collisions* ed I Shimamura and K Takayanagi (New York: Plenum)
[156] Trajmar S, Register D F and Chutjian A 1983 *Phys. Rep.* **97** 219
[157] Allan M 1989 *J. Electron Spectrosc. Relat. Phenom.* **48** 219
[158] Creighton J A 1986 *Surf. Sci.* **173** 665
[159] Moskovits M, DiLella P and Maynard K J 1988 *Langmuir* **4** 67
[160] Jakob P and Menzel D 1989 *Surf. Sci.* **220** 70
[161] Demuth J E, Ibach H and Lehwald S 1978 *Phys. Rev. Lett.* **40** 1044
[162] Schrader B and Meier W 1977 *Raman/IR Atlas of Organic Compounds* (Weinheim: Chemie)
[163] Wong S F and Schulz G J 1975 *Phys. Rev. Lett.* **35** 1429
[164] Furtak T E, Trott G and Loo B H 1980 *Surf. Sci.* **101** 374
[165] Billmann J, Kovacs G and Otto A 1980 *Surf. Sci.* **92** 153

[166] Burstein E, Chen Y J, Chen C Y, Lundquist S and Tossatti E 1979 *Solid State Commun.* **29** 567
[167] Gersten J I, Birke R L and Lombardi J R 1979 *Phys. Rev. Lett.* **43** 147
[168] Bunding K A, Birke R L and Lombardi J R 1980 *Chem. Phys.* **54** 115
[169] Watanabe T, Kawanami O, Honda K and Pettinger B 1983 *Chem. Phys. Lett.* **102** 565
[170] Furtak T E and Roy D 1985 *Surf. Sci.* **158** 126
[171] Furtak T E and Miragliotta J 1986 *Surf. Sci.* **167** 381
[172] Miragliotta J and Furtak T E 1987 *Phys. Rev.* B **35** 7382
[173] Roy D and Furtak T E 1986 *Chem. Phys. Lett.* **124** 299
[174] Rubim J C and Bilmes S A unpublished
[175] Huber H and Ozin G A 1977 *Inorg. Chem.* **16** 64
[176] Yamamoto I and Nanba T 1988 *J. Phys. Soc. Japan* **57** 2111
[177] Smoluchowski R 1941 *Phys. Rev.* **60** 661
[178] Campion A and Mullins D R 1985 *Surf. Sci.* **158** 263
[179] Dumas P, Tobin R G and Richards R L 1986 *Surf. Sci.* **171** 555
[180] Pettenkofer C and Otto A 1985 *Surf. Sci.* **151** 37
[181] Otto A, Pockrand I, Billmann J and Pettenkofer C Chang R K and Furtak T E (ed) 1981 *Surface-enhanced Raman Scattering* (New York: Plenum) p 147
[182] Ertürk Ü and Otto A 1987 *Surf. Sci.* **179** 163
[183] Pettenkofer C, Mrozek I, Bornemann T and Otto A 1987 *Surf. Sci.* **188** 519
[184] Ertürk Ü, Pockrand I and Otto A 1983 *Surf. Sci.* **131** 367
[185] Chesters M A, Parker S F and Raval R 1986 *Surf. Sci.* **165** 179
[186] Horn K and Pritchard J 1976 *Surf. Sci.* **55** 701
[187] Woodruff D P, Hayden B E, Prince K and Bradshaw A M 1982 *Surf. Sci.* **123** 397
[188] Hirschmugl C J, Williams G P, Hoffmann E M and Chabal Y C 1990 *Phys. Rev. Lett.* **65** 480
[189] Toennies J P and Ellis J, private communication
[190] Hirschmugl C J, Ertürk Ü *et al* to be published
[191] Richardson N V and Bradshaw A M 1979 *Surf. Sci.* **88** 255
[192] Höhner G, Toennies J P and Wöll Ch 1990 *Appl. Phys.* A **51** 208
[193] Cardona M 1982 *Light Scattering in Solids II* ed M Cardona and G Güntherodt (Berlin: Springer) ch 2
[194] Hollins P and Pritchard J 1980 *Vibrational Spectroscopy of Adsorbates* ed R F Willis (Berlin: Springer) ch 8
[195] Hayden B E, Kretschmar K and Bradshaw A M 1985 *Surf. Sci.* **155** 553
[196] Raval R, Parker S F, Pemble M E, Hollins P, Pritchard J and Chesters M A 1988 *Surf. Sci.* **203** 353
[197] Pritchard J, Catterick T and Gupta R K 1975 *Surf. Sci.* **53** 1
[198] Dubois L H and Zegarski B R 1985 *Chem. Phys. Lett.* **120** 537
[199] Rowe J E, Shank C V, Zwemer D A and Murray C A 1980 *Phys. Rev. Lett.* **44** 1770
[200] Mullins D R and Campion A 1984 *Chem. Phys. Lett.* **110** 565
[201] Smardzewski R R, Colton R J and Murday J S 1979 *Chem. Phys. Lett.* **68** 53
[202] Ladouceur H D, Tevault D E and Smardzewski R R 1983 *J. Chem. Phys.* **78** 980
[203] Tsang J C Kirtley J R and Theis T N 1982 *J. Chem. Phys.* **77** 641
[204] Bornemann T and Otto A 1989 *Surf. Sci.* **211** 463
[205] Lopez-Rios T, Borensztein Y and Vuye G 1984 *Phys. Rev.* B **30** 659
[206] Reed C E, Giergiel J, Ushioda S and Hemminger J C 1985 *Phys. Rev.* B **31** 1873
[207] Grabhorn H, Schumacher D and Otto A 1990 *Vhdl. DPG (VI)* vol 25, p 1149
[208] Tonscheidt J 1990 *Diplomarbeit* Universität Düsseldorf
[209] Grabhorn H, Otto A, Schumacher D and Persson B N J 1991 *Surf. Sci.* at press
[210] King F W, VanDuyne R and Schatz G C 1978 *J. Chem. Phys.* **69** 4472
[211] Efrima S and Metiu H 1979 *J. Chem. Phys.* **70** 1939
[212] Jennings P J and Jones R O 1988 *Adv. Phys.* **37** 341
[213] Gies P and Gerhardts R R 1988 *J. Phys. Rev.* B **37** 10020
[214] Lang N D and Williams A R 1982 *J. Phys. Rev.* B **25** 2940
[215] Demuth J E, Schmeisser D and Avouris Ph 1981 *Phys. Rev. Lett.* **47** 1166
[216] Schmeisser D, Demuth J E and Avouris Ph 1982 *Chem. Phys. Lett.* **87** 324
[217] Chiu N S, Burrow P D and Jordan K D 1979 *Chem. Phys. Lett.* **68** 121
[218] Wilder J A, Koch E-E and Frank K-H unpublished

[219] Kannen G, Reihl B and Otto A unpublished
[220] *Pyridine, which does not adsorb flat on Ag(111)* [221], is probably bonded by the nitrogen lone pair electrons. The strong decrease of the work function by 1.65 eV [124] indicates strong donation. Bonding to Ag^+ by complex formation within an acetonitrile solution [62] shifts the ν_1 vibration from 992 to 1011 cm^{-1} and the ν_{12} vibration from 1031 to 1038 cm^{-1} No explanation of these shifts by referring to donation is known to us. It follows from symmetry considerations that backdonation into the lowest affinity level b_1 (see figure 12) will strengthen the C–C bonds in the so-called meta position [222]. According to the normal mode analysis of Mizutani and Ushioda [222], *increasing the force constants in the meta position* causes an upward frequency shift of the C–C ring breathing mode ν_1, whereas the C–C–C and C–N–C total symmetric angle bending mode ν_{12} frequency remains constant. This trend agrees with the observations of a pyridine ν_1 E-band, which is shifted upwards (see table 2) and an unshifted ν_{12} band on silver-UHV surfaces [24] and at silver electrodes [2]. According to [222] the ν_{12} mode is shifted upward by the nitrogen–surface bond. Indeed, for pyridine at copper-UHV surfaces and copper electrodes also the ν_{12} E-band is shifted upwards by 7 cm^{-1} [184] and one observes E- and N-bands for both modes (see table 2). We assign this to stronger bonding to the copper substrate.
[221] Bader M, Haase J, Frank K-H, Puschmann A and Otto A 1986 *Phys. Rev. Lett.* **56** 1921
[222] Mizutani G and Ushioda S 1989 *J. Chem. Phys.* **91** 598
[223] Note that this static charge transfer in the adsorbate ground state cannot be deduced from the work function change by adsorption—for instance CO on copper decreases the work function [224] due to stronger 5σ donation compared to $2\pi^*$ backdonation. Note that donation is not incorporated into the Newns–Anderson model.
[224] Tracy J C 1972 *J. Chem. Phys.* **56** 2748
[225] Persson B N J and Persson M 1980 *Solid State Commun.* **36** 175
[226] Seki H 1983 *J. Electroanal. Chem.* **150** 425
[227] Pockrand I 1982 *Chem. Phys. Lett.* **92** 514
[228] Bornemann T, Otto A, Frank K H and Reihl B 1988 *Surf. Sci.* **195** 161
[229] Seki H 1982 *Solid State Commun.* **42** 695
[230] Seki H 1982 *J. Chem. Phys.* **76** 4412
[231] The excitation profiles of the C–C ring breathing mode ν_1 and of the symmetric ring deformation mode ν_{12} of pyridine are different, see lowest frame of figure 21. (The relatively higher SERS intensity of the ν_1 mode at red excitation has also been found on thick cold-deposited silver films—see figure 2 in [232].) The apparent absence of a resonance for the ν_{12} mode corresponds to the peculiar potential dependence of the SERS by this mode of pyridine adsorbed on a silver electrode [126] and to its 'insensitivity' to occupation of the b_1 π^* state—see [220].
[232] Pockrand I, Billmann J and Otto A 1983 *J. Chem. Phys.* **78** 6384
[233] Schulze W, Charle K-P and Kloss U 1985 *Surf. Sci.* **156** 822
[234] Backeshoff E 1986 *Diplomarbeit* Universität Düsseldorf
[235] Domcke W, Berman M, Estrada H, Mündel C and Cederbaum L S 1984 *J. Phys. Chem.* **88** 4862
[236] Hinch B J, Lock A, Toennies J P and Zhang G 1989 *J. Vac. Sci. Technol.* B **7** 1260
[237] Weber M and Liebsch A 1987 *Phys. Rev.* B **35** 7411
[238] Stoner N, Van Hove M A, Tong S Y and Webb M B 1978 *Phys. Rev. Lett.* **40** 243
[239] Anderson A B, McDevitt M R and Urbach F L 1984 *Surf. Sci.* **146** 80
[240] Gies P and Gerhardts R R 1987 *J. Vac. Sci. Technol.* **5** 936
[241] Aers G C and Inglesfield J E 1989 *Surf. Sci.* **217** 367
[242a] Campion A 1988 *Int. Conf. Raman Spectroscopy (Calcutta)* (oral contribution)
[242b] Campion A 1990 *6th Int. Conf. on Vibrations at Surfaces (Shelter island)* (oral contribution)
[243] Ljungbert Å and Apell P 1983 *Solid State Commun.* **46** 47
[244] Penn D R and Rendell R W 1982 *Phys. Rev.* B **26** 3047
[245] Faraci G, Pennisi A R and Margaritondo G 1989 *Phys. Rev.* B **40** 4209
[246] Schmidt-Ott A, Schurtenberger P and Siegmann H C 1980 *Phys. Rev. Lett.* **45** 1284
[247] Müller Ü, Schmidt-Ott A and Burtscher H 1988 *Z. Phys.* B **73** 103
[248] Katrich G A and Naumovets A G 1987 *Physics of Solid Surfaces* ed J Koukal (Amsterdam: Elsevier) p 123
[249] *Otto A, Dudde R and Reihl B unpublished*
[250] Feibelman P J 1982 *Prog. Surf. Sci.* **12** 287

[251] Tsuei K-D, Plummer E W and Feibelman P J 1989 *Phys. Rev. Lett.* **63** 2256
[252] Liebsch A 1989 *Phys. Rev.* B **40** 3421
[253] Liebsch A 1987 *Phys. Rev.* B **36** 7378
[254] Persson B N J and Andersson S 1984 *Phys. Rev.* B **29** 4382
[255] Persson B N J and Zaremba E 1985 *Phys. Rev.* B **31** 1863
[256] Levinson H J, Plummer E W and Feibelman P J 1979 *Phys. Rev. Lett.* **43** 952
[257] Drubbe W, Himpsel F J and Feibelman P J 1988 *Phys. Rev. Lett.* **60** 2070
[258] Gies P and Gerhardts R R 1986 *Europhys. Lett.* **1** 513
[259] Gies P and Gerhardts R R 1986 *Phys. Rev.* B **33** 982
[260] Tom H W K, Mate C M, Zhu X D, Crowell J E, Shen Y R and Somorjai G A 1986 *Surf. Sci.* **172** 466
[261] Song K J, Heskett D, Dai H L, Liebsch A and Plummer E W 1988 *Phys. Rev. Lett.* **61** 1380
[262] Wallden L 1985 *Phys. Rev. Lett.* **54** 943
[263] Persson B N J and Dubois L H 1989 *Phys. Rev.* B **39** 3047
[264] Eickmans J, Goldmann A and Otto A 1983 *Surf. Sci.* **127** 153
[265] Eickmans J, Otto A and Goldmann A 1985 *Surf. Sci.* **149** 293
[266] Lambe J and McCarthy S C 1976 *Phys. Rev. Lett.* **37** 923
[267] Kirtley J R, Theiss T N, DiMaria D J, Tsang J C, Fischetti M V and Brorson S D *Dynamical Phenomena at Surfaces, Interfaces and Superlattices* 1985 ed F Nizzoli, K-H Rieder and R F Willis (Berlin: Springer)
[268] Hänisch M 1992 *Disseration* Universität Düsseldorf, in preparation
Hänisch M and Otto A 1992 *Vhdl. DPG* at press
[269] Kirtley J R, Theiss T N, Tsang J C and DiMaria D J 1983 *Phys. Rev.* B **27** 4601
[270] Pettenkofer C, Pockrand I and Otto A 1983 *Surf. Sci.* **135** 52
[271] Sexton B A and Madix R J 1980 *Chem. Phys. Lett.* **76** 294
[272] The contribution of hole transfer to SERS of cyanide adsorbed at silver electrodes was demonstrated in [130].
[273] Ueba H 1983 *Surf. Sci.* **129** L267
[274] Otto A, Billmann J, Eickmans J, Ertürk and Pettenkofer C 1984 *Surf. Sci.* **138** 319
[275] Koch E E, Barth J, Fock J H, Goldmann A and Otto A 1982 *Solid State Commun.* **42** 897
[276] Chen C Y, Burstein E and Lundquist S 1979 *Solid State Commun.*
[277] Gass A N, Kapusta O I, Klimin S A and Mal'shukov A G 1989 *Solid State Commun.* **71** 749
[278] Pockrand I and Otto A 1981 *Solid State Commun.* **38** 1159
[279] Shen Y R 1986 *Ann. Rev. Mater. Sci.* **16** 69
[280] Richmond G L, Robinson J M and Shannon V L 1988 *Prog. Surf. Sci.* **28** 1
[281] Mal'shukov A G, 1987 *Sov. Phys.-Solid State* **29** 157
[282] Monreal R, Flores F, Gao Y and Lopez-Rios T 1987 *Europhys. Lett.* **4** 115
[283] Das S and Gersten J I 1988 *Phys. Rev.* B **37** 6063
[284] Fal'kovskii L A 1989 *Sov. Phys.-JETP* **68** 661
[285] Zawsdowski A and Cardona M 1990 *Phys. Rev.* B **42** 10732
[286] Pockrand I and Otto A 1980 *Solid State Commun.* **35** 861
[287] According to [200], the background observed on the same kind of sample by our group [49] was higher. Maybe this could explain the 'first-layer effect' of N-type pyridine of about a factor 10 reported by our group [49].
[288] Mal'shukov A G 1990 *Phys. Rep.* **194** 343
[289] Lopez-Rios T, Pettenkofer C, Pockrand I and Otto A 1982 *Surf. Sci.* **121** L541
[290] Gao Y and Lopez-Rios T 1988 *Surf. Sci.* **198** 509
[291] Liao P F and Stern M B 1982 *Opt. Lett.* **7** 483
[292] Bilmes S A, Rubim J C, Otto A and Arvia A J 1989 *Chem. Phys. Lett.* **159** 89
[293] Ozin G A, Huber H and McIntosh D F 1977 *Inorg. Chem.* **16** 3070
[294] Huber H, Kündig E P, Moskovits M and Ozin G A 1975 *J. Am. Chem. Soc.* **97** 2097
[295] McIntosh D F and Ozin G A 1976 *J. Am. Chem. Soc.* **98** 3168
[296] McIntosh D F and Ozin G A 1977 *Inorg. Chem.* **16** 51
[297] Ozin G A, Power W J, Upton T H and Goddard W A III 1978 *J. Am. Chem. Soc.* **100** 4750
[298] Lever A B P P, Ozin G A, Hanlan A J L, Power W J and Gray H B 1979 *Inorg. Chem.* **18** 2088
[299] Huber H, Ozin G A and Power W J 1977 *Inorg. Chem.* **16** 979
[300] Hanlan A J L, Ozin G A and Power W J 1978 *Inorg. Chem.* **18** 2091
[301] Ozin G A anmd Hanlan A J L 1979 *Inorg. Chem.* **18** 2091

[302] Grevels F W and Klotzbücher W E 1981 *Inorg. Chem.* **20** 3002
[303] DeVore T C and Franzen H F 1976 *Inorg. Chem.* **15** 1318
[304] Busby R, Klotzbücher W E and Ozin G A 1977 *Inorg. Chem.* **16** 822
[305] Ozin G A, McIntosh D T, Power W J and Messmer R P 1981 *Inorg. Chem.* **20** 1782
[306] Messmer R P 1975 *The Physical Basis for Heterogeneous Catalysis* ed E Dranglis and R I Jaffee (New York: Plenum) p 261
[307] Radzig A A and Smirnov B M 1985 *Reference Data on Atoms, Molecules and Ions* (Berlin: Springer)
[308] Adelmann D and Gerrity D P 1990 *J. Phys. Chem.* **94** 4055
[309] Pettinger B and Wetzel H 1981 *Surface-enhanced Raman Scattering* ed R K Chang and T E Furtak (New York: Plenum) p 293
[310] Koglin E and Sequaris J-E 1986 *Springer Topics in Current Chemistry* vol 134 (Berlin: Springer) p 3
[311] Nabiev I R, Efremov R G and Chumanov G D 1988 *Sov. Phys.-Usp.* **31** 241
[312] Cotton T M 1988 *Spectroscopy of Surfaces* ed R J H Clark and R E Hester (New York: Wiley) ch 3
[313] Paisley R F and Morris M D 1988 *Prog. Anal. Spectrosc.* **11** 1 1 1
[314] Lee N-S, Hsieh Y-Z, Paisley R F and Morris M D 1988 *Anal. Chem.* **60** 442
[315] Grabbe E S and Buck R P 1989 *J. Am. Chem. Soc.* **111** 8362
[316] Vidugiris G-J A, Gudavicius A V, Razumas V J and Kulys J J 1989 *Eur. Biophys. J.* **17** 19
[317] Hildebrandt P and Stockburger M 1989 *Biochem.* **28** 6710, 6722
[318] Kneipp K, Pohle W and Fabian H 1991 *J. Mol. Struct.* **244** 183
[319] Nie S, Castillo C G, Bergbauer K L, Kuch J F R Jr, Nabiev I R and Yu N T 1990 *Appl. Spectrosc.* **44** 571
[320] Nabiev I R, Chumanov G D and Efremov R G 1990 *J. Raman Spectrosc.* **21** 49
[321] Nabiev I R, Sokolov K V and Voloshin O N 1990 *J. Raman Spectrosc.* **21** 333
[322] Vo-Dinh T 1989 *Chemical Analysis of Polycyclic Aromatic Compounds* ed T Vo-Dinh (New York: Wiley) ch 5
[323] Berthaud A, Laserna J J and Winefordner J D 1988 *J. Pharmaceut. Biomed. Anal.* **6** 599
[324] Barnickel P and Wokaun A 1989 *Mol. Phys.* **67** 1355
[325] Buncick M C, Warmack R J and Ferrell T E 1987 *J. Opt. Soc. Am.* **34** 927
[326] Vo-Dinh T, Meier M and Wokaun A 1986 *Anal. Chim. Acta* **181** 139
[327] Aroca R and Kovacs G J 1988 *J. Mol. Struct.* **174** 53
[328] Busby C C and Creighton J A 1982 *J. Electroanal. Chem.* **140** 379
[329] Bello J M and Vo-Dinh T 1990 *Appl. Spectrosc.* **44** 63
[330] Bell J M, Narayanan V A, Stokes D L and Vo-Dinh T 1990 *Anal. Chem.*6 **62** 2437
[331] Wittke W, Hatta A and Otto A 1989 *Appl. Phys.* A **48** 289
[332] Byahut S and Furtak T E 1990 *Rev. Sci. Instrum.* **61** 27
[333] VanDuyne R P, Haller K and Althorn R I 1986 *Chem. Phys. Lett.* **126** 190
[334] Hildebrandt P, Macor K A and Czernuszewitz R S 1988 *J. Raman Spectrosc.* **19** 65
[335] Shi C, Zhang W, Birke R L and Lombardi J R 1990 *J. Phys. Chem.* **94** 4766
[336] Angel S M and Myrick M L 1989 *Anal. Chem.* **61** 1648
[337] Crookell A, Fleischmann M, Hanniet M and Hendra P J 1988 *Chem. Phys. Lett.* **149** 123
[338] Chase D B and Parkinson B A 1988 *Appl. Spectrosc.* **42** 1186
[339] Angel S M, Katz L F, Archibald D D, Lin L T and Honigs D E 1988 *Appl. Spectrosc.* **42** 1327; 1989 *Appl. Spectrosc.* **43** 367
[340] Angel S M and Archibald D D 1989 *Appl. Spectrosc.* **43** 1097
[341] Fleischmann M, Sockalingum D and Musiani M M 1990 *Spectrochim. Acta* **46** A 285
[342] Carrabba M M, Edmonds R B and Rauh R D 1987 *Anal. Chem.* **59** 2559
[343] Torres E L and Winefordner J D 1987 *Anal. Chem.* **59** 1626
[344] Berten H-O 1990 *Diplomarbeit* Universität Düsseldorf
[345] Sequaris J-M L and Koglin E 1987 *Anal. Chem.* **59** 525
[346] Soper S A and Kuwana T 1989 *Suppl. Spectrosc.* **43** 1180
[347] Koglin E 1989 *J. Planar Chromatogr.* **2** 194
[348] Koglin E 1990 *J. Planar Chromatogr.* **3** 117
[349] Soper S A, Ratzlaff K L and Kuwana T 1990 *Anal. Chem.* **62** 1438
[350] Berthaud A, Laserna J L and Winefordner J D 1987 *Appl. Spectrosc.* **41** 1137
[351] Freeman R D, Hammaker R M, Meloan C E and Fateley W G 1988 *Appl. Spectrosc.* **42** 456

[352] Ni F, Sheng R and Cotton T M 1990 *Anal. Chem.* **62** 1958
[353] Taylor G T, Sharma S K and Mohanan K 1990 *Appl. Spectrosc.* **44** 635
[354] Holze R 1987 *J. Electroanal. Chem.* **224** 253
[355] Venkatachalam R S, Boerio F J, Roth P G and Tsai W H 1988 *J. Polym. Sci.* **26** 2447
[356] Boerio F J 1989 *Thin Solid Films* **181** 423
[357] Boerio F J, Tsai W H and Montando G 1989 *J. Polym. Sci.* B **27** 1017
[358] Tashiro K, Matsushima K and Kobayashi M 1990 *J. Phys. Chem.* **94** 3197
[359] Tsai W H, Boerio F J, Clarson S J and Montando G 1990 *J. Raman Spectrosc.* **21** 311
[360] Perry S S and Campion A 1990 *Surf. Sci.* **234** L275
[361] Wiesner J, Wokaun A and Hoffmann H 1988 *Prog. Colloid Polym. Sci.* **76** 271
[362] Sun S, Birke R L and Lombardi J R 1990 *J. Phys. Chem.* **94** 2005
[363] Aroca R and Guhathakurta-Ghosh U 1989 *J. Am. Chem. Soc.* **111** 7681
[364] Aroca R, Battisti D, Kovacs G J and Loutfy R O 1989 *J. Electrochem. Soc.* **136** 2902
[365] Battisti D and Aroca R 1990 *J. Mol. Struct.* **218** 351
[366] Aroca R and Martin F 1986 *J. Raman Spectrosc.* **17** 243
[367] Zeman E J, Carron K T, Schatz G C and VanDuyne R P 1987 *J. Chem. Phys.* **87** 4189
[368] McConnell A A, Nimmo J A and Smith W E 1989 *J. Raman Spectrosc.* **20** 375
[369] de Groot J, Hester R E, Kaminaka S and Kitagawa T 1988 *J. Phys. Chem.* **92** 2044
[370] Yamada H, Nagata H and Kishibe K 1986 *J. Phys. Chem.* **90** 818
[371] Li L, Liu C, Gu Y, Guo Y and Yin Y 1988 *Chem. Phys. Lett.* **144** 378
[372] Kim J-H, Cotton T M, Uphaus R A and Möbius D 1989 *J. Phys. Chem.* **93** 3713
[373] Brandt E S 1988 *Appl. Spectrosc.* **42** 882
[374] Brandt E S 1989 *Anal. Chem.* **61** 391
[375] Kneipp K, Jahr W and Roewer G 1989 *Chem. Phys. Lett.* **163** 105
[376] Kneipp K 1990 *J. Mol. Struct.* **218** 357
[377] Zhang P, He T, Wang J, Xiu H and Liu F 1989 *J. Photogr. Sci.* **37**
[378] Haegel F-H and Wokaun A 1989 *Chem. Phys. Lett.* **157** 328
[379] Feng Q, Yue W and Cotton T M 1990 *J. Phys. Chem.* **94** 2082
[380] Weitz D A, Garoff S, Gersten J I and Nitzan A 1983 *J. Chem. Phys.* **78** 5324
[381] Efrima S 1985 *J. Phys. Chem.* **89** 2843
[382] Hildebrandt P and Stockburger M 1984 *J. Phys. Chem.* **88** 5935
[383] Pettinger B and Gerolymatou A 1984 *Ber. Bunsenges. Phys. Chem.* **88** 359
[384] Pettinger B and Gerolymatou A 1984 *Surf. Sci.* **156** 859
[385] Pettinger B, Krischer K and Ertl G 1988 *Chem. Phys. Lett.* **151** 151
[386] Pettinger B 1986 *J. Chem. Phys.* **85** 7442
[387] Mo Y, Lei J, Li X and Wachter P 1988 *Solid State Commun.* **66** 127
[388] Kester J J, Furtak T E and Bevolo A J 1982 *J. Electrochem. Soc.* **129** 1716
[389] Kester J J 1983 *J. Chem. Phys.* **78** 7466
[390] Rubim J C, Gutz I G R and Sala O 1983 *J. Mol. Struct.* **101** 1
[391] Youda R, Nishihara N and Aramaki K 1988 *Corrosion Sci.* **28** 87
[392] Carron K T, Yue G and Lewis M L 1991 *Langmuir* **7** 2
[393] Rubim J C 1990 *Chem. Phys. Lett.* **167** 209
[394] Dorain P B, von Raben K U, Chang R K and Laube B L 1981 *Chem. Phys. Lett.* **84** 405
[395] Ishida H and Ishitani A 1983 *Appl. Spectrosc.* **37** 450
[396] von Raben K U, Dorain P B, Chen T T and Chang R K 1983 *Chem. Phys. Lett.* **95** 269
[397] Dorain P B and Boggio J E 1986 *J. Chem. Phys.* **84** 135
[398] McBreen P H and Moskovits M 1987 *J. Catalysis* **103** 188
[399] Boghosian S, Bebelis S, Vayenas C G and Papatheodorou G N 1989 *J. Catalysis* **117** 561
[400] Bates J L and Dorain P B 1989 *J. Chem. Phys.* **90** 7478
[401] Maynard K J and Moskovits M 1989 *J. Chem. Phys.* **90** 6668
[402] Kim J J and Shin G S 1985 *Chem. Phys. Lett.* **118** 493
[403] Garrell R L and Schultz R H 1985 *J. Colloid Interf. Sci.* **105** 483
[404] Stacy A M and VanDuyne R P 1983 *Chem. Phys. Lett.* **102** 365
[405] Hutchinson K, McQuillan A J and Hester R E 1983 *Chem. Phys. Lett.* **98** 27
[406] Guzonas D A, Atkinson G F and Irish D E 1984 *Chem. Phys. Lett.* **107** 193
[407] Guzonas D A, Atkinson G F, Irish D E and Adams W A 1983 *J. Electroanal. Chem.* **150** 457
[408] Pemberton J E 1985 *Chem. Phys. Lett.* **115** 321
[409] Sobocinski R L and Pemberton J E 1990 *Langmuir* **6** 43

[410] Gui J and Devine T M 1989 *Surf. Sci.* **224** 525
[411] Kung H P and Chen T T 1986 *Chem. Phys. Lett.* **130** 311
[412] Kwon M-Y, Lee B-W and Kim J J 1989 *Chem. Phys. Lett.* **162** 238
[413] Tian Z W, Lian Y Z and Lin T Q 1989 *J. Electroanal. Chem.* **265** 277
[414] Chen T T, Smith K E, Owen J F and Chang R K 1984 *Chem. Phys. Lett.* **108** 32
[415] Sanches L A, Lombardi J R and Birke R L 1984 *Chem. Phys. Lett.* **108** 45
[416] DiLella D P and Zhou P 1990 *Chem. Phys. Lett.* **166** 240
[417] Benner R E, von Raben K U, Lee K C, Owen J F, Chang R K and Laube B L 1983 *Chem. Phys. Lett.* **96** 65
[418] Krasser W and Renouprez A J 1982 *Solid State Commun.* **41** 231
[419] Bilmes S A 1990 *Chem. Phys. Lett.* **171** 141
[420] Parker W L, Hexter R M and Siedle A R 1984 *Chem. Phys. Lett.* **107** 96
[421] Fleischmann M, Graves P R and Robinson J 1985 *J. Electroanal. Chem.* **182** 87
[422] Parker W L, Siedle A R and Hexter R M 1986 *J. Catalysis* **99** 482
[423] Zhang P, Wang Y, He T, Zhang B, Wang X, Xiu H and Liu F 1988 *Chem. Phys. Lett.* **153** 215
[424] Hyashi S, Koh R, Ichiyama Y and Yamamoto K 1988 *Phys. Rev. Lett.* **60** 1085
[425] Hayashi S, Koh R, Ichiyama Y and Yamamoto K 1988 *Phys. Rev. Lett.* **60** 1085
[426] Ueba H 1983 *Surf. Sci.* **131** L 432
[427] Wang S-Y, Chou X-Y and Liang N T 1988 *J. Raman Spectrosc.* **19** 365
[428] Shannon O and Campion A 1988 *J. Phys. Chem.* **92** 1385
[429] Pettinger B, Friedrich A and Tiedemann U 1990 *J. Electroanal. Chem.* **280** 49
[430] Lu T and Cotton T M 1987 *J. Phys. Chem.* **91** 5978
[431] Pettinger B and Tiedemann U 1987 *J. Electroanal. Chem.* **228** 219
[432] Leung L-W H and Weaver M J 1987 *J. Am. Chem. Soc.* **109** 5113
[433] Leung L-W H and Weaver M J 1988 *Langmuir* **4** 1076
[434] Feilchenfeld H, Gao X and Weaver M J 1989 *Chem. Phys. Lett.* **161** 321
[435] Fleischmann M and Tian Z Q 1987 *J. Electroanal. Chem.* **217** 385
[436] Fleischmann M, Tian Z Q and Li L J 1987 *J. Electroanal. Chem.* **217** 397
[437] Hengoli G, Musiani M M, Fleischmann M, Mao B and Tian Z Q 1987 *Electrochim. Acta* **32** 1232
[438] Aramaki K and Uehara J 1990 *J. Electrochem. Soc.* **137** 185
[439] Uehara J, Nishihara H and Aramaki K 1990 *J. Electrochem. Soc.* **137** 2677
[440] Walls D J and Bohn P W 1989 *J. Phys. Chem.* **93** 2976
[441] Gao Y and Lopez-Rios T 1986 *Solid State Commun* **60** 55
[442] Mo Y, von Känel H and Wachter P 1984 *Solid State Commun.* **52** 213
[443] Feng Q and Cotton T M 1986 *J. Phys. Chem.* **90** 983
[444] VanDuyne R P, Haushalter J P, Janik-Czachor M and Levinger N 1985 *J. Phys. Chem.* **89** 4055
[445] Knight D S, Weimer R, Pilione L and White W B 1990 *Appl. Phys. Lett.* **56** 1320
[446] Thanos I C G 1986 *Electrochim. Acta* **31** 811
[447] Rubim J C and Dünnwald J 1989 *J. Electroanal. Chem.* **258** 327
[448] Kaul B B, Holt R E, Schlegel V L and Cotton T M 1988 *Anal. Chem.* **60** 1580
[449] Siperko L M 1989 *Appl. Spectrosc.* **43** 226
[450] Allara R C, Murray C A, Bodoff S 1983 *Physicochemical Aspects of Polymer Surfaces* (New York: Plenum) p 33
[451] Pettinger B and Krischer K 1987 *J. Electron Spectrosc. Relat. Phenom.* **45** 133
[452] Zhang P X, Fang Y, Wang W N, Ni D H And Fu S Y 1990 *J. Raman Spectrosc.* **21** 127
[453] Mattei G, Quagliano L G and Pagannone M 1990 *Europhys. Lett.* **11** 373
[454] El'Tsov K N, Zueva G Ya, Klimov A N, Martynov V V and Prokhorov A M 1989 *Chem. Phys. Lett.* **158** 271
[455] Wall K F, Temperini M L A and Chang R K 1986 *Chem. Phys. Lett.* **129** 253
[456] Acker W P, Wall K, Fisch E and Otto A 1986 *Surf. Sci.* **176** 336
[457] Birrs V I and Smith C K 1987 *Electrochim. Acta* **32** 259
[458] Trevor D J, Chidsey C E D and Loiacona D N 1989 *Phys. Rev. Lett.* **62** 929
[459] Kautek W and Gordon II J G 1990 *J. Electrochem. Soc.* **137** 3405
[460] Watanabe T, Yanagihara N, Honda K, Pettinger B and Moerl L 1983 *Chem. Phys. Lett.* **96** 649
[461] Guy A L and Pemberton J E 1985 *Langmuir* **1** 518
[462] Coria-Garcia and Pemberton J E 1988 *ACS Sympos. Series* vol 378 p 398

[463] Roy D and Furtak T E 1984 *J. Chem. Phys.* **81** 4168
[464] Pettinger B and Moerl L 1983 *J. Electron Spectrosc. Relat. Phenom.* **29** 383
[465] Mernagh T P and Cooney R P 1983 *J. Raman Spectrosc.* **14** 138
[466] Ha D H, Lee S K and Kim J J 1987 *Chem. Phys. Lett.* **141** 104
[467] Kannen G and Otto A 1990 *Chem. Phys.* **141** 51
[468] Waser R and Weil K G 1983 *J. Electroanal. Chem.* **150** 89
[469] Ohtsuka I and Iwasaki T 1990 *J. Vac. Sci. Technol.* A **8** 530
[470] Samamaki K, Itoh K, Fujishima A and Gohshi Y 1990 *J. Vac. Sci. Technol.* A **8** 525
[471] Chen T T, von Raben K U, Owen J F, Chang R K and Laube B L 1982 *Chem. Phys. Lett.* **91** 494
[472] Aktsipetrov O A, Mishina E D, Murzina T V, Petukhov A V and Petukhova A L 1989 *Sov. Phys. – Dokl.* **34** 348
[473] Funtikov A M, Sigalaev S KL and Kazarinov V E 1987 *J. Electroanal. Cem.* **228** 197
[474] Macomber S H and Furtak T E 1983 *Solid State Commun.* **45** 267
[475] Bryant M A and Pemberton J E 1990 *Langmuir* **6** 751
[476] Jung E C, Rhee B K, Kim Y D and Jung C S 1990 *Solid State Commun.* **74** 1063
[477] Philpott M R, Barz F, Gordon J G II and Weaver M J 1983 *J. Electroanal. Chem.* **150** 399
[478] Baltruschat H and Heitbaum J 1986 *Surf. Sci.* **166** 113
[479] Sobocinski R L and Pemberton J E 1988 *Langmuir* **4** 836
[480] Moerl L and Pettinger B 1982 *Solid State Commun.* **43** 315
[481] Ha D H and Kim J J 1988 *Phys. Rev.* B **38** 12704
[482] Ha D H and Kim J J 1990 *Chem. Phys. Lett.* **167** 215
[483] Pemberton J E, Guy A L, Sobocinski R L, Tuschel D D and Cross N A 1988 *Appl. Surf. Sci.* **32** 33
[484] Marinyuk V V, Lazorenko-Manevich R M and Kolotyrkin Ya m 1982 *Solid State Commun.* **43** 721
[485] Pemberton J E 1984 *J. Electroanal. Chem.* **167** 317
[486] Takahashi M and Ito M, 1990 *J. Electron Spectrosc. Relat. Phenom.* **54/55** 913
[487] Tuo L C, Chen T T, Chou Y C and Liang N T 1989 *Surf. Sci.* **222** L861
[488] Albano E V, Daiser S, Ertl G, Miranda R and Wandelt K 1983 *Phys. Rev. Lett.* **51** 2314
[489] Seki H and Chuang T J 1983 *Chem. Phys. Lett.* **100** 393
[490] Albano E V, Daiser S, Miranda R and Wandelt K 1985 *Surf. Sci.* **150** 367
[491] Wirgin A and Lopez-Rios T 1984 *Opt. Commun.* **48** 416
[492] Lopez-Rios T and Wirgin A 1984 *Solid State Commun.* **52** 197
[493] Liver N, Nitzan A and Gersten J L 1984 *Chem. Phys. Lett.* **111** 449
[494] Chew H and Kerker M 1985 *J. Opt. Soc. Am.* **32** 1025
[495] Takemori T and Inoue M 1988 *J. Phys. Soc. Japan* **57** 3188
[496] Wirgin A 1990 *Chem. Phys. Lett.* **170** 538
[497] Seki H, Chuang T J, Escobar J F, Morawitz H and Albano E V 1985 *Surf. Sci.* **158** 254
[498] Seki H, Chuang T J, Philpott M R, Albano E V and Wandelt K 1985 *Phys. Rev.* B **31** 5533
[499] Aktsipetrov O A, Vasil'ev S I and Panov V I 1988 *Sov. Phys.–JETP* **67** 1010
[500] Aktsipetrov O A, Vasil'ev S I and Panov V I 1988 *JETP Lett.* **47** 226
[501] Lopez-Rios T and Gao Y 1985 *J. Vac. Sci. Technol.* B **3** 1539
[502] Schröder E 1969 *Z. Phys.* **225** 26
[503] Kaspar W and Kreibig U 1977 *Surf. Sci.* **69** 619
[504] Beer K D, Tanner W and Garell R L 1989 *J. Electroanal. Chem.* **258** 313
[505] McMahon J J 1990 *Proc. XIIth Int. Conf. Raman Spectroscopy* ed J E During and J F Sullivan (New York: Wiley)
[506] Busby C C 1984 *Surf. Sci.* **140** 294
[507] Chen T T, Owen J F and Chang R K 1984 *Dynamics on Surfaces* ed B Pullmann, J Jortner, A Nitzan and B Gerber (Dordrecht: Reidel) p 365
[508] Saito H, Ikezawa Y and Toda G 1984 *Chem. Phys. Lett.* **110** 291
[509] Brotman A, Burstein E and Jiang J D 1985 *Surf. Sci.* **158** 1
[510] Ueba H 1983 *Surf. Sci.* **131** 347
[511] Lombardi J R, Birke R L, Lu T and Xu J, 1986 *J. Chem. Phys.* **84** 4174
[512] Apell P, Flores F, Martin-Rodero A and Monreal R 1988 *Phys. Scr.* **38** 180
[513] Lippitsch M E 1984 *Phys. Rev.* B **29** 3101
[514] Afara S M and Dignam M J 1989 *J. Chem. Phys.* **90** 713

[515] Jha S S 1985 *Surf. Sci.* **158** 190
[516] Jha S S, Kirtley J R and Tsang J C 1980 *Phys. Rev.* B **22** 3973
[517] Kirtley J R, Jha S S and Tsang J C 1980 *Solid State Commun.* **35** 509
[518] Adrian F J 1982 *J. Chem. Phys.* **77** 5307
[519] Pettinger B 1981 *Chem. Phys. Lett.* **78** 404
[520] Chen T T, Owen J F, Chang R K and Laube B L 1982 *Chem. Phys. Lett.* **89** 356
[521] McMahon J J, Dougherty T P, Riley D J, Babacock G T and Carter R L 1985 *Surf. Sci.* **158** 381
[522] Lin H J and Chou Y C 1986 *Chem. Phys. Lett.* **125** 53
[523] Guzonas D A, Irish D E and Atkinson G F 1990 *Langmuir* **6** 1102
[524] Yamada H, Nagata H, Toba K and Nakao Y 1987 *Surf. Sci.* **182** 269
[525] Yamada H, Toba K and Nakao Y 1987 *J. Electron Spectrosc. Relat. Phenom.* **45** 113
[526] Brotmann A and Burstein E 1985 *Phys. Scr.* **32** 385
[527] Jiang J D, Burstein E and Kobayashi H 1986 *Phys. Rev. Lett.* **57** 1793
[528] Jiang J D and Burstein E 1988 *Ind. J. Pure Appl. Phys.* **26**
[529] Joo T H, Kim K and King M S 1984 *Chem. Phys. Lett.* **112** 65
[530] Feilchenfeld H and Siiman O 1986 *J. Phys. Chem.* **90** 2163
[531] Fornasiero D and Grieser F 1987 *J. Chem. Phys.* **87** 3213
[532] Yamada H, Nagata H and Teranishi H 1986 *J. Phys. Chem.* **90** 2384
[533] Greaves S J and Griffith W P 1988 *J. Raman Spectrosc.* **19** 503
[534] Takenaka T, Umemura J and Nakagawa T 1988 *Bull Inst. Chem. Res. Kyoto Univ.* **66** 591
[535] Gosztola D and Weaver M J 1989 *Langmuir* **5** 776
[536] Osawa M and Suetaka W 1987 *Surf. Sci.* **186** 583
[537] Tadayyoni M A, Farquharson S and Weaver M J 1984 *J. Chem. Phys.* **80** 1363
[538] Blue D, Helwig K and Moskovits M 1989 *J. Phys. Chem.* **93** 8080
[539] Eesley G L and Smith J R 1979 *Solid State Commun.* **31** 815
[540] Murray C A and Bodoff S 1984 *Phys. Rev. Lett.* **52** 2273
[541] Murray C A and Bodoff S 1985 *Phys. Rev.* B **32** 671
[542] Giergiel J, Ushioda S and Hemminger J C 1986 *Phys. Rev.* B **33** 56 57
[543] Mrozek I and Otto A 1987 *J. Electron Spectrosc. Relat. Phenom.* **45** 143
[544] Eesley G L 1981 *Phys. Lett.* **81A** 193
[545] Stolberg L, Richer J, Lipkowski J and Irish D E 1986 *J. Electroanal. Chem.* **207** 213
[546] Stolberg L, Lipkowski J and Irish D E 1991 *J. Electroanal. Chem.* **300** 563